National Library
of Canada

Canadian Theses Service

Ottawa, Canada
K1A 0N4

Bibliothèque nationale
du Canada

Service des thèses canadiennes

NOTICE

The quality of this microform is heavily dependent upon the quality of the original thesis submitted for microfilming. Every effort has been made to ensure the highest quality of reproduction possible.

If pages are missing, contact the university which granted the degree.

Some pages may have indistinct print especially if the original pages were typed with a poor typewriter ribbon or if the university sent us an inferior photocopy.

Reproduction in full or in part of this microform is governed by the Canadian Copyright Act, R.S.C. 1970, c. C-30, and subsequent amendments.

AVIS

La qualité de cette microforme dépend grandement de la qualité de la thèse soumise au microfilmage. Nous avons tout fait pour assurer une qualité supérieure de reproduction.

S'il manque des pages, veuillez communiquer avec l'université qui a conféré le grade.

La qualité d'impression de certaines pages peut laisser à désirer, surtout si les pages originales ont été dactylographiées à l'aide d'un ruban usé ou si l'université nous a fait parvenir une photocopie de qualité inférieure.

La reproduction, même partielle, de cette microforme est soumise à la Loi canadienne sur le droit d'auteur, SRC 1970, c. C-30, et ses amendements subséquents.

NL-339 (r. 88/04) c

Canada

UNIVERSITY OF ALBERTA

DEFORMATIONS OF PIPELINES EMBEDDED IN FROZEN SOIL

BY

© BALVANTRAI B. RAJANI

©

A THESIS
SUBMITTED TO THE FACULTY OF GRADUATE STUDIES AND
RESEARCH IN PARTIAL FULFILMENT OF THE REQUIREMENTS
FOR
THE DEGREE OF DOCTOR OF PHILOSOPHY

DEPARTMENT OF CIVIL ENGINEERING

EDMONTON, ALBERTA
SPRING, 1992

National Library of Canada
Bibliothèque nationale du Canada

Canadian Theses Service
Service des thèses canadiennes

Ottawa, Canada
K1A 0N4

The author has granted an irrevocable non-exclusive licence allowing the National Library of Canada to reproduce, loan, distribute or sell copies of his/her thesis by any means and in any form or format, making this thesis available to interested persons.

L'auteur a accordé une licence irrévocable et non exclusive permettant à la Bibliothèque nationale du Canada de reproduire, prêter, distribuer ou vendre des copies de sa thèse de quelque manière et sous quelque forme que ce soit pour mettre des exemplaires de cette thèse à la disposition des personnes intéressées.

The author retains ownership of the copyright in his/her thesis. Neither the thesis nor substantial extracts from it may be printed or otherwise reproduced without his/her permission.

L'auteur conserve la propriété du droit d'auteur qui protège sa thèse. Ni la thèse ni des extraits substantiels de celle-ci ne doivent être imprimés ou autrement reproduits sans son autorisation.

ISBN 0-315-73276-8

Canada

UNIVERSITY OF ALBERTA

RELEASE FORM

NAME OF AUTHOR:	Balvantrai B. Rajani
TITLE OF THESIS:	Deformations of Pipelines Embedded in Frozen Soil
DEGREE:	Doctor of Philosophy
YEAR THIS DEGREE GRANTED:	1992

PERMISSION IS HEREBY GRANTED TO THE UNIVERSITY OF ALBERTA LIBRARY TO REPRODUCE SINGLE COPIES OF THIS THESIS AND TO LEND OR SELL SUCH COPIES FOR PRIVATE, SCHOLARLY OR SCIENTIFIC RESEARCH PURPOSES ONLY.

THE AUTHOR RESERVES OTHER PUBLICATION RIGHTS, AND NEITHER THE THESIS NOR EXTENSIVE EXTRACTS FROM IT MAY BE PRINTED OR OTHERWISE REPRODUCED WITHOUT THE AUTHOR'S WRITTEN PERMISSION.

BBRajani
(Student's signature)

9807-151 Street,
Edmonton. Alberta T5P 1S9.
(Permanent address)

Date: April 21, 1992

UNIVERSITY OF ALBERTA

FACULTY OF GRADUATE STUDIES AND RESEARCH

THE UNDERSIGNED CERTIFY THAT THEY HAVE READ, AND RECOMMEND TO THE FACULTY OF GRADUATE STUDIES AND RESEARCH FOR ACCEPTANCE, A THESIS ENTITLED **DEFORMATIONS OF PIPELINES EMBEDDED IN FROZEN SOIL** SUBMITTED BY BALVANTRAI B. RAJANI IN PARTIAL FULFILMENT OF THE REQUIREMENTS FOR THE DEGREE OF DOCTOR OF PHILOSOPHY.

Dr. N.R. Morgenstern

D C Sego
Dr. D.C. Sego

PK Robertson
Dr. P.K. Robertson

Dr. A.E. Elwi

JR Colbourne.
Dr. J.R. Colbourne

Dr. B. Ladanyi (External Examiner)

Date: April 13, 1992

DEDICATION

"*... to Sonia, Asha and Anjali* "

and

"*... to Ba and Bapuji* "

ABSTRACT

In the late seventies and early eighties, the concept of transporting gas through a chilled pipeline was proposed. While a chilled gas pipeline satisfies environmental requirements and proves economical from a thermo-dynamical viewpoint, it introduces a structural problem for the pipeline itself. This is because the pipeline is subjected to differential movements (frost heave) when it traverses from a non-frost susceptible soil to a frost susceptible soil, i.e. discontinuous permafrost. Here this important aspect is addressed both analytically and experimentally.

The uplift behaviour of a shallow pipeline embedded in an elasto-plastic medium is examined. An analytical solution for a beam on an elasto-plastic foundation is developed and a characteristic non-dimensional load displacement and stress-displacement relationships are presented. An approximate 3D solution that accounts for embedment and breakaway condition behind the pipeline is proposed, making use of the load displacement curves developed for rigid anchors by Rowe and Davis (1982).

Recognizing that ice and ice rich soils creep, the behaviour of a pipeline embedded in a creeping medium is examined. Approximate solutions for a beam in a creeping foundation are developed and characteristic non-dimensional load-displacement relationships are presented. A comparison of these approximate solutions provides upper and lower bound solutions which are consistent with finite element analyses. Furthermore, the simplified solutions can be readily adapted for analyzing the uplift behaviour of shallow pipelines. Simulations of laterally loaded steel and timber piles in frozen ground as well as analysis of a pipeline at Caen, France, were carried out to demonstrate the robustness of the developed model.

The experimental behaviour of scaled model pipelines embedded in polycrystalline ice is studied in order to confirm our understanding of the behaviour of a chilled buried pipeline subjected to frost heave. Two model pipelines with slightly different radius to thickness ratios were subjected to prescribed displacement rates and their behaviour was observed until the pipeline was strained beyond current acceptable limits. The observed and predicted responses are compared and acceptable agreement between the responses is obtained, giving confidence in the predictive Winkler model.

ACKNOWLEDGEMENTS

I am deeply grateful to my supervisor, Dr. N.R. Morgenstern, for his interest, guidance and encouragement throughout the development of this thesis. I would like to thank Dr. D.C. Sego for useful discussions on the aspects of snow preparation and constant load creep tests on polycrystalline ice. The laboratory work was carried out with the skillful assistance of Mr. G. Cyre, Ms. C. Hereygers, Mr. S. Gamble and Mr. J. Khajuria of the Geotechnical Laboratory.

I wish to express my gratitude to my wife, Sonia, and daughters, Asha and Anjali, for their invaluable support and understanding throughout the course of this study. Without their patience and encouragement it would have proved very difficult to finish this thesis. I also recognize and appreciate the lifelong influence of my parents. Throughout this study, friends and colleagues have offered encouragement and fruitful discussions.

The research work reported in this thesis was supported by The Natural Sciences and Engineering Research Council and Esso Resources Canada Limited. The financial support granted through awards by Gulf Canada Resources Limited (administered by The University of Alberta) and Foothills Pipe Lines Limited (administered by The Association of Canadian Universities for Northern Studies (ACUNS)) is gratefully acknowledged.

TABLE OF CONTENTS

CHAPTER PAGE

1. FROZEN SOIL PIPELINE INTERACTION

Introduction 1
Outline of thesis 4

2. PIPELINES AND LATERALLY LOADED PILES IN AN ELASTO-PLASTIC MEDIUM

Introduction 6
Beam embedded in an elasto-plastic medium 10
An approximate 3D solution for a buried beam 17
Finite element analysis 21
  Uplift resistance of a buried pipeline 24
  Laterally loaded pile with and without separation 27
Conclusions 33
References 34
Nomenclature 38

3. BEHAVIOUR OF A SEMI-INFINITE BEAM IN A CREEPING MEDIUM

Introduction 40
Review of previous work 44
Beam embedded in a creeping medium 46
  Linear viscous medium i.e. $n = 1$ 53
  Creeping medium i.e. $n \neq 1$ 55
  Upper bound: Rayleigh-Ritz 55

  Lower bound: Martin's inequality 57
  Finite elements 62
Comparison between the different solutions 65
Conclusions 66
References 75
Nomenclature 80

4. LATERAL LOADS ON PILES AND UPLIFT OF PIPELINES IN PERMAFROST

Introduction 82
Brief review of previous work 85
Simulation of laterally loaded piles in frozen soil 89
  Pile load tests at Inuvik, N.W.T. 92
  Model solid steel piles in ice (Nixon, 1984) 101
  Model aluminium and steel piles in sand (Foriero and Ladanyi, 1991) 105
Simulation of pipeline subjected to differential frost heave 110
Conclusions 129
References 131
Nomenclature 136

5. UPLIFT OF MODEL STEEL PIPELINES EMBEDDED IN POLYCRYSTALLINE ICE

Introduction 138
Equipment design 141
  Proportioning of the model pipeline and polycrystalline ice block sample 142
  Preparation of a polycrystalline ice block sample 146
  Loading arrangement 154
  Instrumentation 156
Elastic and creep properties of polycrystalline ice 159
Structural properties of pipeline steel 304 167

Observation of strain time histories in model pipelines 168
Comparison of experimental behaviour with analysis 186
Conclusions 188
References 191
Nomenclature 197
Appendix 198

6. CONCLUSIONS

Frozen soil pipeline interaction 202
Recommendations for future studies 204

List of Tables

Table 3.1 Indentation factors 48

Table 3.2 J integrals for particular values of n 57

Table 4.1 Details on laterally loaded pile tests 84

Table 4.2 Geotechnical properties for clayey silt at Inuvik, N.W.T. 93

Table 4.3 Elastic and creep properties for ice 102

Table 4.4 Assumed elastic and creep properties for sand 106

Table 4.5 Geotechnical properties for sand and silt at Caen, France 118

Table 5.1 Summary of critical strain criterion for pipelines 145

Table 5.2 Comparison of prototype and model pipeline characteristics 148

Table 5.3 Summary of constant load creep test on samples of polycrystalline ice 167

Table 5.4 Creep properties of polycrystalline ice at - 2°C. 168

List of Figures

Figure 1.1 A comparison of frost heave and thaw settlement deformed shapes for pipelines 3

Figure 2.1 Vertical uplift of pipeline due to frost heave 12

Figure 2.2 Load-displacement curves for rigid anchors - no separation (after Rowe and Davis, 1982) 19

Figure 2.3 Load-displacement curves for rigid anchors - with separation (after Rowe and Davis, 1982) 20

Figure 2.4 Non-dimensional load-displacement curves for a beam on elasto-plastic foundation - analytical vs 3D finite elements 22

Figure 2.5 Non-dimensional maximum moment-displacement curves for a beam on elasto-plastic foundation - analytical vs 3D finite elements 23

Figure 2.6 Finite element model for an embedded pipeline 26

Figure 2.7 Non-dimensional load-displacement curves for a laterally loaded pile with and without separation - 3D finite elements (data from Pollalis, 1982) 30

Figure 2.8 Non-dimensional load-displacement curves for a laterally loaded pile without separation - analytical vs 3D finite elements 31

Figure 2.9 Non-dimensional load-displacement curves for a laterally loaded pile with separation - analytical vs 3D finite elements 32

Figure 3.1 Differential frost heave at the interface of discontinuous permafrost 42

Figure 3.2 Indentation factors for a semi-infinite creeping medium (von Mises material) 49

Figure 3.3 Beam embedded in a creeping medium 50

Figure 3.4 Geometrical interpretation of Martin's inequality 59

Figure 3.5 Tip displacement with time for a semi-infinite beam on a linear viscous creeping foundation - comparison of different methods 67

Figure 3.6 Tip displacement with time for a semi-infinite beam on a non-linear creeping foundation - Raleigh - Ritz 68

Figure 3.7 Tip displacement with time for a semi-infinite beam on a non-linear creeping foundation - Martin's inequality 69

Figure 3.8 Tip displacement with time for a semi-infinite beam on a non-linear creeping foundation - finite elements 70

Figure 3.9 Tip displacement with time for a semi-infinite beam on a non-linear ($n = 3$) creeping foundation - comparison of different methods 71

Figure 3.10 Tip displacement with time for a semi-infinite beam on a non-linear (n = 5) creeping foundation -comparison of different methods 72

Figure 3.11 Tip displacement with time for a semi-infinite beam on a non-linear (n = 7) creeping foundation - comparison of different methods 73

Figure 4.1 Typical signature of pile head displacement and displacement rate for a laterally loaded pile in frozen creeping medium 90

Figure 4.2 Comparison of predicted and observed pile head displacement time history for timber pile T-2-L at Inuvik, N.W.T. 96

Figure 4.3 Comparison of predicted and observed pile head displacement time history for timber pile T-3-L at Inuvik, N.W.T. 97

Figure 4.4 Comparison of predicted and observed pile head displacement time history for steel tubular pile S-4-L at Inuvik, N.W.T. 99

Figure 4.5 Comparison of predicted and observed pile head displacement time history for steel tubular pile S-5-L at Inuvik, N.W.T. 100

Figure 4.6 Comparison of predicted and observed pile head displacement time history for steel model piles in ice 103

Figure 4.7 Comparison of predicted and observed pile head displacement rates time history for steel model piles in ice 104

Figure 4.8 Comparison of predicted and observed pile head displacement time history for aluminium pile 1-A1 (with slurry) 108

Figure 4.9 Comparison of predicted and observed pile head displacement time history for steel rod pile 16-S1 (no slurry) 109

Figure 4.10 Vertical displacement and stress wave history profiles during 1st freeze period for pipeline at Caen, France (after Dallimore and Crawford, 1984) 112

Figure 4.11 Vertical displacement and stress wave history profiles during 2nd freeze period for pipeline at Caen, France (after Dallimore and Crawford, 1984) 113

Figure 4.12 Vertical displacement and stress wave profiles for a semi-infinite beam on elastic foundations as function of the characteristic length β 116

Figure 4.13 Instantaneous elastic modulus for sand and silt at Caen from constant load and constant displacement rate tests 120

Figure 4.14 Frost heave in sand and silt during 1st freeze period at Caen, France 123

Figure 4.15 Frost heave in sand and silt during 2nd freeze period at Caen, France 124

Figure 4.16 Predicted vertical displacement and stress history profiles during 1st freeze period (fixed/free end conditions) for pipeline at Caen, France 127

Figure 4.17 Predicted vertical displacement and stress wave profiles during 2nd freeze period (fixed/free end conditions) for pipeline at Caen, France 128

Figure 5.1 Exploded view of PVC box for block sample ice 147

Figure 5.2 Schematic diagram for snow production using a mini-snow gun 151

Figure 5.3 Test frame for mounting sample box (not to scale) 153

Figure 5.4 Exploded view of freezing plate wafer (not to scale) 155

Figure 5.5 Typical strain gauge arrangement and hanger system for applying displacements 157

Figure 5.6 Constant load creep test for polycrystalline ice sample T1-10/91 164

Figure 5.7 Constant load creep test for polycrystalline ice sample B7-02/92 165

Figure 5.8 Corrected normalized strain rate versus axial stress for polycrystalline ice at -2°C. 166

Figure 5.9 Experimental stress-strain characteristics of pipeline models A and B (stainless steel 304) 169

Figure 5.10a End displacement and load time histories for pipeline model A 171

Figure 5.10b End displacement and load time histories for pipeline model B 172

Figure 5.11a End displacement and temperature time histories for pipeline model A 173

Figure 5.11b End displacement and temperature time histories for pipeline model B 174

Figure 5.12a Strain time histories for points in the immediate vicinity of the peak strains for pipeline model A 175

Figure 5.12b Strain time histories for points in the immediate vicinity of the peak strains for pipeline model B 176

Figure 5.13a Vertical displacement profile histories for pipeline model A 177

Figure 5.13b Vertical displacement profile histories for pipeline model B 178

Figure 5.14a Experimental flexural strain profile histories for pipeline model A 179

Figure 5.14b Experimental flexural strain profile histories for pipeline model B 180

Figure 5.15a Comparison of final flexural strain profiles before thaw, strains determined from deformed shape and predicted strains for pipeline model A 182

Figure 5.15b Comparison of final flexural strain profiles before thaw and predicted strains for pipeline model B 183

Figure 5.16 Out-of-roundness profiles exaggerated 20 times along the pipeline model A in the final deformed form 185

Figure 5.17a Comparison of measured and predicted flexural strain profiles for pipeline model A 189

Figure 5.17b Comparison of measured and predicted flexural strain profiles for pipeline model B 190

Figure 5.A1 Constant load creep test for polycrystalline ice sample T2-11/91 199

Figure 5.A2 Constant load creep test for polycrystalline ice sample A4-01/92 200

Figure 5.A3 Constant load creep test for polycrystalline ice sample B7-02/92 201

List of Plates

Plate 5.1 General loading arrangement of an embedded model pipeline 158

Plate 5.2 Thin sections of ice polycrystalline samples from upper 0.10 m of block sample A using the hot-plate and microtome 161

Plate 5.3 Thin sections of ice polycrystalline samples from top and bottom block sample B using hot-plate 162

Chapter 1

FROZEN SOIL PIPELINE INTERACTION

Introduction

Over the past decade it has become evident that in the not too distant future the fossil energy demand in the North American Continent will increase considerably. Concurrently, public concern over the environment has put greater restraints on the ways and means of the exploitation and production of these hydrocarbon resources. Consequently, natural gas is gaining preference over coal and oil since it burns so much cleaner. These facts make it ultimately imperative to tap the large gas reserves found in the northern arctic regions of Canada.

In the late seventies and early eighties the concept of transporting gas through a chilled pipeline was proposed. The principal advantages of using a chilled gas pipeline system are twofold:

1. An economical throughput is obtained by using low pipeline temperatures. The energy balance of the system would be aided by the low ambient temperatures that exist in the northern arctic regions of Canada during a large part of the year.

2. The environment safeguards are met by not inducing thawing of the permafrost and thus preserving existing flora and fauna. While a chilled gas pipeline satisfies environmental requirements and proves economical from a thermo-dynamical viewpoint, it does introduce a structural problem for the pipeline. This is because the pipeline is subjected to differential movements (frost heave) when it traverses from a non-frost susceptible soil to a frost susceptible soil, i.e. discontinuous permafrost. This is schematically shown in Figure 1.1. A similar problem arises when a warm pipeline traverses previously frozen ground which subsequently subsides on thawing and thus induces additional stresses. However, there exists a fundamental difference between the above mentioned situations. Soils susceptible to a high frost heave are normally highly saturated soils which, when frozen, have a fairly high stiffness. Although the localized frozen soil stiffness is not as high as that of the pipe, there is much more active soil around the pipe that is frozen and consequently the relative influence is magnified in the frozen state. The newly heaving frozen soil constrains the pipeline much more that the unfrozen thawed soil due to both its higher stiffness and larger active region around the pipe. A given pipeline configuration can therefore tolerate far more differential thaw settlement than frost heave since frozen ground is substantially stiffer. The higher restraint consequently induces higher strains and stresses in the pipeline.

Ever since the chilled gas pipeline was proposed, the effects of frost heave on a pipeline were identified as an important issue. While the mechanics of frost heave, frost susceptibility and mechanical properties of

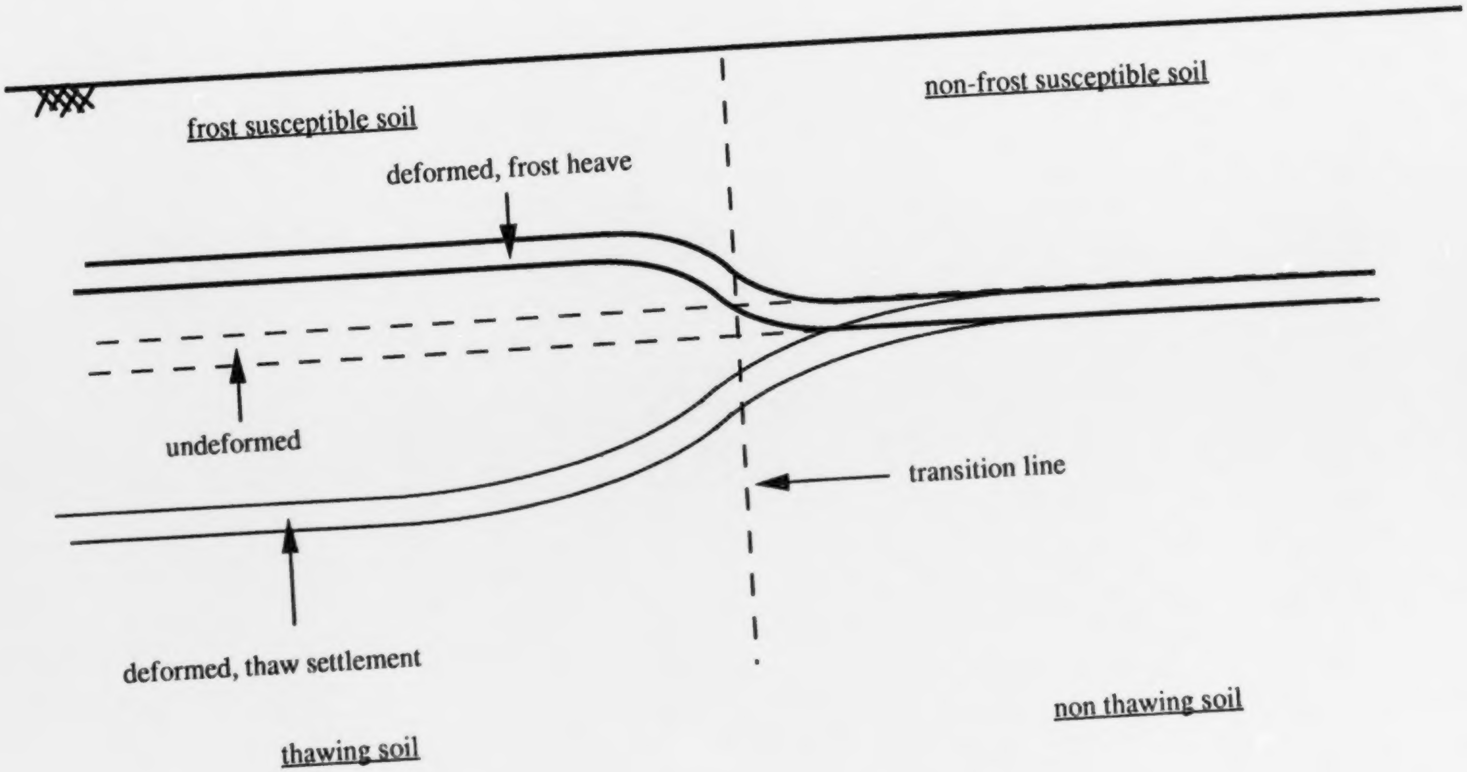
frost susceptible soil
non-frost susceptible soil
deformed, frost heave
undeformed
transition line
deformed, thaw settlement
thawing soil
non thawing soil

Figure 1.1 A comparison of frost heave and thaw settlement deformed shapes for pipelines.

frozen ground have been well studied, there is still a lack of proper understanding of the interaction between frozen soils and pipelines.

Outline of thesis

This thesis is written in paper format and consequently each chapter describes a particular aspect that is identified with the problem of frozen soil pipeline interaction. The second chapter describes how the behaviour of a pipeline embedded at shallow depths can be suitably determined from a solution of a beam embedded in an elasto-plastic medium. The analytical model is also used to verify other three dimensional finite element solutions obtained in relation to laterally loaded piles

The third chapter deals with approximate solutions for a beam embedded in a creeping medium. Simple analytical models representing upper and lower bound solutions are developed. These solutions compare favorably with simple Winkler finite element solutions. In chapter four the latter solutions are used to evaluate the creep response of laterally loaded piles and the response of an experimental pipeline subjected to frost heave at Caen, France. The robustness of the model is demonstrated by predictions which compare well with the observed performance.

Chapter five describes the experimental and test set-up of scaled model pipelines subjected to steady displacement. Two model pipelines were embedded in polycrystalline ice and the experimental responses were compared to solutions obtained using numerical procedures. Tests were also carried out to characterize the structural steel as well as the creep properties of polycrystalline ice. The simple numerical procedures developed in this thesis are able to reproduce the principal characteristics of the interaction of a pipeline embedded in frozen materials. Conclusions and recommendations for future studies are presented in Chapter 6.

Chapter 2

PIPELINES AND LATERALLY LOADED PILES IN AN ELASTO-PLASTIC MEDIUM[1]

Introduction

Over the past two decades several proposals have been put forward for the construction of a gas pipeline from the arctic to the southern populated areas (ASCE, 1978). These pipelines must be buried because of regulatory control. One method that has been suggested is to transport gas at below freezing temperatures and thus avoid the thawing of permafrost soils. However, this would lead to freezing of previously unfrozen soils in zones of shallow and discontinuous permafrost. It is to be expected that a frozen annulus will develop in a frost susceptible soil around the gas pipeline leading to significant water migration to the freezing front and the formation of ice lenses. Consequently, frost heave will be induced, thus forcing the pipeline to move upwards. The pipeline can undergo substantial straining leading to wrinkling buckles specially when the pipeline traverses a transition zone between two soils with different frost susceptibilities or between unfrozen and already frozen soil. Ever since the chilled gas pipeline concept was proposed, the effect of frost heave on pipelines has been identified as an important issue that should be addressed.

---

[1] A version of this chapter has been submitted for publication to The Journal of Geotechnical Engineering, ASCE.: Rajani, B. and Morgenstern, N., 1991. Pipelines and laterally loaded piles in an elasto-plastic medium.

However, it is appropriate to note that similar interactions are present in a variety of situations such as that of a laterally loaded pile embedded in a stiff soil or permafrost, a pipeline subjected to fault movement, a pipeline subjected to landslide movement, etc. The significant differences between that of a pipeline and pile would be the imposed loads (prescribed displacements versus imposed loads) and the near surface effects would have to be accounted for with the shallow burial of the pipeline.

In order to understand soil-pipeline interaction, specially in the context of a frozen surrounding medium, a number of aspects need to be considered. These include (i) the mechanics of frost susceptibility and frost heave which is essentially constitutes the loading process, (ii) the modelling of mechanical properties of frozen ground and (iii) the modelling of mechanical response of the pipeline. Though each of these aspects has been well studied individually, there is a lack of proper understanding of the interaction between frozen soil and pipelines.

Frost susceptibility and frost heave have become reasonably well understood and have been studied (Penner and Ueda (1978); Nixon *et al.*, (1981); Konrad and Morgenstern (1983, 1984)). These aspects will not be discussed further here. Although the prediction of frost heave is not an easy task, it can be estimated reasonably with currently available experience and knowledge.

The mechanical behaviour of frozen soil has been studied by Sayles (1973), Sayles and Haines (1974), Sego and Morgenstern (1983) and others. It is now widely accepted that ice-rich frozen soil behaves like a creeping material. The most likely circumstances of a pipeline subjected to frost heave will be associated with primary and secondary creep phases of straining. The classical studies of Glen (1955) indicate that the flow law of ice-rich soils is that of the Norton type. The Norton creep relationship rewritten in the generalized form as proposed by Ladanyi (1972) is:

$$[2.1] \qquad \frac{\dot{\varepsilon}}{\dot{\varepsilon}_o} = \left(\frac{\sigma}{\sigma_o}\right)^n \quad \text{or} \quad \dot{\varepsilon} = B\sigma^n$$

where $\dot{\varepsilon}$ is the axial strain rate, σ is the axial stress, $\dot{\varepsilon}_o$ and σ_o are proof strain rates and proof stress, B and n are creeping constants. Typically, n is about 3 (Morgenstern *et al.*, 1980) for ice at low stresses and icy silts (McRoberts *et al.*, 1978). In search for a dependence of n and B on temperature, Morgenstern *et al.* (1980) found from analyses of available creep data that ice behaves more as a linearly viscous material at temperatures close to 0^{o} C. The constant B is found to be temperature and material dependent. Sego and Morgenstern (1983, 1985) have studied the behaviour of laboratory prepared polycrystalline ice and have indeed confirmed the applicability of the Norton-type power law. In the past, considerable attention has also been paid to the behaviour of polycrystalline ice primarily for glaciology studies as well as laboratory studies related to geotechnical problems. It provides a good material to work with since control can be exercised over its characteristics in the laboratory. Sego and Morgenstern (1985) studied the indentation problem in polycrystalline ice both experimentally and numerically using finite elements and they were able to simulate comparable behaviour.

We have seen above that the analysis of the interaction of frost heave with a pipeline is a complex problem in which many processes need to be examined for a proper understanding of the complete system. In the present work, we propose to decouple the frost heave process in the frost susceptible soil from the pipeline in the non-frost susceptible soil. This implies that we should apply an attenuated frost heave rate at the transition zone of the two types of media rather than the free field frost heave rate (that which is usually measured in the laboratory). Presently, we assume that it can be readily approximated.

Previous attempts at solving this problem and specially that related to pipelines have been made by Nixon *et al.* (1983) and Selvadurai (1988). Nixon *et al.* (1983) simplified the problem to that of plane strain conditions and applied the free field frost heave over a predetermined section of the frost susceptible soil and studied its attenuation specifically at the interface of the frost and non-frost susceptible soils. However, the pipeline was considered as a passive component of the whole system and hence its interaction effects were not studied. Using the thermo-elastic analogy, Selvadurai (1988) analyzed the elastic behaviour of an embedded pipeline at shallow depth. As indicated previously, frozen soil hardly behaves as an elastic material and hence the application of this analysis is limited.

The motivation for studying the behaviour of a pipeline (beam) on elasto-plastic foundation is that for ice, n is found to be within the range of 3 to 4 and this is sufficiently large so as to be analogous to a rigid-plastic material ($n \rightarrow \infty$). Of course, the material behaviour is linearly viscous when $n = 1$ in a Norton type relationship. It is this former aspect that is of interest because it permits us to establish bounds on the true behaviour. In this chapter we present the solution for a beam on elasto-plastic foundation and an approximate 3D solution is also proposed. These results are then compared with 3D finite element analyses and they indeed confirm the validity of the simplified 3D solution.

Since the development of the solution is of a general nature in that it can be readily adapted to the analysis of a pipeline or a pile, we shall refer to either structure as a beam and the surrounding medium as the foundation. Yamada (1988) reported an analysis along the same lines where the beam was of finite length and applied to the problem of bonded-joint cracking.

Beam embedded in an elasto-plastic medium

For the present analysis we assume that the beam is buried in a homogeneous and isotropic elasto-plastic medium and when subjected to uplift the beam exhibits a double curvature. We recognize that, in fact, for shallow pipelines this may not be totally valid. The elasto-plastic behaviour of the medium is represented by a bi-linear force-displacement relation. If the elastic subgrade modulus is represented by k_s, then the foundation stiffness, k_s', is given by $k_s' = bk_s$, where b is the beam width (pile or pipeline diameter). Typically, the maximum force/unit length, F_z, resistance available for sand (Trautmann *et al.*, 1985) and for clay corresponding to the undrained state can be expressed respectively by:

$$F_z = \gamma b z N_z \tag{2.2a}$$

$$F_z = \overline{N}_c b s_u = \overline{N}_c b c = \overline{N}_c b \sigma_y \tag{2.2b}$$

where z is the depth of embedment and N_z is the dimensionless factor that depends on material properties of the sand, γ is the medium weight density, s_u is the undrained strength (= c, the cohesion for a purely cohesive material that follows the Mohr-Coulomb failure criterion) and $\overline{N}_c$ is a factor analogous to the bearing capacity factor which will be discussed in detail later. In the case of an elasto-plastic medium the undrained shear strength could be replaced by the yield strength, σ_y. Also, the limiting elastic displacement, U_z, is expressed as F_z/k_s'.

A consequence of the double curvature mentioned earlier is that the transition point O (Figure 2.1) is a point of inflexion at which the bending moment is zero. If on the other hand, we choose to look at the problem as that of a pile subjected to lateral load P, then the equivalent problem of a pipeline subjected to frost heave would be given by a prescribed displacement of $w_o = P\beta/2k_s'$ where $\beta = \sqrt[4]{k_s'/4EI}$ where E and I are beam elastic modulus and moment of inertia respectively, β is the so called characteristic length. We also note that the resulting problem is statically indeterminate. We shall formulate the problem in terms of the load, P, but the corresponding prescribed end displacement solution can be obtained as

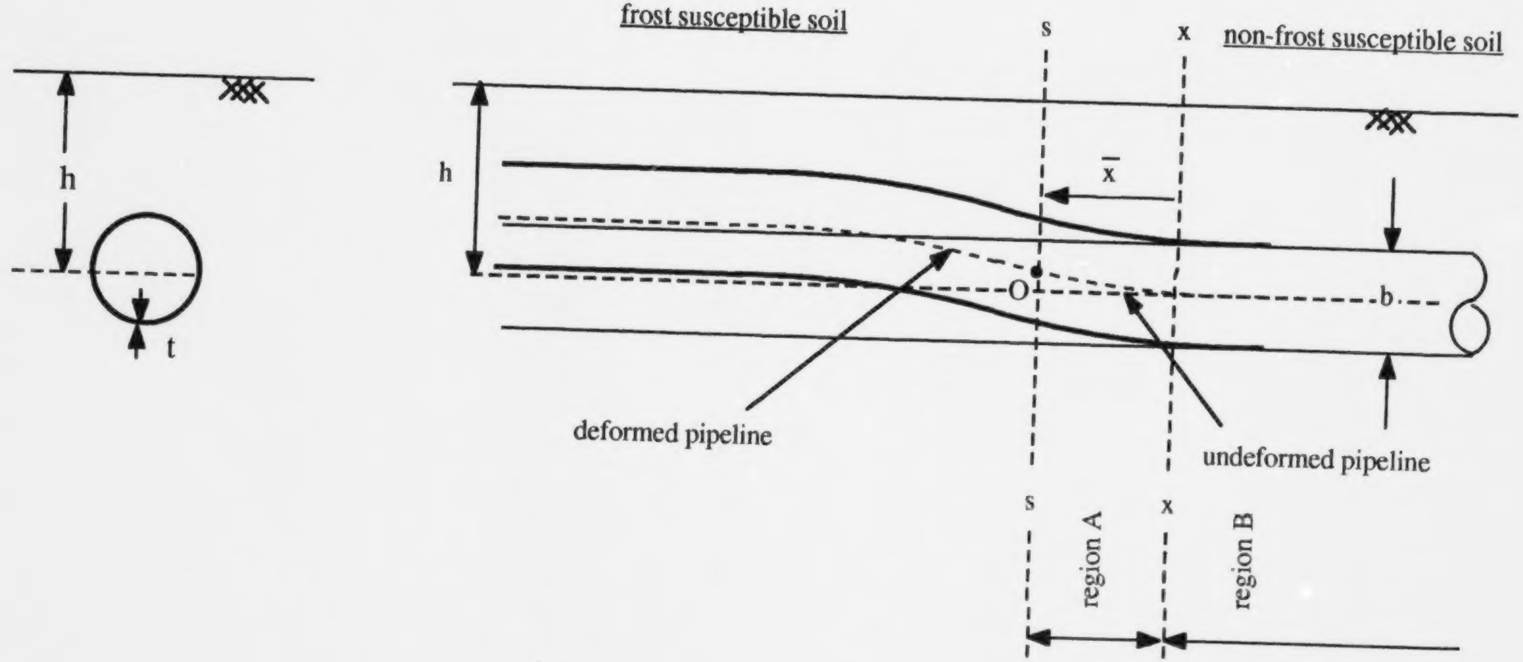
h
t
frost susceptible soil
s
x
non-frost susceptible soil
h
$\bar{x}$
O
b
deformed pipeline
undeformed pipeline
s
x
region A
region B

Figure 2.1. Vertical uplift of pipeline due to frost heave.

indicated above. A sequence of events as a result of the interaction between the beam and the surrounding foundation take place as the load is monotonically increased and these can be described as follows:

- on initial application of the end load, P (load level P_1), the embedded beam as well as the soil behave elastically.

- as the load is increased to a load level P_2, ultimate passive resistance will be developed in part of the surrounding soil medium but the pipe will remain elastic. Referring to Figure 2.1, we define an axis x-x that distinguishes two regions: region A where the medium is in an elasto-plastic state and region B where the medium is still elastic. The position of the axis x-x will shift from initial position (s-s) where it is initially coincident with the edge where the load or prescribed displacement is applied. The shift from the far edge to the axis x-x is denoted by $\overline{x}$ at any particular loading stage.

- as the load is further increased to, say, load level P_3, the distance $\overline{x}$ increases until a plastic hinge begins to develop in the beam or wrinkles develop in the beam depending on the structural characteristics of the beam.

Our object here is to trace this load resistance behaviour for the first two events.

Stage $0 \leq P \leq P_1$ and $w \leq U_z$

As noted earlier, for a load $0 \leq P \leq P_1$ and as long as the displacement w does not exceed the elastic displacement limit of the soil, $w \le U_z$, the solution for a beam on elastic foundation is perfectly valid and the corresponding differential equation, boundary conditions and solution (Hetenyi, 1968) are:

$$EI\frac{d^4w}{dx^4} + k_s' w = 0 \tag{2.3}$$

and at x = 0, we have $-M = EIw'' = 0$ and $-S = EIw''' = P$. The displacement is given by:

$$w = \frac{2P\beta}{k_s'} e^{-\beta x} \cos\beta x \tag{2.4}$$

for $0 \le x \le \infty$.

Stage $P_1 \le P \le P_2$ and $w \ge U_z$

As soon as the beam displaces sufficiently so as to exceed the elastic displacement limit, U_z, then a maximum force resistance will be acting on that portion of the beam while the rest of the beam-foundation is still elastic. The equilibrium equations for the two regions described earlier are:

$$\text{region A:} \quad -\bar{x} \le x \le 0 \qquad EI\frac{d^4w_A}{dx^4} = -F_z \tag{2.5}$$

$$\text{region B:} \quad 0 \le x \le \infty \qquad EI\frac{d^4w_B}{dx^4} + k_s' w_B = 0 \tag{2.6}$$

where $\bar{x}$ has been defined earlier.The corresponding solution for the differential equations are:

$$w_A = -\frac{F_z x^4}{24EI} + \frac{C_1 x^3}{6} + \frac{C_2 x^2}{2} + C_3 x + C_4 \tag{2.7}$$

$$w_B = e^{-\beta x}\left[C_5 \cos\beta x + C_6 \sin\beta x\right] \tag{2.8}$$

where C_i, i = 1, 2,...6 are constants. In the above equations we have seven unknowns: six C_i constants and $\bar{x}$. The necessary boundary conditions are:

[2.9a] at $x = -\bar{x}$ for moment: $-M = EIw'' = 0$

and shear: $-S = EIw''' = P$

for displacement and slope compatibility, and moment and shear equilibrium at $x = 0$, we have

[2.9b] displacement: $w_A = w_B$

for slope $w'_A = w'_B$

for moment: $w''_A = w''_B$

for shear: $w'''_A = w'''_B$

The last boundary condition is obtained from the fact that at $x = 0$ the rate of variation of shear is equal to the maximum force/unit length. i.e.,

$$EI\frac{d^4 w_A}{dx^4} = EI\frac{d^4 w_B}{dx^4} = -F_z \tag{2.9c}$$

The seven boundary conditions given in equations [2.9] permit the evaluation of the seven unknown constants. They are:

[2.10]
$$\begin{aligned} C_1 &= (P - \bar{x}F_z)/EI \\ C_2 &= \bar{x}(P - \bar{x}F_z/2)/EI \\ C_3 &= \beta(-2\bar{x}\beta^2 P + \bar{x}^2\beta^2 F_z - F_z)/k_s' \\ C_4 &= C_5 \\ C_5 &= F_z/k_s' \\ C_6 &= -C_2/2\beta^2 \end{aligned}$$

and
$$\bar{x}\beta = 2P\beta/F_z - 1$$

We note from the last equation of set [2.10] that the region A increases (i.e. $\bar{x}$ increases) as P increases and that $\bar{x}$ is zero until at least:

[2.11]
$$P \geq F_z/2\beta \quad \text{and} \quad P_e = F_z/2\beta$$

The displacement at the point of application of the load can be evaluated as a function of the applied load to determine what is commonly termed as the characteristic curve. Interestingly enough, the expression so obtained can be conveniently expressed in non-dimensional form i.e.,

[2.12]
$$\bar{w} = \bar{N}_c\left(\frac{1}{2} + \frac{2}{3}\frac{\bar{P}}{\bar{N}_c} + \frac{8}{3}\frac{\bar{P}^4}{\bar{N}_c^4}\right)$$

where $\bar{w} = wk_s'/bc$ and $\bar{P} = P\beta/bc$. In the design of a pipeline or a pile, we would normally be interested in the maximum bending moment or stress. The maximum bending moment in the beam depends on the load level as well as on which side of the transition axis (x-x) the maximum curvature develops. Three specific load levels are identified and expressed in non-dimensional form:

[2.13a] $$\frac{M\beta}{P} = e^{-\beta x} \sin\beta x \quad \text{where} \quad \beta x = \pi/4 \quad \text{and} \quad P \leq P_e$$

[2.13b] $$\frac{M\beta}{P} = \frac{e^{-\beta\hat{x}}\overline{N}_c}{2\overline{P}}\left[\sin\beta\hat{x} + \left(2\frac{\overline{P}}{\overline{N}_c} - 1\right)\cos\beta\hat{x}\right]$$

where $$\tan\beta\hat{x} = \frac{\left(\overline{N}_c - \overline{P}\right)}{\overline{P}} \quad \text{and } \overline{P} \geq 2\overline{P}_e$$

[2.13c] $$\frac{M\beta}{P} = \frac{3}{2}\frac{\overline{P}}{\overline{N}_c} + 4 - \frac{2\overline{N}_c}{\overline{P}}$$

where $$\beta\hat{x} = 1 - \frac{\overline{P}}{\overline{N}_c} \quad \text{and } \overline{P}_e \leq \overline{P} \leq 2\overline{P}_e$$

Equations [2.13a and 2.13b] correspond to the case when the maximum bending moment occurs to the right of the x-x axis and [2.13c] corresponds to the case when the maximum bending moment occurs to the left of the axis x-x. Nonetheless, the point ($\hat{x}$) of maximum moment increases as the load is monotonically increased.

An approximate 3D solution for a buried beam

Rowe and Davis (1982) examined the undrained behaviour for vertical uplift as well as horizontal movement of a rigid thin anchor in a saturated clay. Their study was limited to 2D plane strain conditions and they considered the influences of anchor embedment, layer depth, overburden pressure and breakaway condition or separation as well as other aspects on load displacement behaviour. The numerical solutions were obtained using finite element techniques assuming that the soil was purely cohesive and behaved according to the Mohr-Coulomb criterion. Additional assumptions made in their study can be referred to in the cited reference. In the case of a cohesive soil and for the specific case of undrained loading response, the cohesion is equal to the undrained shear strength. Consequently, for the analysis of the uplift behaviour of the pipeline and the laterally loaded pile the maximum resistance, F_z, can be expressed as indicated in [2.2b]. In the present analysis we propose to use findings of Rowe and Davis (1982) related to vertical uplift of anchors to study the uplift behaviour of pipelines and those related to horizontal movement of anchors to study lateral pile behaviour. Essentially we make use of the load displacement curves (commonly referred to as characteristic curves) for vertical uplift of anchors (Figures 2.2 and 2.3) and horizontal movement of anchors where full bonding or immediate breakaway is allowed for between the anchor and soil. The specific solutions were obtained for an anchor lying on the surface, i.e. $h/b = 0$ and for an anchor deeply buried. i.e. $h/b = \infty$. These provide lower and upper bounds solutions for the uplift capacity as expressed in [2.2b]. For a vertical anchor and embedment ratio of $h/b = 0$ we have the Prandtl solution and $\overline{N}_c$ is 5.14. The corresponding $\overline{N}_c$ value for $h/b = \infty$ is 11.42. Rowe and Davis (1982) found in their analyses that it was particularly difficult to define failure and they proposed a definition that failure is considered to be reached when the displacement is a selected multiple of that which would have been reached had the conditions remained entirely plastic. In fact, they showed through their analysis that

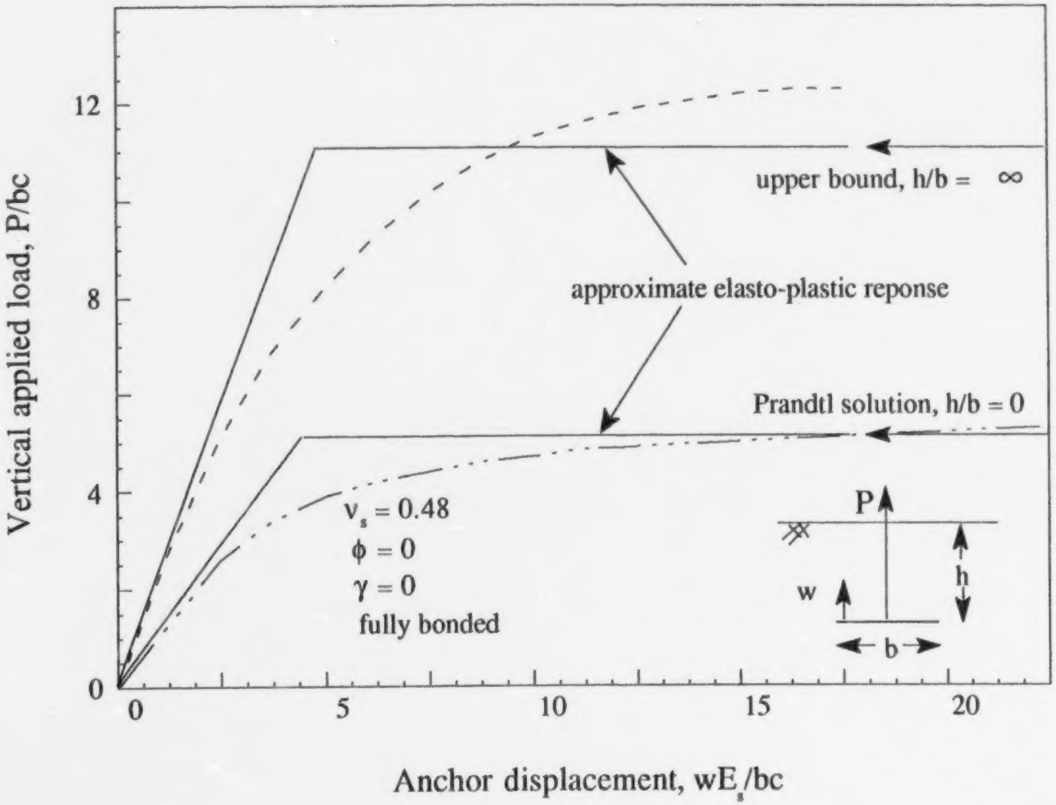

Figure 2.2. Load-displacement curves for rigid anchors - no separation (after Rowe and Davis, 1982).

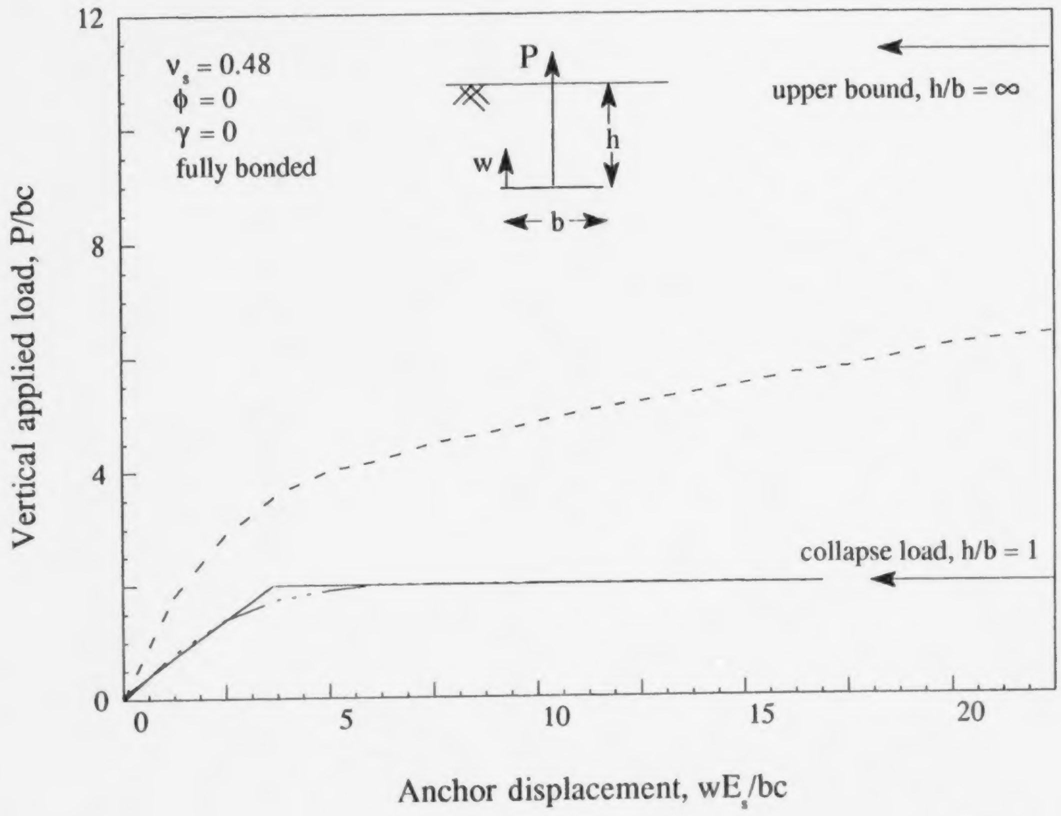

Figure 2.3. Load-displacement curves for rigid anchors - with separation (after Rowe and Davis, 1982).

for h/b > 3, the value of $\overline{N}_c$ (= 11.42) is essentially constant for a vertical anchor and its variation from 5.14 for h/b = 0 is practically linear till h/b = 3. Consequently, we propose to use the equivalent bi-linear representations of the vertical and horizontal load-displacement curves for anchors to represent the response of the soil in order to obtain an approximate 3D characteristic curves for the uplift behaviour of a buried beam and the response of a laterally loaded pile. As we shall see, this also permits us to obtain an economical solution for the beam embedded in a medium where separation is permitted to take place between the beam and the surrounding soil.

The characteristic curves for uplift resistance of a buried beam obtained by making use of the above indicated load displacement curves are shown in Figures 2.4 and 2.5. The effect of separation may be of considerable importance for the lateral behaviour of a pile, while it is believed that the pipeline-frozen soil interface could sustain adhesion and thus limit if not avoid separation. The loads and displacements obtained in Figures 2.4 and 2.5 are within the range of small displacement formulation.

Finite element analysis

The following points should be kept in mind in order to compare the finite element solutions with the proposed approximate solutions using load displacement characteristics for anchors developed by Rowe and Davis (1982):

- finite element solutions for anchors as developed by Rowe and Davis

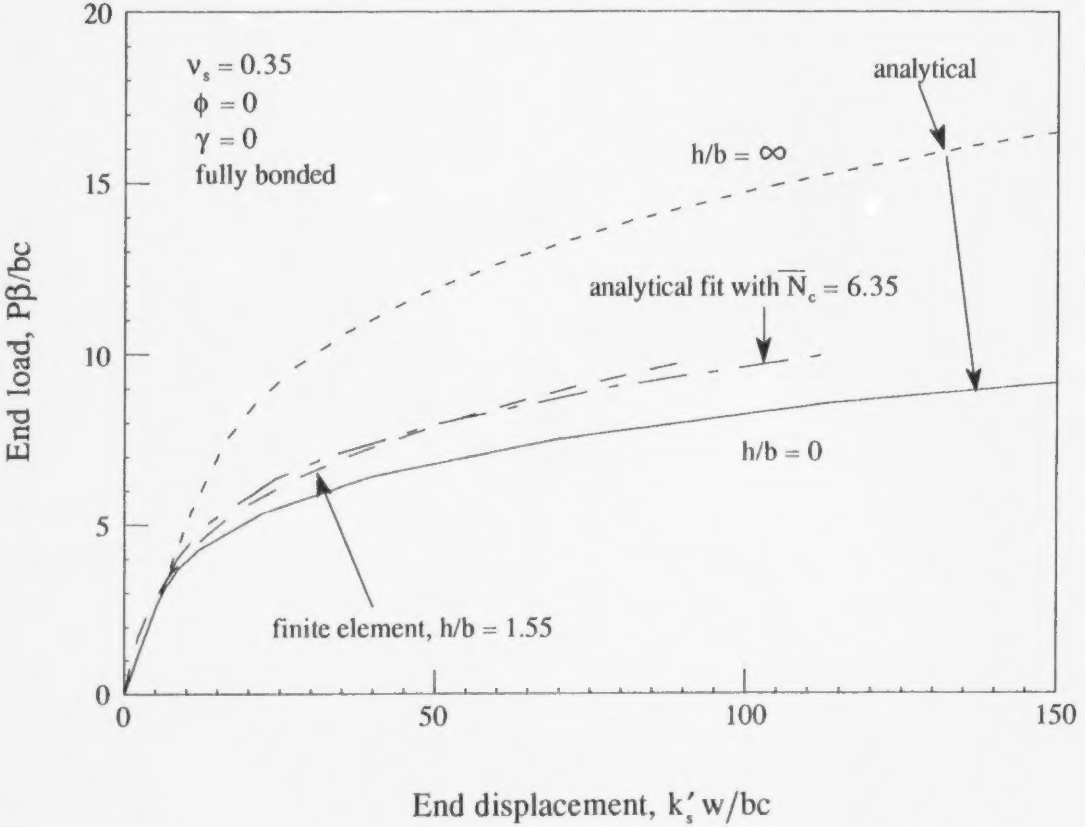

Figure 2.4. Non-dimensional load-displacement curves for a beam on elasto-plastic foundation - analytical vs 3D finite elements.

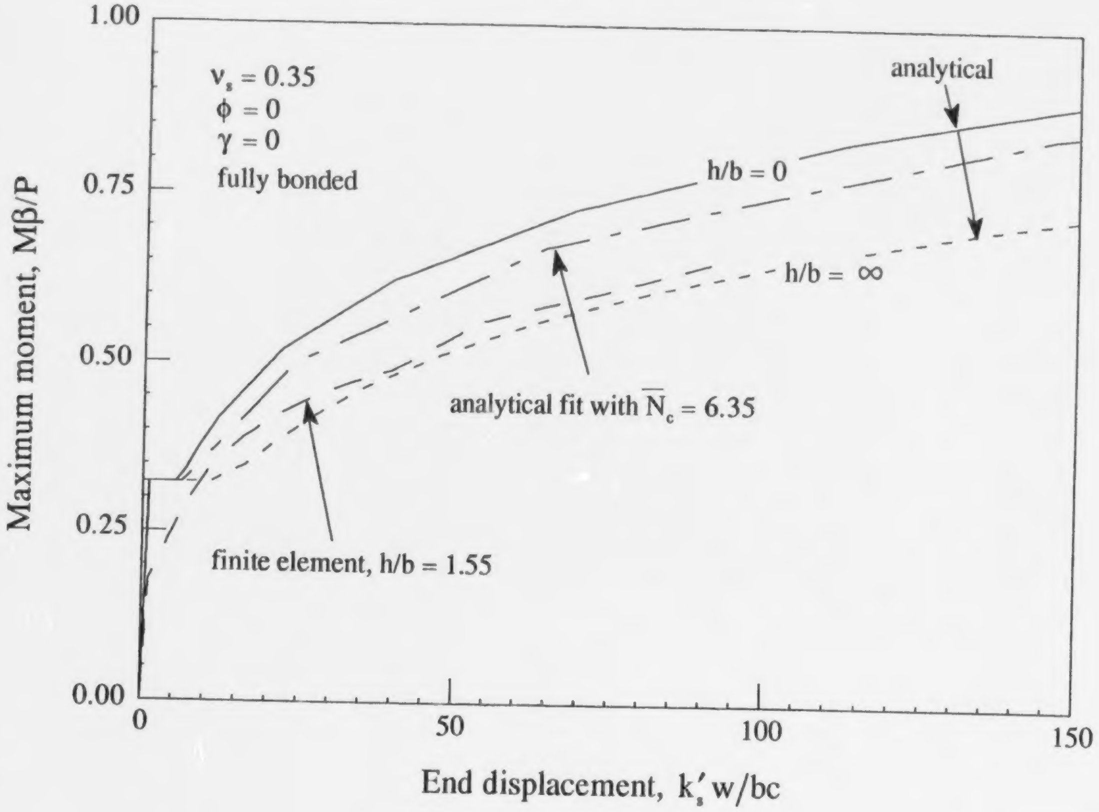

Figure 2.5. Non-dimensional maximum moment-displacement curves for a beam on elasto-plastic foundation - analytical vs 3D finite elements.

(1982) represent a plane strain condition. Meanwhile, the embedded beam (pipeline or pile) in a surrounding medium (frozen soil or soil) is between a plane stress and a plane strain condition.

- while the load displacements curves for vertical anchors given by Rowe and Davis (1982) can be directly used for the study of uplift resistance of the pipelines, the corresponding use for understanding the behaviour of a laterally loaded pile is not so obvious. For the latter case, the uppermost part of the pile can be envisaged as an anchor that steadily grows in depth (Figure 2.8) as the load is increased.

- a relation between the elastic modulus of the continuum and the so called foundation subgrade modulus used for the simplified problem as proposed by Vesic (1961) is given by:

$$k_s' = \frac{0.65E_s}{1-\nu_s^2}\sqrt[12]{\frac{E_s b^4}{EI}} \qquad [2.14]$$

Uplift resistance of a buried pipeline

In order to validate the approximate 3D solution for a beam embedded at finite depth, a finite element model for the embedded pipe was solved. A common problem in three dimensional finite elements is that the computational effort increases dramatically with discretization. This is of special significance when non-linear analysis is being carried out. As a consequence, we found that the discretization pattern was largely governed by the number of shell elements used along the circumference for representing the tube. We also wanted to ensure that the curvature of the tube was adequately represented. Hence, a choice was made to use the 4-noded thin shell element as formulated by Bathe and Dvorkin (1986) and available in Adina (1987). In order to avoid element locking, a 2 x 2 Gauss integration rule in the r-s plane was used. The surrounding medium was represented by 8-node brick finite elements and its material properties were described by the von Mises failure criterion. The finite element discretization of 12 x 5 x 12 in the x, y, z directions is shown in Figure 2.6. In fact, only one half of the problem needs to be solved if we take advantage of the symmetry. In solving the problem, essentially the same results were obtained when an 8-noded thin shell element and the corresponding 20-node brick element were used with a coarser discretization.

The finite element solution for displacement and maximum moment obtained for embedment ratio of h/b=1.55 are shown in Figures 2.4 and 2.5. An embedment ratio of 1.55 was chosen based on the premise that for regulatory approval a minimum cover of about 1 m is required and we envisaged a gas pipeline diameter of, say, 1066 mm. We observe that the finite element solution falls within the bounds established by the approximate analytical solutions. Subsequently, the approximate solution was obtained as indicated above using a depth factor, $\overline{N}_c$, of 6.35. It should be emphasized that this value of $\overline{N}_c$ was obtained by trial and error procedure and without applying any rigorous analysis such as a least square analysis. We note that though the load-displacement matches quite well, the bending moment-displacement match is closer to that of $h/b = \infty$ case. We

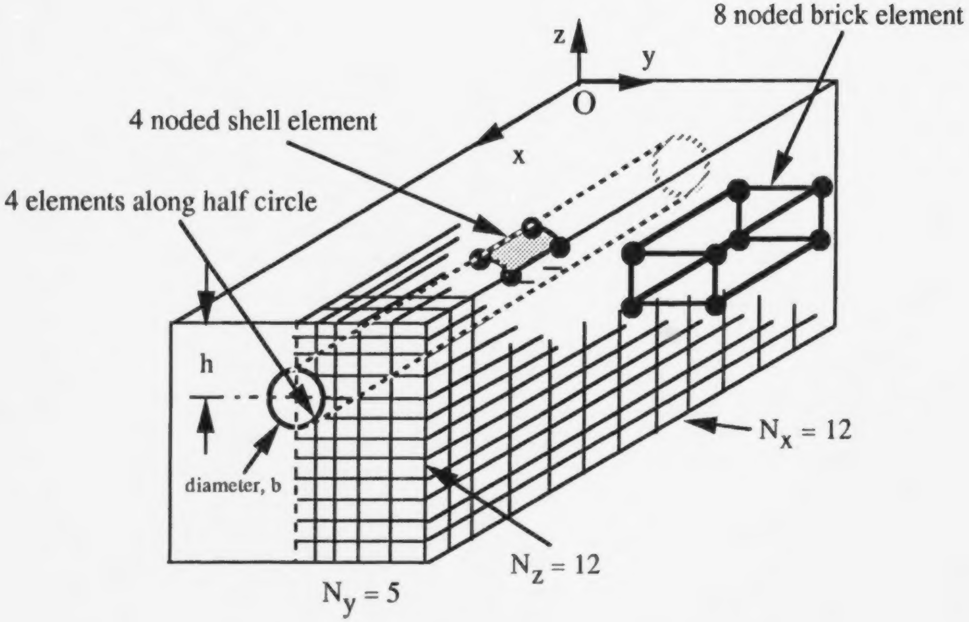
8 noded brick element
z
y
O
x
4 noded shell element
4 elements along half circle
h
diameter, b
$N_x = 12$
$N_z = 12$
$N_y = 5$

Figure 2.6. Finite element model for an embedded pipeline.

should keep in mind that the stress predictions using the displacement finite element technique are known to be poor and this would be especially expected in light of the coarse discretization used for the pipeline. It can be appreciated that a variety of approximate solutions can be easily obtained by varying this depth factor that corresponds to the specific h/b ratio.

Laterally loaded pile with and without separation

Pollalis (1982) examined the behaviour of a laterally loaded pile allowing for separation to take place as the lateral load was increased monotonically. The soil medium was considered to be elasto-plastic but both elastic shear modulus and the undrained shear strength increased linearly with depth since such a situation is usually encountered in normally consolidated clays. The laterally loaded pile was simulated using cubic beam finite elements for the pile and solved using 3D brick finite elements for the surrounding medium. The separation was accounted for by using springs elements and details can be found in the fore-mentioned reference. The constitutive model as proposed by Kavvadas (1982) for non-linear behaviour of the surrounding soil was used. However, before proceeding to compare the finite element solutions with the approximate solutions it is important to bear in mind that the solutions obtained by Pollalis (1982) consider shear strength increasing linearly with depth while the above proposed solution for a beam embedded in an elasto-plastic medium as well as the solutions for anchors obtained by Rowe and Davis (1982) are only pertinent for a homogeneous medium. Also, we should keep in mind that the solutions for an embedded anchor are those corresponding to that of a plane strain situation. Here, we attempt to obtain (at least qualitatively) a solution for a complex 3D situation using simplified 2D solutions and no suggestion is made that the analysis is rigorous. Nonetheless, it does provide insight into the mechanisms involved in the behaviour of a laterally loaded pile.

Recently, Trochanis *et al.* (1991a) performed a 3D finite element analysis of laterally loaded piles that accounts for a non-linear response of the soil as well as slippage and separation between the pile and the surrounding soil. Subsequently, Trochanis *et al.* (1991b) developed a discrete numerical Winkler model that adequately represents the cited non-linearities and it was validated by solving the same problem using 3D finite element analysis. A good comparison was obtained for typical test problems. A particular problem that was solved using the discrete numerical Winkler model was that of a laterally loaded pile embedded in an homogeneous cohesive soil.

The solutions as indicated by Pollalis (1982) are expressed in terms of different non-dimensional load-displacement parameters that we have selected in the above solution. Hence, the 3D finite element solution given by Pollalis (1982) was transformed to conform to our non-dimensional parameters. It is also important to note that when separation is not allowed for, Pollalis (1982) obtains an immediate non-linear response since a linearly varying elastic modulus with depth is used for the surrounding soil medium. Consequently, data from Pollalis (1982) was adjusted to include the initial elastic behaviour.

Figure 2.7 shows the 3D normalized finite element solutions as indicated above. It indeed shows that our normalization is more consistent than that proposed by Pollalis (1982). His parameter, $\overline{\alpha} = EI/\overline{\sigma}_D b^4$, is brought naturally into our normalization and the response obtained is within a very narrow band. It is also evident that the responses obtained by Pollalis (1982) were within a narrow range of parameters and hence to compare his results with our approximate solution an extrapolation procedure was used. In order to account for the linear variation of soil properties with depth and obtain a fair comparison between the approximate analyses and the 3D finite element method, we amplified the 3D finite element response by 1.5 (this factor is based on equivalence of the strain energy for the two systems). Figure 2.8 shows the 3D finite element solution as compared with the upper and lower bounds obtained using approximate analysis. The approximate solution can be seen to steadily increase from the h/b = 0 case to reach a steady state solution where h/b is in the range 1 to 3. In spite of the limitations cited above, it can be observed that the approximate analysis remarkably traces the trend of the more accurate finite element solution. The data from specific analysis of a laterally loaded pile that accounts for separation given by Trochanis *et al.* (1991b) was transformed to our non-dimensional parameters and the responses are indicated in Figures 2.8 and 2.9.

The separation between the back of the pile and the soil can be accounted for in an approximate manner if we use the corresponding limiting solutions for horizontal anchors as given by Rowe and Davis (1982). Though the limiting resistance depends on the particular collapse criteria used, the upper and lower resistances can be estimated to be in the range 2c and 4c. Figure 2.9 shows the comparison of the characteristic

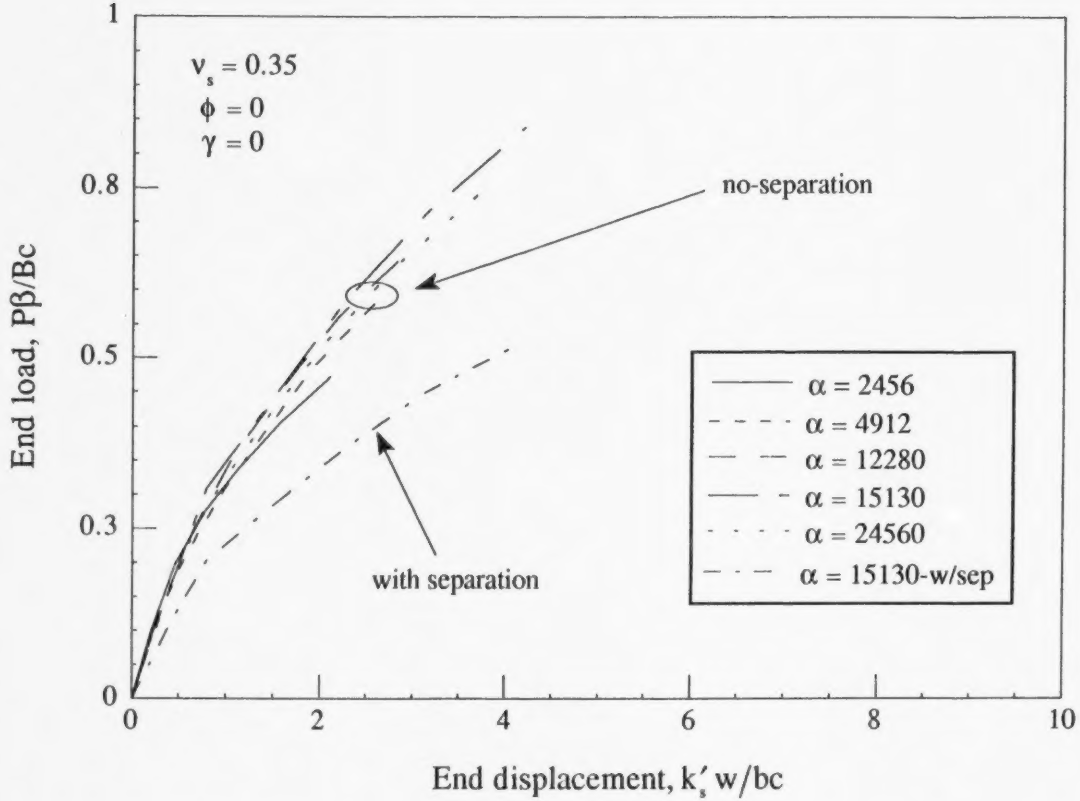

Figure 2.7. Non-dimensional load-displacement curve for a laterally loaded pile with and without separation - 3D finite elements (data from Pollalis, 1982).

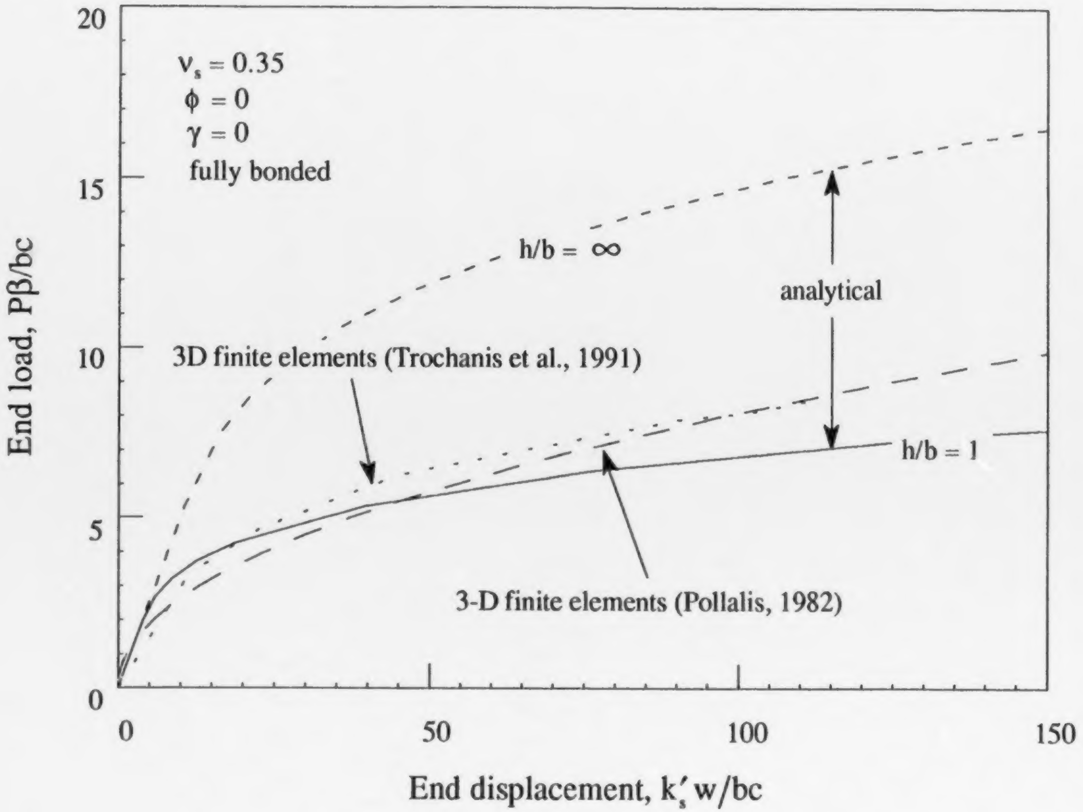

Figure 2.8. Non-dimensional load-displacement curve for a laterally loaded pile without separation - analytical vs 3D finite elements.

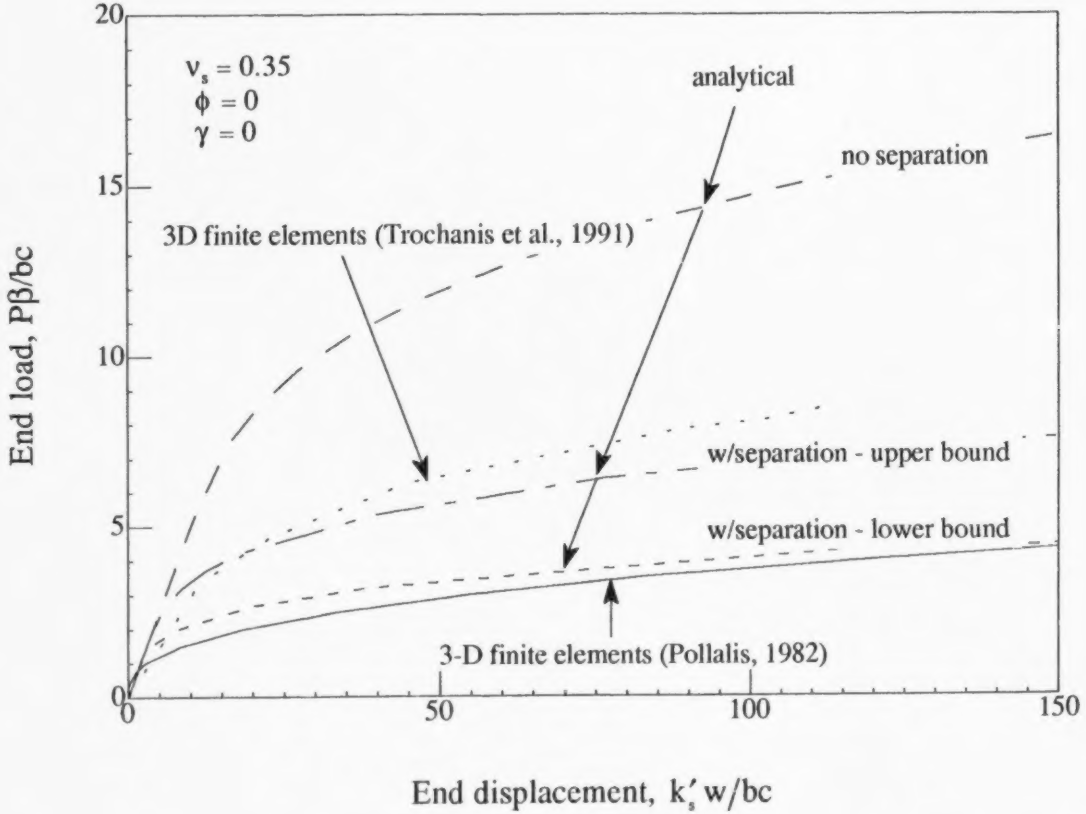

Figure 2.9. Non-dimensional load-displacement curve for a laterally loaded pile with separation - analytical vs 3D finite elements.

load-displacement curves obtained using the proposed analytical approximate solution, the 3D finite element solution (Pollalis, 1982) and the discrete Winkler model (Trochanis *et al.*, 1991). We note that the trend of the load-resistance curve is similar to that of the lower bound (h/b = 1) case and perhaps this observation provides a rational understanding of this commonly used criterion for ignoring the resistance offered by the soil medium in this region.

Conclusions

A simple analytical formulation for a beam on an elastic-plastic foundation is presented. The 2D plane stress load-displacement solutions developed by Rowe and Davis (1982) have been incorporated with the analytical formulation to obtain an approximate 3D solution. This approximate solution was compared with the 3D finite element solution for a shell pipe embedded in an elasto-plastic medium. We have demonstrated that the bounds established by the approximate solutions are quite adequate. The approximate solution can be fine tuned to the finite element solution using the bearing capacity factor, $\overline{N}_c$. We found that a value of $\overline{N}_c = 6.35$ matches the displacements well but the match of the stresses is not all that satisfactory. The approximate solution was also used to predict the effective lateral pile head stiffness and similar trends are predicted.

References

Adina - A finite element program for automatic dynamic incremental nonlinear analysis. 1987. Report ARD 87-1, ADINA R&D, Inc., Boston, MA.

American Society of Civil Engineers. 1978. An overview of the Alaska highway gas pipeline: The world's largest project. National Convention of the American Society of Civil Engineers in Pittsburg, Penn. vi + 130p.

Bathe, K.J. and Dvorkin, E. 1986. A formulation of general shell elements - the use of mixed interpolation of tensorial components. International Journal for Numerical Methods in Engineering, **22**(3): 697-722.

Glen, J.W. 1955. The flow law of polycrystalline ice. Proceedings of the Royal Society, London, **228A**: 519-538.

Kavvadas, M. 1982. Non-linear consolidation around driven piles in clays. Sc. D. thesis, Massachusetts Institute of Technology, Department of Civil Engineering. Boston, MA.

Konrad, J.-M. and Morgenstern, N. 1983. Frost susceptibility of soils in terms of their segregation potential. Proceedings, Permafrost: Fourth International Conference, Fairbanks, National Academy Science, Washington, p. 660-665.

Konrad, J.-M. and Morgenstern, N. 1984. Frost heave of chilled pipelines buried in unfrozen soils. Canadian Geotechnical Journal, **21**: 100-115.

Ladanyi, B. 1972. An engineering theory of creep of frozen soils. Canadian Geotechnical Journal, **9**: 63-80.

McRoberts, E.C., Law, T. and Murray, T. 1978. Creep testing on undisturbed ice-rich silt. Proceedings of the Third International Permafrost Conference. Edmonton, p. 539-545.

Morgenstern, N.R., Roggensack, W.D. and Weaver, J.S. 1980. The behaviour of friction piles in ice and ice-rich soils. Canadian Geotechnical Journal, **17**: 405-415.

Nixon, J., Ellwood, J. and Slusarchuk, W. 1981. In-situ frost heave testing using cold plates. Proceedings of the Fourth Canadian Permafrost Conference, Calgary, NRCC No. 20124. Section 7.

Nixon, J.F., Morgenstern, N.R. and Ressor, S.N. 1983. Frost heave-pipeline interaction using continuum mechanics. Canadian Geotechnical Journal, **20**: 251-261.

Penner, E. and Ueda, T. 1978. A soil frost susceptibility test and a basis for interpreting heaving rates. Proceedings of the Third International Permafrost Conference. Edmonton, p. 722-727.

Pollalis, S.N. 1982. Analytical and numerical techniques for predicting the lateral stiffness of piles. Ph.D. thesis, Massachusetts Institute of Technology, Department of Civil Engineering. Boston, MA.

Rowe, R.K. and Davis, E.H. 1982. The behaviour of anchor plates in clay. Geotechnique, **32**(1): 9-23.

Sayles, F.H. 1973. Triaxial and creep tests in frozen Ottawa sands. Proceedings of the Second International Conference on Permafrost, North American Contribution, Yakutsk, USSR, National Academy of Sciences, Washington, D.C., p. 384-391.

Sayles, F.H. and Haines, D. 1974. Creep of frozen silt and clay. U.S, Army Cold regions research and engineering laboratory, Hanover, NH. Technical report 252. 50p.

Sego, D.C. and Morgenstern, N. 1983. Deformation of ice under low stresses. Canadian Geotechnical Journal, **20**(4): 587-602.

Sego, D.C. and Morgenstern, N. 1985. Punch indentation of polycrystalline ice. Canadian Geotechnical Journal, **22**(2): 226-233.

Selvadurai, A.P.S. 1988. Mechanics of soil-pipeline interaction. Proceedings of the Annual Conference of The Canadian Society for Civil Engineering, Calgary, **3**: 151-173.

Trochanis, A.M., Bielak, J. and Christiano, P. 1991a. Three-dimensional nonlinear study of piles. ASCE Journal of Geotechnical Engineering

Division, **117**(3): 429-447.

Trochanis, A.M., Bielak, J. and Christiano, P. 1991b. Simplified model for analysis of one or two piles. ASCE Journal of Geotechnical Engineering Division, **117**(3): 448-466.

Trautmann, C.H., O'Rourke, T.D. and Kulhawy, F. 1985. Uplift force-displacement response of a buried pipe. ASCE Journal of Geotechnical Engineering Division, **111**(9): 1061-1076.

Vesic, A.S. 1961. Bending of beams resting on isotropic elastic solid. Proceedings of ASCE, **87**(EM2): 35-51.

Yamada, S.E. 1988. Beams on partially yielded foundation. ASCE Journal of Engineering Mechanics Division, **114**(3): 353-363.

Nomenclature

The following symbols are used in this chapter:

b = beam width, pipeline or pile diameter

B = creep proportionality constant

c = cohesion

C_i = constants

E = beam elastic modulus

E_s = soil elastic modulus

F_z = medium resistance per unit length

h = embedment depth

I = beam moment of inertia

k_s' = foundation subgrade modulus

M = bending moment

P = non-dimensional load parameter

n = creep exponent in Norton relation

$\overline{N}_c$ = bearing capacity type factor

N_z = non-dimensional parameter for evaluating soil resistance

s_u = undrained shear strength

S = shear

w = displacement in the z-direction

$\overline{w}$ = non-dimensional displacement parameter

x = longitudinal coordinate axis

$\overline{x}$ = region in plastic state

$\hat{x}$ = point of maximum bending moment

z = axis normal to x-axis

$\overline{\alpha}$ = non-dimensional parameter defined by Pollalis (1982) (= $EI/\overline{\sigma}_D b^4$)

$\dot{\varepsilon}_o$ = proof strain rate

γ = soil weight density

ν_s = soil Poisson's ratio

σ_o = proof stress

$\overline{\sigma}_D$ = stress at tip of pile (used by Pollalis,1982)

σ_y = yield stress of surrounding medium

Chapter 3

BEHAVIOUR OF A SEMI-INFINITE BEAM IN A CREEPING MEDIUM[1]

Introduction

The understanding of soil-pipeline interaction and specially in the context of a frozen surrounding medium is important for pipeline as well as pile design. The different aspects that need to be considered, particularly when involved with the design of pipelines, are: (i) the mechanics of frost susceptibility and frost heave which essentially constitute the loading process, (ii) the modelling of mechanical properties of frozen ground and (iii) the mechanical response of the pipeline. Though each of these aspects has been well studied individually, there is a lack of proper understanding of the interaction between frozen soil and pipelines subjected to uplift.

The state of knowledge in each of the identified aspects related to frozen ground was summarized in the last chapter. The analysis of the interaction of frost heave with a pipeline is a complex problem in which many processes need to be examined for a proper understanding of the complete system. In the present work, we propose to decouple the frost heave process in the frost susceptible soil from the pipeline in the non-frost susceptible soil. This implies that we can apply an attenuated frost heave rate at the transition zone of the two types of media rather than the free field frost heave rate (that which is usually measured in the laboratory). This is illustrated in Figure 3.1 using data from the Caen experiments (Dallimore and Crawford,1984) where the pipeline is embedded in both sand and silt. The attenuation of the free field frost heave is probably a function of the dimensions and mechanical properties of the adjacent frozen ground. Ladanyi and Lemaire (1984) attempted to back-analyze the Caen experiments using a simplified model based on the elastic Winkler foundation that accounted for free field frost heave in an idealized manner. Here, we assume that the attenuated relation can be readily approximated from the stress dependence of the free field frost heave rate (Konrad and Morgenstern, 1982).

---

[1] A version of this chapter has been submitted for publication to The Canadian Geotechnical Journal: Rajani, B. and Morgenstern, N., 1991. Behaviour of a semi-infinite beam in a creeping medium.

Previous attempts at solving this problem related to pipelines have been made by Nixon *et al.* (1983) and Selvadurai (1988). Nixon *et al.* (1983) simplified the problem to that of plane strain conditions and applied the free field frost heave over a predetermined section of the frost susceptible soil and studied its attenuation specifically at the interface of the frost and non-frost susceptible soils. However, the pipeline was considered as a passive component of the whole system and hence its interaction effects were not studied. Selvadurai (1988) analyzed the elastic behaviour of an embedded pipeline at shallow depth using the thermo-elastic analogy.

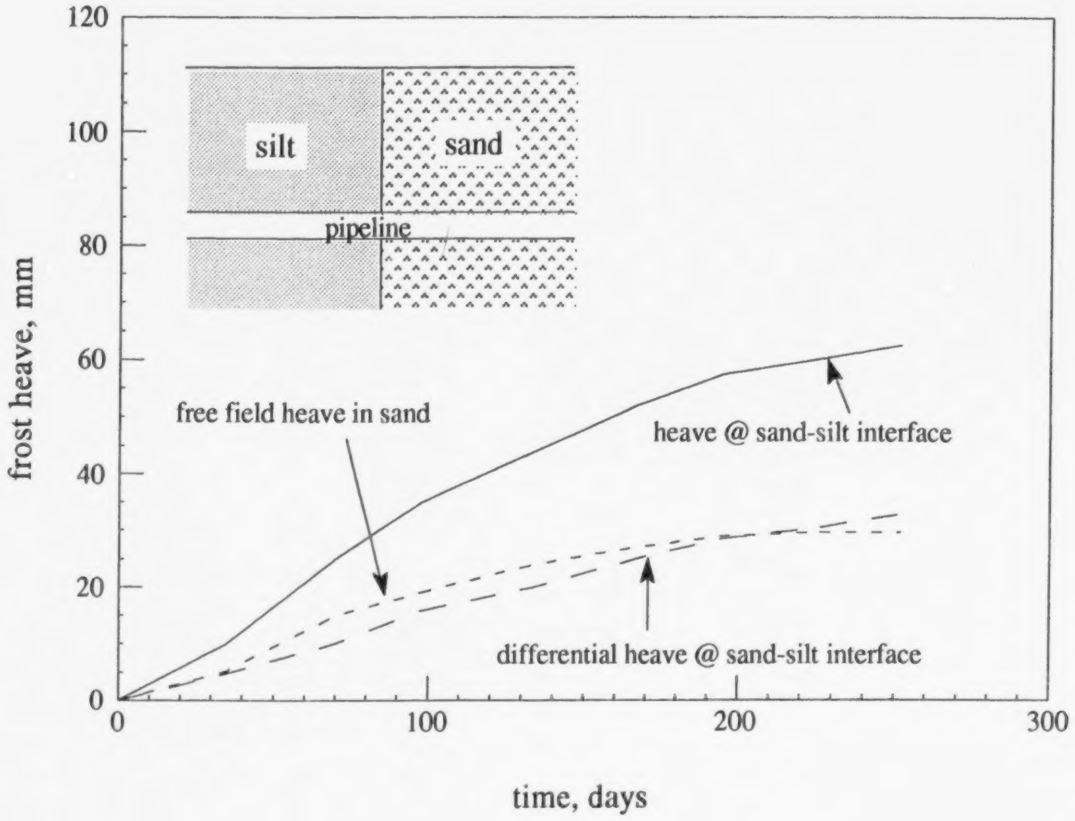

Figure 3.1. Differential frost heave at the interface of discontinuous permafrost.

Frozen soil hardly behaves as an elastic material and hence the application of this analysis is limited.

The classical studies of Glen (1955) indicate that the flow law of ice-rich soils is that of the Norton type. The Norton creep relationship, rewritten in the generalized form as proposed by Ladanyi (1972), is:

$$\frac{\dot{\varepsilon}}{\dot{\varepsilon}_o} = \left(\frac{\sigma}{\sigma_o}\right)^n \quad \text{or} \quad \dot{\varepsilon} = B\sigma^n \tag{3.1}$$

where $\dot{\varepsilon}$ is the axial strain rate, σ is the axial stress, $\dot{\varepsilon}_o$ and σ_o are proof strain rates and proof stress, B and n are creeping constants. Typically, n is about 3 (Morgenstern *et al.*, 1980) for ice at low stresses and icy silts (McRoberts *et al.*, 1978). In search for the dependence of n and B on temperature, Morgenstern *et al.* (1980) found from analyses of available creep data that ice behaves more as a linearly viscous material at temperatures close to 0^oC. The constant B is found to be temperature and material dependent.

The motivation for studying the behaviour of a pipeline (beam) on an elasto-plastic foundation is that, for ice, n is found to be within the range of 3 to 4 and this is sufficiently large so as to be analogous to a rigid-plastic material ($n \rightarrow \infty$). Of course, the material behaviour is linearly viscous when $n = 1$ in a Norton type relationship. The former aspect was studied in the last chapter and here we confine ourselves to n between the bounds indicated above. In this chapter we present the solution of a beam on a creeping foundation and an approximate 3-D solution is proposed.

Since the development of the solution is of a general nature in that it can be readily adapted to the analysis of a pipeline or a pile free at the head, we shall refer to either structure as a beam and the surrounding medium as the foundation.

Review of previous work

Flügge (1975) presented the solution of a finite beam on a linear viscous foundation i.e. $n = 1$. Flügge's solutions are based on the *correspondence principle* which states that, when a viscoelastic system is subjected to a constant load or displacement, then displacements or stresses depend on time and are calculated in the same manner as those in an elastic system, except that the elastic material properties are replaced by viscoelastic parameters. As indicated by Flügge (1975), the conditions of equilibrium, kinematics and constitutive relationships must be satisfied for the *correspondence principle* to be applicable for the analysis of viscoelastic systems. It is important to point out that this procedure, in which the time variable is separated in the analysis, is also often referred to as Hoff's *elastic analogy* (1954). The application of the *correspondence principle* is not limited to linear elastic systems as shown by Hoff (1954). A direct consequence of the *correspondence principle* or Hoff's *elastic analogy* is that the distribution of stresses in space within the system remains constant. This phenomenon is often referred to as *stationary creep* and it needs to be contrasted with *secondary creep* where creep occurs with a constant rate of strain.

In an indeterminate structure where the material behaves according to the secondary creep law [3.1], a redistribution of stresses occurs during the transient phase and the structure behaves as though the material were subjected to primary creep. Hence, to distinguish this phenomenon from primary creep, which is a material property, it is often referred to as *statical creep*. In the present analysis, we are dealing with an indeterminate structure (i.e. beam in a creeping foundation), we will observe *statical creep* which should not be confused with *primary creep*.

Most of the developments for the solution of a beam in a creeping medium have taken place with particular reference to laterally loaded piles in permafrost. Furthermore, all these developments consider the foundation to be of the Winkler type and which makes the problem more amenable to a simple solution. Early solutions proposed by Ladanyi (1973) and Rowley *et al.* (1973) were essentially along the same lines as the non-linear analysis of laterally loaded piles in unfrozen ground i.e. non-linear p-y representation of the frozen ground. Nixon (1984) dealt with a short rigid pile as well as a flexible pile embedded in frozen soil that follows the secondary creep law [3.1]. In the case of a flexible pile, Nixon (1984) established a differential equation treating the foundation as a creeping Winkler foundation and solved it numerically using the finite difference technique. More recently, Foriero and Ladanyi (1990) have proposed a solution where the lateral reaction due to creep is represented by Maxwell springs and the creep displacements of the surrounding medium are evaluated using finite elements. Almost always, the effectiveness of the different methods have been demonstrated by comparing the predictions with pile load test carried out by Rowley *et al.* (1973, 1975).

After looking in detail at the different solutions and strategies it is evident that comparing the solutions on a case by case basis does not permit us to gain insight and hence develop an understanding of the role of the different parameters. A more comprehensive analytical framework is desirable.

Consequently, in the present chapter, we attempt to obtain upper and lower bound analytical approximate solutions that enhance the understanding of the behaviour of a laterally loaded beam in a creeping medium. In a non-linear finite element analysis of lateral loads in unfrozen soil, discrete springs are often used in which the spring characteristics that are assigned correspond to the non-linear behaviour of the foundation response. Using simple energy concepts, we develop simple relations for defining spring characteristics when the foundation follows the material law as described by [3.1]. This permits the use of conventional finite element programs for analyzing these types of problems. In the previous chapter, the solution to the problem of a beam in an elasto-plastic foundation, i.e. the limiting solution when $n \to \infty$ was presented.

Beam embedded in a creeping medium

For the present analysis we assume that the beam is buried in a homogeneous and isotropic, elastic and non-linear viscous medium, and that when subjected to uplift, the beam deforms anti-symmetrically. We recognize that, in fact, for shallow pipelines this may not be totally valid. The creep behaviour of the medium is represented by a Norton-type relation [3.1]. If the elastic subgrade modulus is represented by k_s, then the foundation stiffness, k_s', is given by $k_s' = bk_s$, where b is the beam width (pile or pipeline diameter). Nixon (1978) has related the displacement rate ($\dot{w}$) of a long cylinder to the stress on the loaded area and this is given by:

[3.2a]
$$\dot{w} = (I_f Bb/2)p^n$$

where p is the intensity of pressure on the loaded area, I_f is the influence factor dependent on n and the geometry of the loaded beam. Since the beam width is b, then the reaction per unit length q is given by:

[3.2b]
$$\dot{w} = \frac{(I_f Bb/2)}{(b)^n} q^n = B'q^n$$

and $B' = (I_f Bb/2)/(b)^n$ is the creep compliance coefficient for the foundation. The above relation can be rewritten in the general form:

[3.3]
$$F_z = I_n b\sigma_o \left(\frac{\dot{w}/b}{\dot{\varepsilon}_o} \right)^{1/n}$$

where $F_z (= pb)$ is the resistance per unit length offered by the surrounding medium and $I_n (= (2/I_f)^{1/n})$ is the indentation factor. Indentation factors for a von Mises material as determined by Nixon (1978), Ladanyi (1983), Ponter *et al.* (1983) and Foriero and Ladanyi (1989) are shown in Table 3.1. We note from [3.3] that as $n \rightarrow \infty$ the indentation factor becomes Prandtl's bearing capacity factor, N_c. While indentation factors for a flat indenter and a circular disk (plane strain) as determined by expressions in Table 3.1 approach Prandtl's limiting value, the cavity expansion solution for a strip footing is unbounded. The slight difference in the solution for the long cylinder and the flat indenter studied by Ponter *et al.* (1983) is due to the shape of the two indenters. The variation of the indentation factor with creep coefficient n is shown in Figure 3.2 and demonstrates that it is preferable to use the indentation factor as proposed by Foriero and Ladanyi (1989).

A consequence of the double curvature mentioned earlier is that the transition point O (Figure 3.3) is a point of inflexion implying a stress boundary condition of zero moment. If on the other hand, if we choose to look at the problem as that of a pile subjected to a lateral load P, then the equivalent problem of a pipeline subjected to frost heave would be given by

Table 3.1. Indentation factors.

Feature	Indentation factor I_n	Reference
cavity expansion strip footing solution	$I_n = (n/\sqrt{3})(8/\pi\sqrt{3})^{1/n}$	Nixon (1978), Ladanyi (1983)
flat indenter on semi-infinite half-space	$I_n = \phi/(\phi\psi)^{1/n}$ where $\phi = (\pi + 2)/\sqrt{3}$ and $\psi = 0.445$	Ponter *et al.* (1983)
long cylinder streamline solution (plane strain)	$I_n = \frac{2\pi}{\sqrt{3}}\left(\frac{8}{\sqrt{3}}\right)^{1/n} \frac{n^2}{(n+1)(n+3)}$	Foriero and Ladanyi (1989)

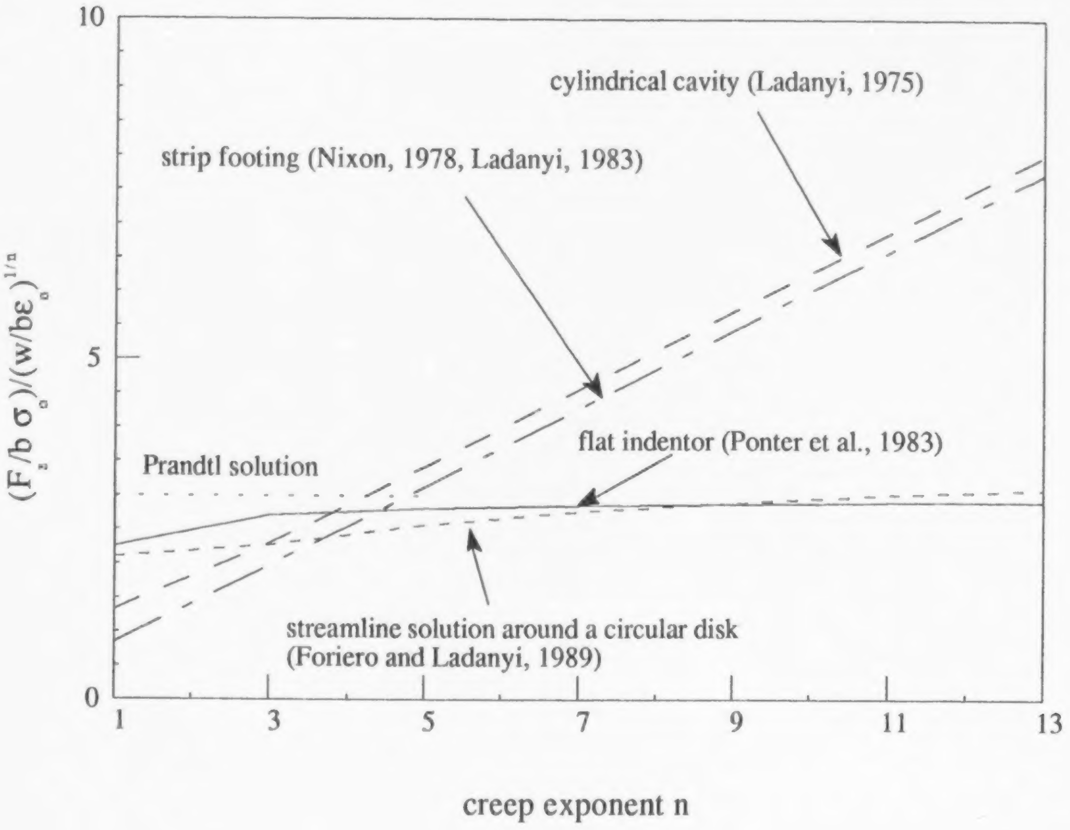

Figure 3.2. Indentation factors for a semi-infinite creeping medium (von Mises material).

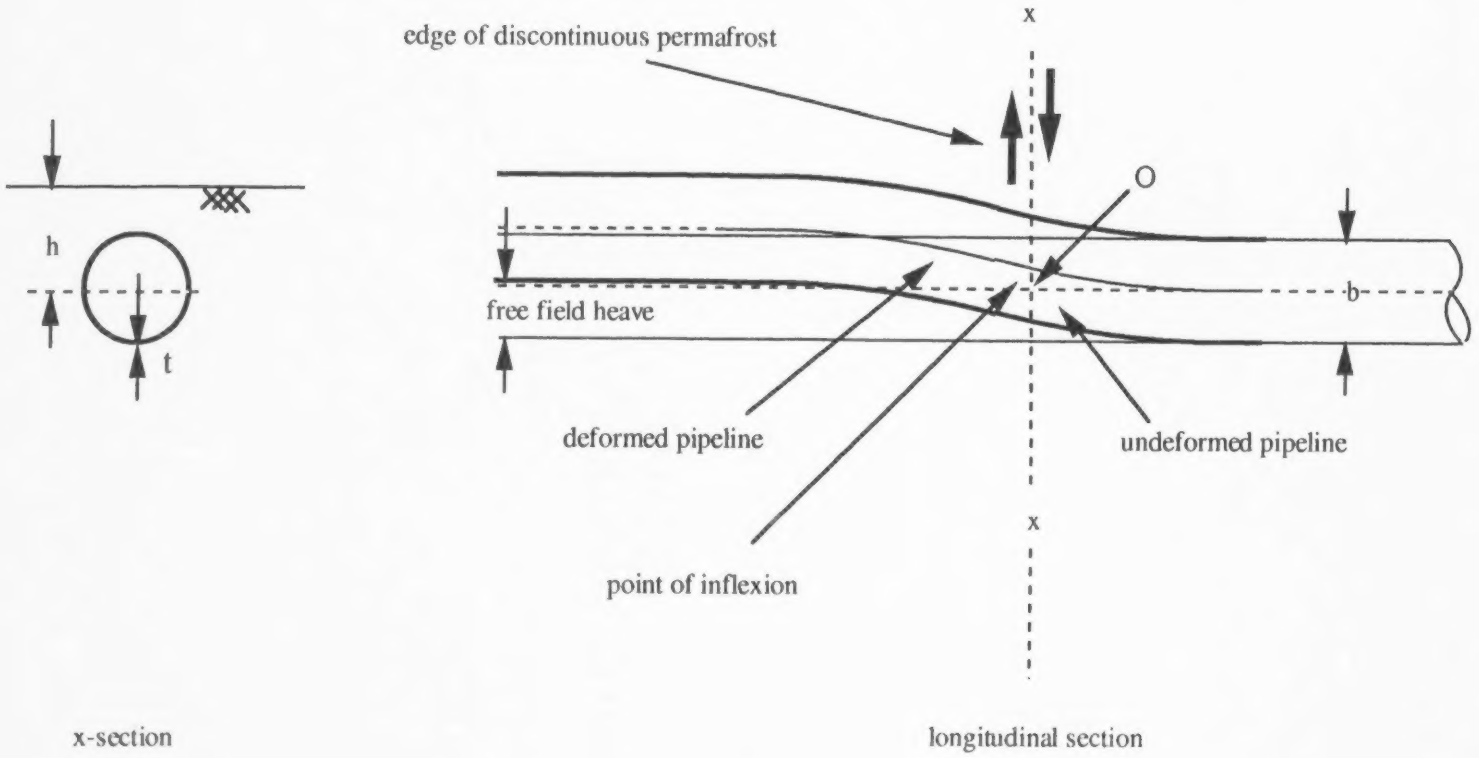
edge of discontinuous permafrost
x
O
h
t
b
free field heave
deformed pipeline
undeformed pipeline
x
point of inflexion

x-section

longitudinal section

Figure 3.3. Beam embedded in a creeping medium.

a prescribed displacement of $w_o = P\beta/2k_s'$.where $\beta^4 = k_s'/4EI$. We also note that the resulting problem is statically indeterminate.

The variational approach to determine the governing differential equation for equilibrium is adopted to establish bounded solutions. We will invoke the stationary condition for the total potential (Π), i.e. $\delta\Pi = 0$. The problem can be conveniently separated into two time frames. On initial application of the load P, i.e. @ t = 0 there will be an immediate elastic response (w_e) and this response can be determined by the usual beam on elastic foundation type solutions. Subsequent creep response (w_c) will depend on the interaction of the beam and the creeping characteristics of the foundation material. The total (accumulated) response can be estimated by the application of superposition of states which can be expressed as:

$$w(t) \approx w_e(0) + \int_0^t \dot{w}_c(t)dt \tag{3.4}$$

The above approximation defines the superposition of an elastic response, determined as if there were no creep, and a pure creep response, determined as if there were no elastic response.

The elastic response can be obtained readily from Hetenyi (1974). The total potential (Π) in rate form for the creep steady state response of the semi-infinite beam under end load P, where the beam follows the small-displacement elastic Euler-Bernoulli relation and the foundation obeys the Norton-type creep law, is given by:

[3.5] $$\Pi = \frac{1}{2}\int_0^\infty \dot{w}_c'' M dx + \frac{n}{(1+n)}\int_0^\infty q\dot{w}_c dx - P\dot{w}_c(0)$$

where $\dot{w}_c$ is the creep displacement rate at the point of application of the load, P. Upon substituting for the moment, M, according to the Euler-Bernoulli theory, i.e. $-M = EIw''$ and the medium reaction, q, from equation [3.2b], we get after integration by parts,

[3.6a] $$EI\frac{\partial^4 w_c}{\partial x^4} + \left(\frac{\dot{w}_c}{B'}\right)^{1/n} = 0$$

[3.6b] $$EIw_c'' \big|_{x=0} = 0$$

[3.6c] $$\left[EIw_c''' + P\right]\big|_{x=0} = 0$$

The governing differential equation is given by [3.6a] and the natural boundary conditions are the relations in [3.6b] and [3.6c]. We note that these natural boundary conditions correspond to the physical conditions of moment and shear equilibrium at $x = 0$. The differential equation expressed in [3.6a] is similar to that obtained by Nixon (1984). Analytical solutions for equation [3.6a] are very difficult to obtain for $n \neq 1$ and hence we have to resort to either approximate or numerical techniques. However, for a linear viscous foundation, i.e. $n = 1$, an exact solution for the equation can be found. There exists an interest in a solution for this particular case from a practical point of view. Morgenstern *et al.* (1980) have shown that frozen soil behaviour can be idealized as a linear viscous material when the temperatures are near freezing ($0^{o}C$). Moreover, the solution for a linear viscous foundation is readily comparable to solutions obtained by other approximate methods and provides insight into the general behaviour which is often obscured by other solution techniques.

Linear viscous medium i.e. $n = 1$

We obtain the following solution upon integrating equation [3.6a] with respect to time and applying the boundary conditions expressed by [3.6b] and [3.6c]:

$$[3.7] \qquad w_c = 2P\beta_c B't\, e^{-\beta_c x} \cos\beta_c x$$

where $\beta_c^4 = 1/4EIB't$. Hence, the total response can be determined as stated in [3.4] and is given by:

$$[3.8] \quad w = (2P\beta/k_s')\left[e^{-\beta x}\cos\beta x + (k_s'B't)^{3/4} e^{-\beta_c x}\cos\beta_c x\right] \quad \text{for} \quad t > 0$$

The end displacement at the point of application of the load is:

$$[3.9] \qquad w = \frac{2P\beta}{k_s'}\left[1 + (k_s'B't)^{3/4}\right]$$

In the case of a beam on an elastic foundation, the characteristic length, β, represents the relative elastic stiffnesses of the beam and foundation. The solution given by [3.7] for the creeping foundation results in an equivalent characteristic length that is an inverse function of time, t, and the creep parameter B'. This solution clearly demonstrates why the technique of solving a beam on a creeping foundation using a time-dependent k-modulus has been successful.

An approximate upper bound solution for a beam on a linear viscous foundation according to the Rayleigh-Ritz method described later is:

[3.10] $$w = \frac{2P\beta}{k_s'}\left[8 - 7e^{-k_s'B't/6}\right]$$

The reason why a separate solution has to be sought when n = 1 will be discussed when dealing with the Raleigh-Ritz method of analysis. A lower bound solution for a beam on a linear viscous foundation obtained based on Martin's inequality described later is given by:

[3.11] $$w = \frac{2P\beta}{k_s'}\left[1 + 3k_s'B't/7\right]$$

The total response as expressed by [3.8] clearly shows that the initial static response sets up a stationary stress wave along the beam-foundation system and the subsequent creep response sets up another stress wave that is of similar shape to that of the elastic response. Furthermore, the creep stress response is modified by the so-called reduced k-modulus and propagates with time towards the semi-infinite end. Though this argument has been demonstrated for linear viscous foundations, similar effects will be present for foundations with $n \neq 1$. These findings are in complete accordance qualitatively with field experimental results of a buried chilled pipeline facility at Caen, France as reported by Dallimore and Crawford

(1984).

Creeping medium i.e. $n \neq 1$

As stated before, for a creeping foundation, direct solution of the differential equations becomes almost impossible for $n \neq 1$. Consequently, we have to resort to approximate techniques where we can obtain reasonable estimates and bounds. In this chapter, we will approach the problem using two methods that guarantee upper and lower bounds. The two methods are essentially based on the minimization of the total potential Π , the first approach being the Rayleigh-Ritz method and the second approach is based on the application of Martin's inequality.

Upper bound: Rayleigh-Ritz

The theorem of minimum potential energy dissipation states that, for the particular case of a beam on a creeping foundation, amongst all kinematically admissible curvatures (κ^k) and displacement rates ($\dot{w}^k$), the actual curvatures and displacement rates minimize the functional Π of [3.5]:

$$\Pi\left(\kappa^k, \dot{w}^k\right) = \int_0^{\infty} \left[EI\kappa^k \dot{\kappa}^k + \frac{n}{(1+n)} \left(\frac{\dot{w}^k}{B'} \right)^{1/n} \dot{w} \right] dx \tag{3.12}$$

Since κ^k, $\dot{w}^k$ must be kinematically admissible, they must satisfy the natural boundary conditions obtained in [3.6]. An obvious choice for $\dot{w}^k$ that satisfies the required boundary conditions is that which corresponds to the spatial elastic solution. Hence, we assume for $\dot{w}^k$:

[3.13] $$w(x,t) = u(t)w_e(x)$$

In the above assumed solution, u(t) is the function that depends on time. We also note that this assumed solution is also in accordance with the correspondence principle or Hoff's elastic analogy. Substituting [3.13] in [3.12] and carrying out the minimization with respect to displacement rate, $\dot{u}$, we obtain:

[3.14] $$u(t) = \frac{2P\beta}{k'_s}\left[8 - 7\left(1 + rk'_sB'(P\beta)^{n-1}t\right)^{1/(1-n)}\right]$$

where $$r = \frac{0.875^{n-1}(n-1)}{16J_1^n}$$ and $$J_1 = \int_0^\infty (e^{-z}\cos z)^{1+1/n}\,dz$$

Equation [3.14] identifies the dimensionless time as $rk'_sB'(P\beta)^{n-1}t$ and we shall see that it appears recurrently in the rest of the analysis. Once again, the static response has been factored out in order to isolate the displacement amplification due to creep alone. The J_1 integral can be evaluated for particular values of n and sample values are given in Table 3.2. The J_2 integral given in Table 3.2 is defined after equation [3.24].

Equation [3.14] breaks down for the particular case when n = 1 and it is necessary to obtain a particular solution [3.9], but the procedure remains the same. It is to be expected that the solution will deteriorate with increasing values of n as equilibrium will be steadily violated. The

Table 3.2. J integrals for particular values of n.

Creep exponent, n	J_1 integral	J_2 integral
1	0.375000	0.375000
3	0.538126	0.209375
5	0.595879	0.146635
7	0.625020	0.113014

Rayleigh-Ritz procedure together with a series solution as proposed by Heteyni (1974) for beams on elastic foundations could lead to an improvement in the accuracy of the solution. However, to do so analytically would be somewhat involved algebraically. An added advantage of this modified procedure lies in cases of beams of variable cross section EI or in which a non-linear moment curvature relation exists.

Lower bound: Martin's inequality

In general terms, Martin's inequality (Boyle and Spence, 1983) for the power creep law can be stated as:

$$\frac{n}{n+1}\int_V \sigma_B \dot{\varepsilon}_B dV + \frac{1}{n+1}\int_V \sigma_A \dot{\varepsilon}_A dV \geq \int_V \sigma_A \dot{\varepsilon}_B dV \qquad [3.15]$$

where we identify σ_B, $\dot{\varepsilon}_B$ with the actual solution σ, $\dot{\varepsilon}$ and σ_A, $\dot{\varepsilon}_A$ with statically admissible surface tractions along the beam-foundation interface. Martin's inequality derivation is based on a postulate for material stability formulated by Drucker (1951) which in turn ensures that the constitutive relation is monotonic i.e. the increase in stress causes an increase in strain rate. A geometrical interpretation of [3.15] can be deduced from Figure 3.4. The first and second terms of [3.12] correspond to strain and complementary energy dissipations in the areas represented by the polygons JMKOL and JNMOL respectively. It then becomes obvious why the inequality holds true for any monotonic functional relation. In our particular beam-foundation system, the beam is assumed to behave entirely elastically and only the foundation is composed of the creeping material. Rewriting [3.15] in terms of the moments and curvature rates and taking into account the two different components of the system, we have:

$$[3.16] \qquad \frac{1}{2}\int_0^\infty \dot{w}''_B M_B dx + \frac{1}{2}\int_0^\infty \dot{w}''_A M_A dx + \frac{1}{(n+1)}\int_0^\infty q_A \dot{w}_A dx + \frac{n}{(n+1)}\int_0^\infty q_B \dot{w}_B dx \geq \int_0^\infty \dot{w}''_B M_A dx + \int_0^\infty \dot{w}_B q_A dx$$

where $\dot{w}$, $\dot{w}''$, M, q, refer to transverse displacement, curvature, moment and foundation reaction respectively. Upon substituting for $\dot{w}$ using the creep material relation defined by [3.2] and M by the Euler-Bernoulli moment curvature relation and if we let the B state correspond to the true solution (without subscript), we obtain:

$$[3.17] \qquad \frac{1}{2}\int_0^\infty \dot{w}'' M dx + \frac{1}{2}\int_0^\infty \frac{\dot{M}_A M_A}{EI} dx + \frac{B'}{(n+1)}\int_0^\infty q_A^{n+1} dx + \frac{nB'}{(n+1)}\int_0^\infty q^{n+1} dx \geq \int_0^\infty \dot{w}'' M_A dx + \int_0^\infty \dot{w} q_A dx$$

Integrating the first term on the right and left hand sides of inequality

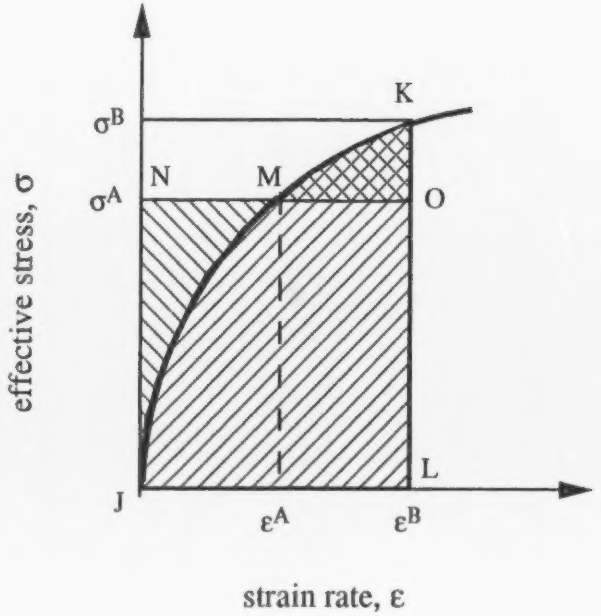
K
σ^B
N
M
σ^A
O
effective stress, σ
J
L
ε^A
ε^B
strain rate, ε

Figure 3.4. Geometrical interpretation of Martin's inequality.

[3.16] by parts twice and after rearranging terms, we obtain:

$$\frac{1}{2}\dot{w}'M\Big|_0^{\infty} - \frac{1}{2}\dot{w}\frac{dM}{dx}\Big|_0^{\infty} + \dot{w}\frac{dM_A}{dx}\Big|_0^{\infty} - \dot{w}'M_A\Big|_0^{\infty} + \int_0^{\infty}\left(-\frac{d^2M_A}{dx^2} + \frac{1}{2}\frac{d^2M}{dx^2} - q_A + \frac{n}{(n+1)}q\right)\dot{w}dx \geq -\frac{1}{2}\int_0^{\infty}\frac{\dot{M}_A M_A}{EI}dx - \frac{B'}{(n+1)}\int_0^{\infty} q_A^{n+1}dx \qquad [3.18]$$

The essential boundary conditions are given by the first two terms on the *lhs* of the inequality and the natural boundary conditions are given by the following two terms. We have not imposed any conditions on M_A or q_A except that they be statically admissible. One must find adequate functions of M_A and q_A that satisfy the integral on the *lhs* of the inequality [3.18]. We then select a function for q and M on the basis of elastic beam foundation systems that will ensure that M_A and q_A satisfy the stated boundary conditions. Two governing differential equations can be set from the integral on the *lhs* of the inequality. They are:

$$\frac{d^2M_A}{dx^2} + \frac{n}{(n+1)}q = 0 \qquad [3.19a]$$

$$\frac{1}{2}\frac{d^2M}{dx^2} - q_A = 0 \qquad [3.19b]$$

The true static elastic foundation reaction set up is given by:

$$q = -4P\beta e^{-\beta x}\cos\beta x \qquad [3.20]$$

On substitution in equation [3.19a] and integrating once we find that the shear at $x = 0$ is given by:

$$S = -\frac{2nP}{(1+n)} \tag{3.21}$$

We note that the natural boundary condition is satisfied when $n = 1$ and deteriorates on increasing n value. Hence, we should expect that the solution will be poor for high values of n. A further integration of [3.19a] leads to an expression for M_A:

$$M_A = \frac{2n}{(n+1)}\frac{P}{\beta}e^{-\beta x}\sin\beta x \tag{3.22}$$

The expression for M_A satisfies the natural boundary conditions stated earlier. Recognizing that $d^2M/dx^2 - q = 0$ from beam theory, we can subsequently obtain an expression for q_A:

$$q_A = -2P\beta e^{-\beta x}\cos\beta x \tag{3.23}$$

Following substitution of expressions for M_A and q_A in the *rhs* of the inequality and upon application of the correspondence principle as stated in [3.12], we obtain after integration:

$$u(t) \geq \frac{(-1)^{n+1}2^{n+1}(n+1)}{(n^2+4n+2)}J_2B'k_s't(P\beta)^{n-1} \tag{3.24}$$

where $J_2 = \int_0^\infty (e^{-z}\cos z)^{n+1}dz$. J_2 has been tabulated for different values of n in Table 3.2. Once again we note the recurrent dimensionless time parameter in [3.24]. A much improved solution is obtained if the corrected shear as stated in [3.21] is used. The corresponding solution is given by:

$$u(t) \geq \frac{(-1)^{n+1} 2^{n+1} (n+1)}{(4n^2 + 4n - 1)} J_2 B' k_s' t (P\beta)^{n-1} \tag{3.25}$$

Nonetheless, it should be emphasized that the solution should deteriorate for large values of n but, as we shall see later that for the range of values of n that we are concerned with, a good approximate solution is obtained.

Finite elements

While the above solutions provide insight into the behaviour and understanding of the system, they do limit the analysis to ideal situations, i.e. homogeneous medium. In the last three decades the finite element method has proved immensely useful in solving problems previously intractable by analytical or approximate means. The solution of beams on non-linear foundations is now routinely carried out using available finite element codes. Adina (1984) is one code that has incorporated within it a truss element with the Norton-Bailey creep law. However, the characterization, (i.e., spacing of springs, cross section area, length, etc) of the truss springs has to be done with care so that equivalence is maintained between the beam on a continuous creeping foundation and the beam on a discretized foundation.

It is natural to expect that, as the spacing of the discretized truss springs becomes small, the resulting approximation will be accurate. In a practical situation we wish to get away with as few truss springs as possible. Boresi *et al.* (1978) has shown that spacing, s, of truss springs can be estimated by:

[3.26] $$s = \pi / 4\beta$$

We note that although the above criterion is developed for a beam on an elastic foundation, we observe from the development of the solution for a beam on a linear viscous foundation that the characteristic length β_c is essentially the same as β except that the effective foundation modulus is time dependent (inverse relation). Consequently, for the steady state solution, if necessary, the spacing (s) could be steadily increased with time and thus the spacing of the springs guided by [3.26] is more than adequate for the complete analysis.

The material characteristic of the truss spring has to be adequately represented for the elastic response as well as the creep response. Hence, if we arbitrarily fix the length of the springs to say, L, then conflicting definitions of cross-sectional areas arise in attempting to satisfy both responses. A plausible way to remedy this situation is to first satisfy the requirements of creep response and then redefine the elastic modulus of the spring. In order that the spring represents adequately the creep response, the rate of work done by the spring should be equal to that done by the continuous creeping medium, i.e.,

[3.27] $$(Q\dot{w})_{\text{spring}} = (bqs\dot{w})_{\text{creeping foundation}}$$

where Q and q are the axial and foundation reactions in the spring and continuous medium respectively. If the material properties of both the spring and the continuous foundation are defined as in [3.1] and [3.2], then on substitution in [3.27] we obtain the cross section area of the spring, A_{spring} as:

$$A_{spring} = bs\left(2L/bI_f\right)^{1/n} \qquad [3.28]$$

Subsequently, the elastic modulus of the springs, E_{spring}, has to be:

$$E_{spring} = sLk_s'/A_{spring} \qquad [3.29]$$

The above characterization of creep springs is independent of the particular geometry and loading of the beam-foundation system. A pertinent question that may be posed is how long should the beam-foundation system be so as to simulate a semi-infinite condition. Den Hartog (1952) has provided an elegant argument for this problem that essentially concludes that if $\beta X \geq 4$ (where X is the length of beam-foundation system) then the beam-system can be treated as a semi-infinite beam. Since we are dealing with a non-linear viscous creeping foundation the corresponding creep characteristic length should be used, i.e.:

$$X^{creep}_{semi-infinite} \geq 4\sqrt[4]{4EIB't(P\beta)^{n-1}} \qquad [3.30]$$

We note from the above that length ($X^{creep}_{semi-infinite}$) of the beam-foundation system extends with time and should be added to the length obtained for elastic response. Hence, provision should be made at the outset for the time span of the analysis so that adequate length of the beam-foundation system is always ensured.

Various techniques have been proposed for carrying out time integration for solving creep problems. An implicit time integration, α-method, was used in the analysis, as explained by Bathe (1982). When $\alpha = 0$ the method reduces to the Euler forward method and when $\alpha > 0$ it is the implicit method. One particular advantage of the implicit time integration scheme is that the method is unconditionally stable for $\alpha > 1/2$ for any time step size, though it may not necessarily converge to the correct solution.

Comparison between the different solutions

As indicated before through the approximate analyses, the non-dimensional time factor, $\bar{t}$, $(= k_s' B' (P\beta)^{n-1} t)$ has been identified and conveniently provides a basis for adequate comparisons between the different methods. It has become customary to evaluate the response for the types of problems considered in this chapter to either measures of the displacement or displacement rates and here we use the former measure since both features can be readily appreciated from a single plot. Figure 3.5 shows the comparison between all the methods discussed in this chapter for a linear viscous foundation creeping material. The approximate upper and lower bounds provide reasonably good estimates if we compare them to the available exact solution. The finite element solution is comparably close to the exact solution and could be improved with finer discretization and using smaller time steps in the time integration procedure. Figures 3.6, 3.7, and 3.8 show displacement-time histories for Raleigh-Ritz, Martin's inequality and finite element solutions respectively for varying values of n. The solutions as obtained using the Raleigh-Ritz and the finite element methods clearly show the role of statical creep indicated earlier. Also, these methods reveal an interesting phenomenon that there exists a particular non-dimensional time when the response is independent of the creep exponent n. As expected this effect is masked when a lower bound solution is obtained using Martin's inequality. If we compare the steady state responses in terms of displacement rates then the comparison is good. Similarly, Figures 3.9 - 3.11 show the same previous responses except that each solution is compared to each other for particular n values of 3, 5 and 7 respectively. The solution obtained using Martin's inequality is insensitive to $n < 5$ but diverges for $n > 5$ and thus no longer represents a lower bound. This is to be expected as discussed earlier since one of the natural boundary conditions (end shear) is increasingly violated for increasing n values. If, on the other hand, the response is measured in terms of steady state (displacement rates) then all the approximate methods compare well.

Conclusions

The various solutions have highlighted the role of the different parameters in the total response of a beam embedded in a creeping foundation. Simplified analytical upper and lower bounds for a beam in a creeping foundation subjected to an end load have been developed. A simple finite element modelling procedure has been outlined that facilitates the general solution for this type of problems if a truss spring with

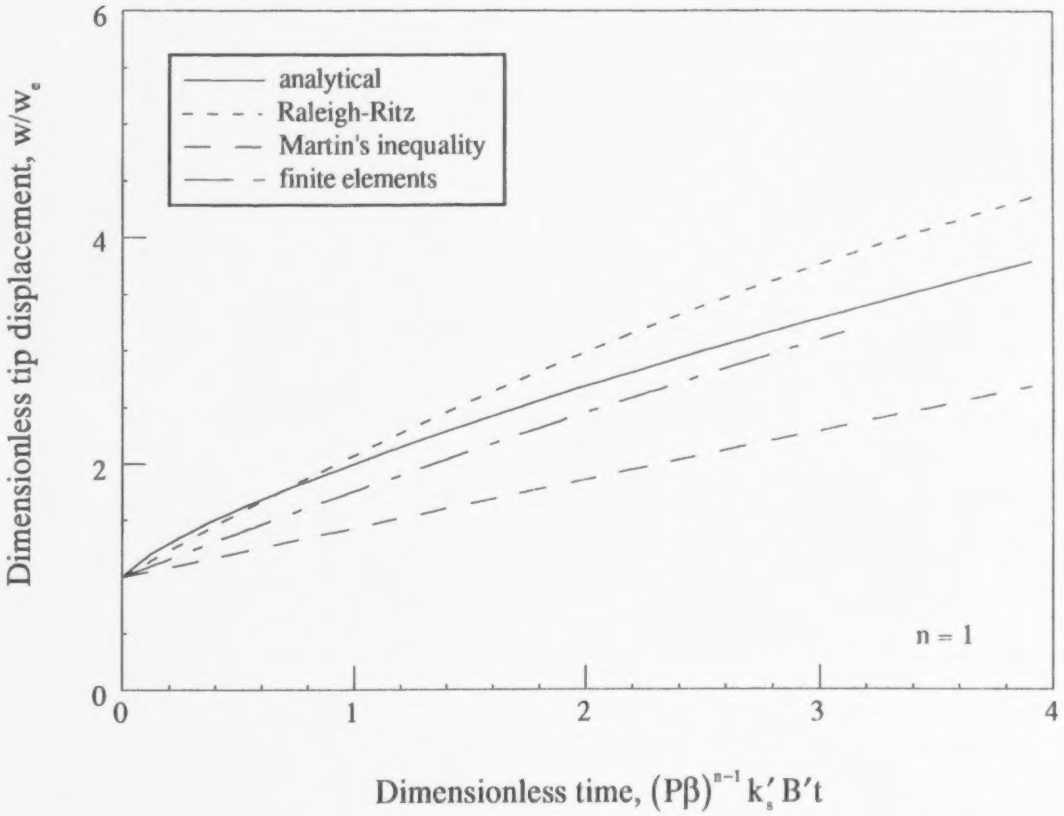

Figure 3.5. Tip displacement vs time for a semi-infinite beam on linear viscous creeping foundation - comparison of different methods.

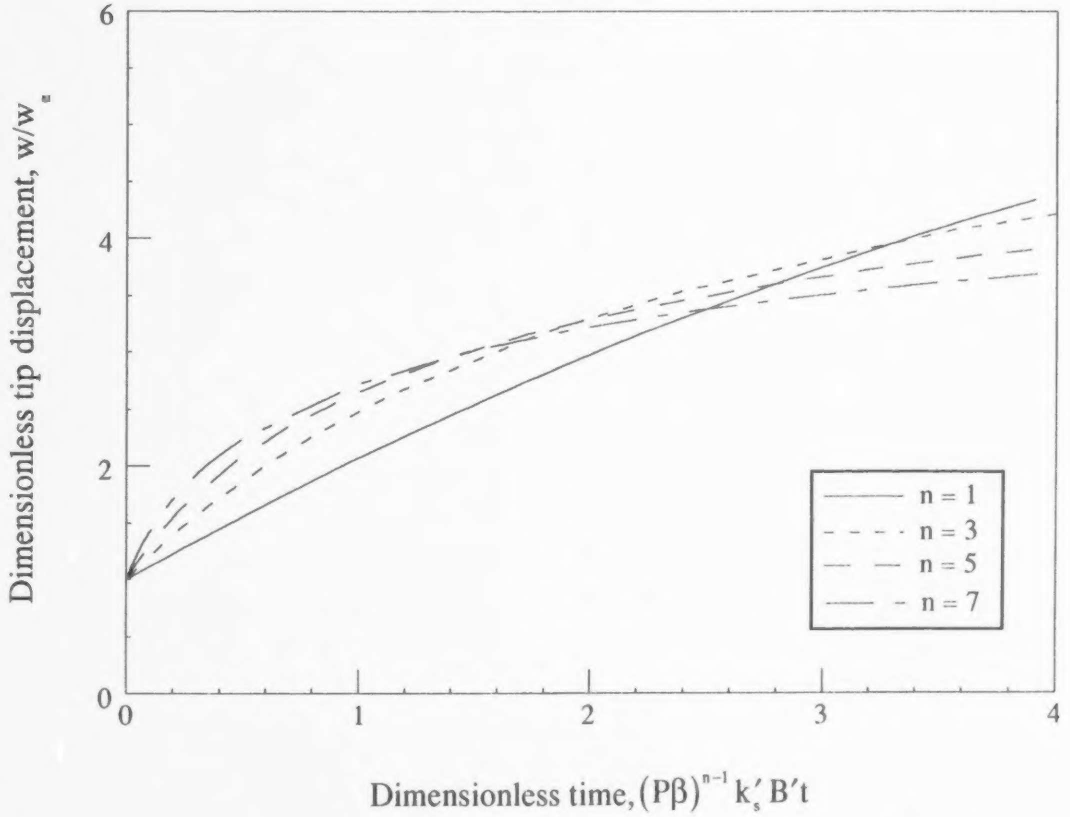

Figure 3.6. Tip displacement vs time for a semi-infinite beam on a non-linear creeping foundation - Raleigh-Ritz.

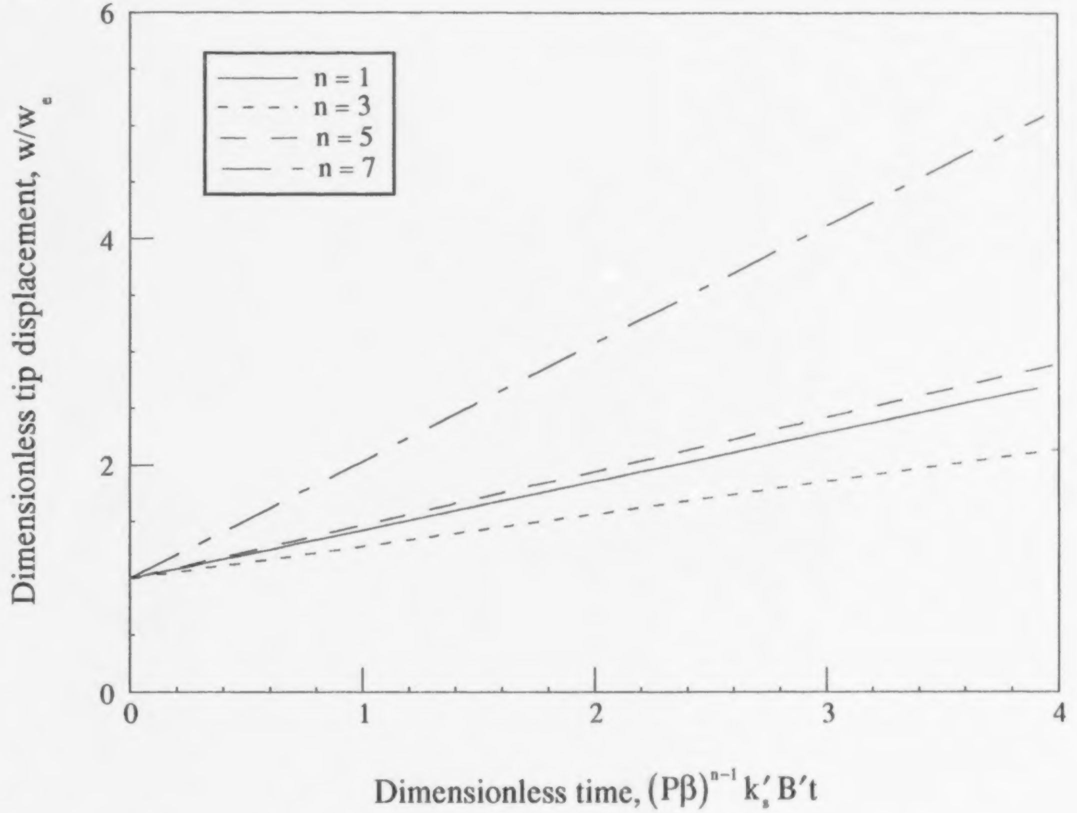

Figure 3.7. Tip displacement vs time for a semi-infinite beam on a non-linear creeping foundation - Martin's inequality.

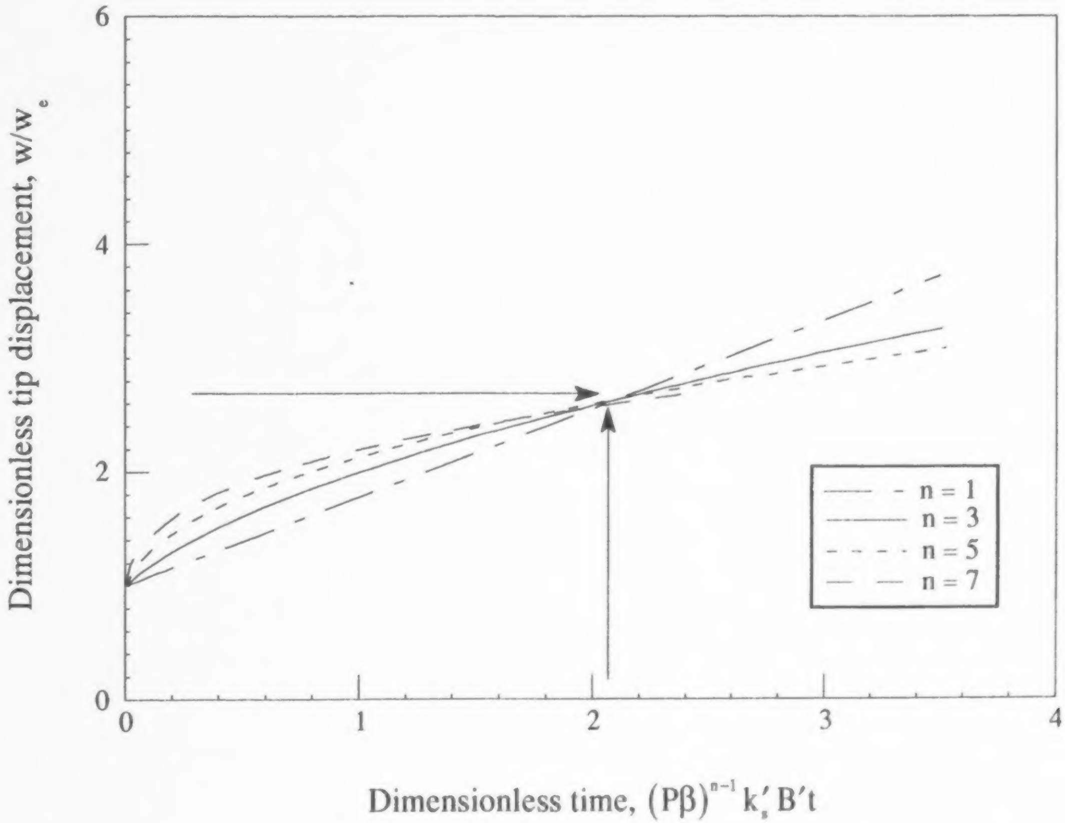

Figure 3.8. Tip displacement vs time for a semi-infinite beam on a non-linear creeping foundation - finite elements.

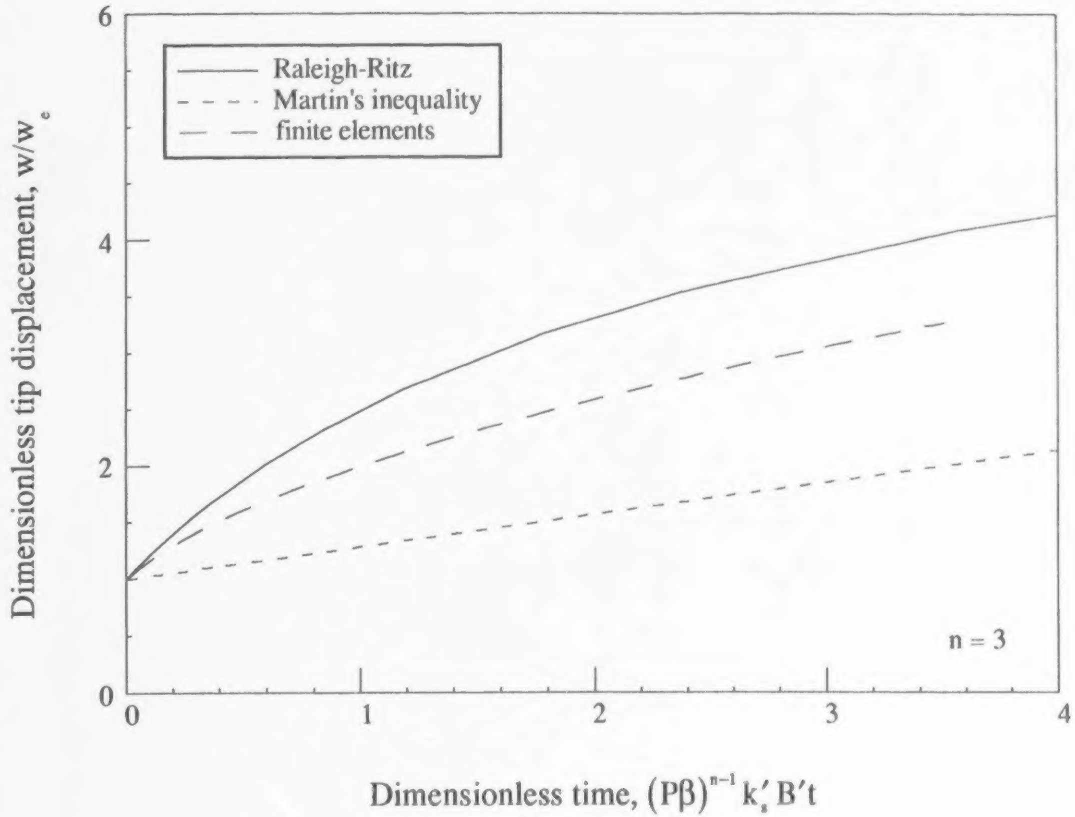

Figure 3.9. Tip displacement vs time for a semi-infinite beam on a non-linear (n = 3) creeping foundation - comparison of different methods.

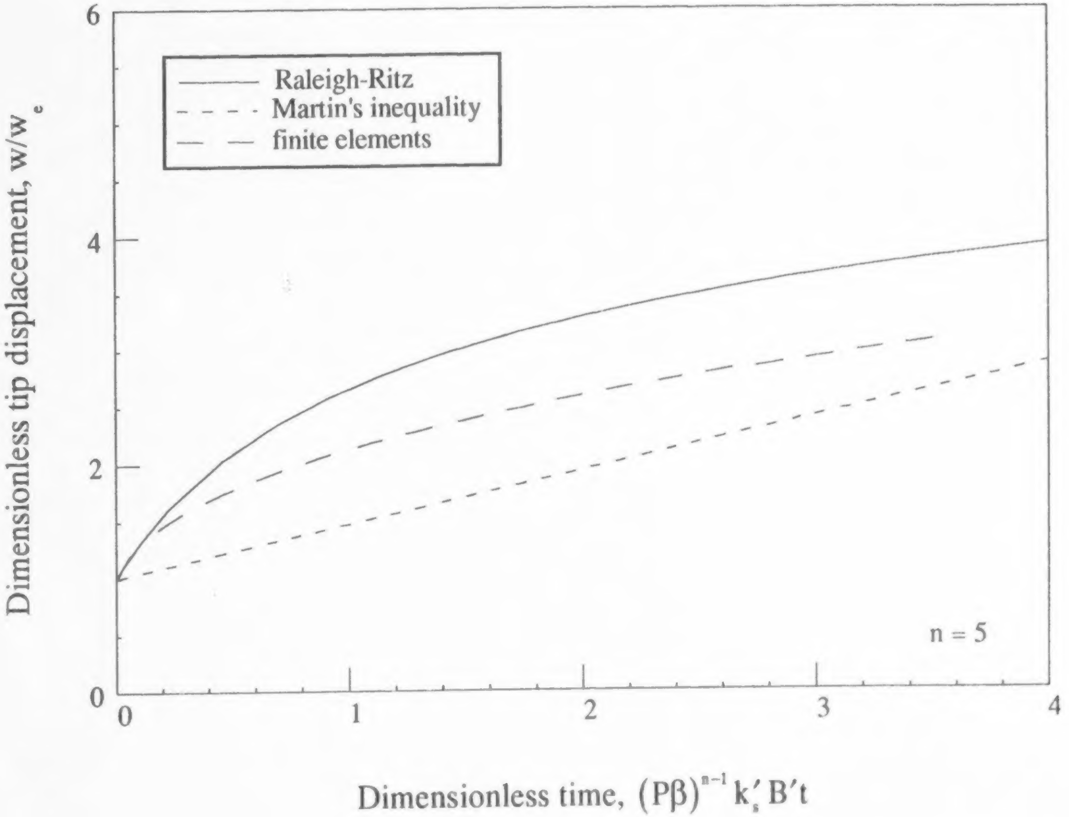

Figure 3.10. Tip displacement vs time for a semi-infinite beam on a non-linear ($n = 5$) creeping foundation - comparison of different methods.

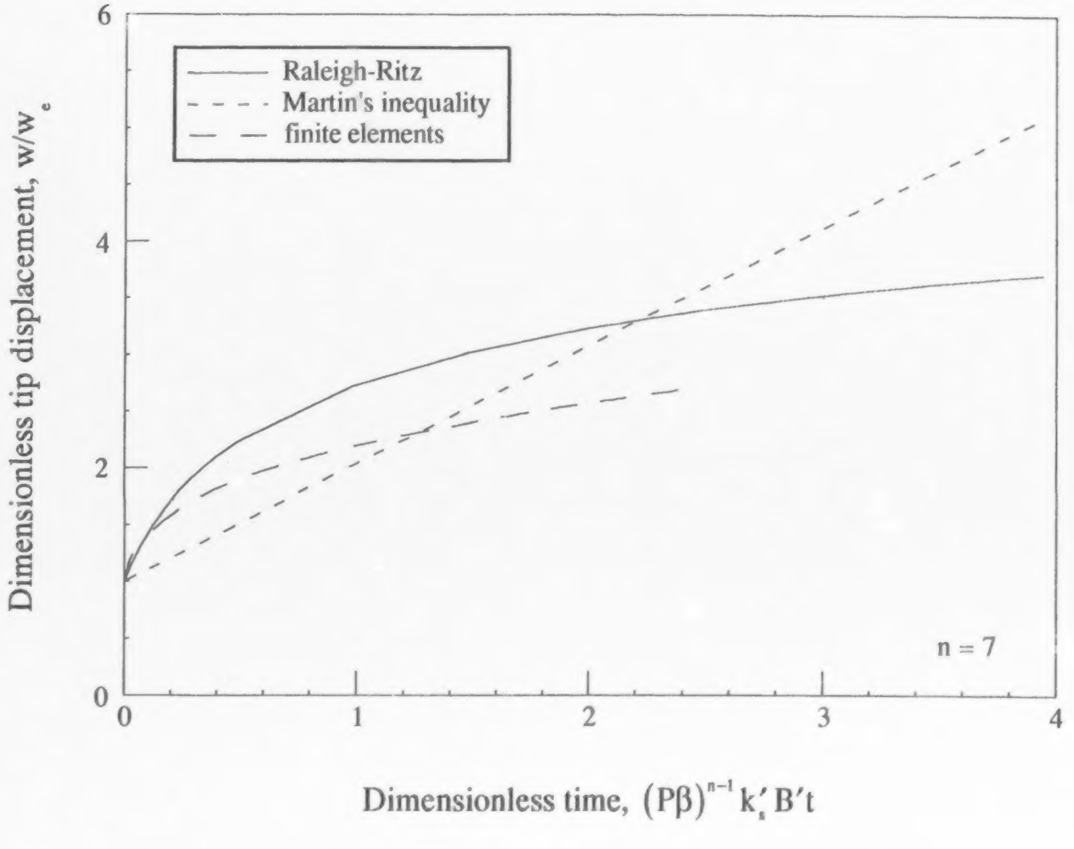

Figure 3.11. Tip displacement vs time for a semi-infinite beam on a non-linear (n = 7) creeping foundation - comparison of different methods.

Norton's creep law is available in a general finite element code. The finite element analysis confirms the bounds established using variational principles. While the upper bound established using the Raleigh-Ritz approach exhibits all the basic characteristics shown to exist by the finite element method, the lower bound estimates are poor because of the inability of the selected functions to satisfy the natural boundary conditions for all values of the creep exponent n. Nonetheless, the analytical solutions developed here remain upper and lower bounds as long as $n \leq 5$. All the results have been obtained in non-dimensional form which permits rapid evaluation for design purposes.

In the previous chapter we have demonstrated how the bearing capacity factor, N_c can be adjusted to account for finite shallow burial. Through [3.3] we have shown how the indentation factor I_n tends towards the Prandtl bearing capacity factor, N_c, for large values of n. Consequently, the indentation factor I_n can be similarly adjusted to account for shallow burial of pipelines.

The solutions permit the rapid evaluation of the amplification of the elastic response of a beam embedded in a creeping foundation. In order to obtain an accurate creep response it is equally important to obtain a proper estimate of the elastic response. The application of the above solutions for pipelines and laterally loaded piles will be treated in a subsequent publication.

References

Adina - A finite element program for automatic dynamic incremental nonlinear analysis. 1987. Report AE 84-1, ADINA R&D, Inc., Boston, MA.

American Society of Civil Engineers. 1978. An overview of the Alaska highway gas pipeline: The world's largest project. National Convention of the American Society of Civil Engineers in Pittsburg, Penn. vi + 130p.

Bathe, K.J. 1982. Finite element procedures in engineering analysis. Prentice-Hall, New Jersey. xiii + 735p.

Boresi, A.P., Sidebottom, O.M., Seely, F.B., and Smith, J. O. 1978. Advanced mechanics of materials. 3rd edition. John Wiley & Sons, New York.

Boyle, J. T. and Spence, J. 1983. Stress analysis for creep. Butterworths, London. vii + 283p.

Dallimore, S.R. and Crawford, H. 1985. Experimental observations of differential heaving and thaw settlement around a chilled pipeline In Pipelines and frost heave. Proceedings of a seminar held at Centre de Geomorphologie, Caen, France. pp. 75 + v.

Den Hartog, J.P. 1952. Advanced strength of materials. McGraw Hill Book

Co., New York. ix + 379p.

Drucker, D.C. 1952. A more fundamental approach to plastic stress-strain relations. Proceedings, 1st U.S. National Congress on Applied Mechanics, ASME, New York. p. 487.

Flügge, W. 1975. Viscoelasticity. Springer-Verlag, Berlin. vii + 194p.

Foriero, A. and Ladanyi, B. 1989. A streamline solution for laterally loaded piles in permafrost. Canadian Geotechnical Journal, **26**(4): 568-574.

Foriero, A. and Ladanyi, B. 1990. Finite element simulation of behaviour of laterally loaded piles in permafrost. ASCE Journal of Geotechnical EngineeringDivision, **116**(2): 266-284.

Glen, J.W. 1955. The flow law of polycrystalline ice. Proceedings of the Royal Society, London, **228A**: 519-538.

Hetenyi , M. 1974. Beams on elastic foundation. University of Michigan Press, Ann Arbor. ix + 255p.

Hoff, N.J. 1954. Approximate analysis of structures in the presence of moderately large creep deformation. Quarterly of Applied Mathematics, **12**: 49-55.

Konrad, J.-M. and Morgenstern, N. 1982. Effects of applied pressure on freezing soils. Canadian Geotechnical Journal, **19**: 494-505.

Konrad, J.-M. and Morgenstern, N. 1984. Frost heave of chilled pipelines buried in unfrozen soils. Canadian Geotechnical Journal, **21**: 100-115.

Konrad, J.-M. and Morgenstern, N. 1983. Frost susceptibility of soils in terms of their segregation potential. Proceedings, Permafrost: Fourth International Conference, Fairbanks, National Academy Science, Washington, pp. 660-665.

Ladanyi, B. 1972. An engineering theory of creep of frozen soils. Canadian Geotechnical Journal, **9**: 63-80.

Ladanyi, B. 1973. Design procedure for laterally loaded piles at Dawson City. Report of Investigation for Mackenzie Valley Pipe Line Research, Ltd., Calgary, Alberta.

Ladanyi, B. 1975. Bearing capacity of strip footings in frozen soils. Canadian Geotechnical Journal, **12**: 393-407.

Ladanyi, B. 1983. Shallow foundations on frozen soil: creep settlement. ASCE Journal of Geotechnical Engineering Division, **109**(11): 1434-1448.

Ladanyi, B. and Lemaire, G. 1984. Behaviour of buried pipeline under differential frost heave conditions. Proceedings of Cold Regions Engineering Speciality Conference. Canadian Society of Civil

Engineering. Montreal. pp. 161-176.

McRoberts, E.C., Law, T. and Murray, T. 1978. Creep testing on undisturbed ice-rich silt. Proceedings of the Third International Permafrost Conference. Edmonton. pp. 539-545.

Morgenstern, N.R., Roggensack, W.D. and Weaver, J.S. 1980. The behaviour of friction piles in ice and ice-rich soils. Canadian Geotechnical Journal, **17**: 405-415.

Nixon, J.F. 1978. First Canadian Geotechnical Colloquium:Foundation design approaches in permafrost areas. Canadian Geotechnical Journal, **15**: 96-112.

Nixon, J., Ellwood, J. and Slusarchuk, W. 1981. In-situ frost heave testing using cold plates. Proceedings of the Fourth Canadian Permafrost Conference. Calgary, NRCC No. 20124. Section 7.

Nixon, J.F., Morgenstern, N.R. and Ressor, S.N. 1983. Frost heave-pipeline interaction using continuum mechanics. Canadian Geotechnical Journal, **20**: 251-261.

Nixon, J.F. 1984. Laterally loaded piles in permafrost. Canadian Geotechnical Journal, **21**(3):431-438.

Penner, E. and Ueda, T. 1978. A soil frost susceptibility test and a basis for interpreting heaving rates. Proceedings of the Third International

Permafrost Conference. Edmonton. pp. 722-727.

Rowley, R.K., Watson, G.H. and Ladanyi, B. 1973. Vertical and lateral pile load test in permafrost. Proceedings, Second International Conference of Permafrost, Yakutsk, North American Contribution. pp. 712-721.

Rowley, R.K., Watson, G.H. and Ladanyi, B. 1975. Prediction of pile performance in permafrost under lateral load. Canadian Geotechnical Journal, **12**: 510-523.

Sayles, F.H. and Haines, D. 1974. Creep of frozen silt and clay. U.S, Army Cold Regions Research and Engineering Laboratory, Hanover, NH. Technical report 252. 50p.

Sego, D.C. and Morgenstern, N. 1983. Deformation of ice under low stresses. Canadian Geotechnical Journal, **20**(4): 587-602.

Sego, D.C. and Morgenstern, N. 1983. Punch indentation of polycrystalline ice. Canadian Geotechnical Journal, **22**(2): 226-233.

Selvadurai, A.P.S. 1988. Mechanics of soil-pipeline interaction. Proceedings of the Annual Conference of The Canadian Society for Civil Engineering, Calgary, **3**: 151-173.

Nomenclature

The following symbols are used in this chapter:

A_{spring} = x-sectional area for discretized foundation spring

b = beam width, pipeline or pile diameter

B = creep proportionality constant

B' = creep foundation compliance for plane strain

c = cohesion

E = beam elastic modulus

E_s = soil elastic modulus

E_{spring} = elastic modulus for discretized foundation spring

h = embedment depth

I = beam moment of inertia

I_f = creep influence factor

I_n = creep indentation factor

J_1, J_2 = integrals dependent on creep exponent n

k_s' = foundation subgrade modulus

L = length of discretized foundation spring

M = bending moment

p = reaction intensity pressure

P = non-dimensional load parameter

n = creep exponent in Norton relation

N_c = Prandtl bearing capacity factor

q = reaction per unit length

Q = axial force in discretized foundation spring

s = discrete spring spacing

S = shear

$\bar{t}$ = non-dimensional time parameter

$u, \dot{u}$ = displacement and displacement rates time dependent functions

$w_c, \dot{w}_c$ = creep displacement and displacement rates

w_e = elastic displacement

$\dot{w}$ = accumulated transverse displacement

w = transverse displacement in the z-direction

$\overline{w}$ = non-dimensional displacement parameter

x = longitudinal coordinate axis

$X^{\text{creep}}_{\text{semi-infinite}}$ = additional length of beam-foundation system for discretization during creep

z = axis normal to x-axis

α = implicit integration parameter

β, β_c = elastic and linear viscous characteristic lengths

$\dot{\varepsilon}_o$ = proof strain rate

γ = soil weight density

Π = total potential

ν_s = soil Poisson's ratio

σ, σ_o = stress and proof stress

σ_y = yield stress of surrounding medium

Chapter 4

LATERAL LOADS ON PILES AND UPLIFT OF PIPELINES IN PERMAFROST[1]

Introduction

The first significant interest in understanding the behaviour of laterally loaded piles in frozen soil evolved on the initiation of the construction of the Alyeska oil pipeline in 1975. As the pipeline expands or contracts due to temperature changes, important lateral movements of the pipeline occur which impose lateral loads on the piles supporting the elevated pipeline. The interest in laterally loaded piles has continued as additional development in frozen terrain has taken place.

The proposal for a chilled gas pipeline to carry gas from the Northern Canadian frontier regions has been under discussion since the late 1970's. During the design stage, when the first preliminary studies were carried out, it was identified that the pipeline would be subjected to significant differential frost heave and thus inducing high stresses when it crossed regions of discontinuous permafrost. The mechanism of frost heave for different soil types is fairly well understood now to enable a reasonable prediction of frost heave rate.

---

[1] A version of this chapter has been submitted for publication to The Canadian Geotechnical Journal: Rajani, B. and Morgenstern, N., 1991. Lateral loads on piles and uplift of pipelines in permafrost.

From the analysis and behavioural viewpoint, striking similarities exist between the two above-mentioned structures. It is well known that the behaviour of lateral piles is largely governed by the restraint offered by the uppermost portion of the surrounding medium. The shallow burial of pipelines in a stiff creeping medium is similar to the pile problem except that the piles are oriented vertically as opposed to pipelines which are horizontal. Another important difference between the two structures lies in the nature of the loading process: the pipeline is subjected to imposed displacements while the piles are usually subjected to imposed loads.

In anticipation of the construction of arctic pipelines and a few years prior to the construction of the Alyeska oil pipeline, a major field study was carried out in order to understand the behaviour of laterally loaded piles in frozen soil as reported by Rowley *et al.* (1973, 1975). Pile lateral load tests were performed on two timber and three steel tubular piles. Creep soil properties for the surrounding clayey silt were determined at the site using pressuremeters. In fact till now, no other comprehensive test data exist except for an incomplete load test data given by Domaschuk *et al.* (1988). Nixon (1984) performed laboratory pile load tests on solid model steel piles embedded in pure ice. Recently Foriero and Ladanyi (1991) have reported tests on model piles embedded in frozen sand. The relevant data for all four sets of pile load tests are summarized in Table 4.1.

Table 4.1. Details on laterally loaded pile tests.

Reference	pile type	pile size L (m)	 b (m)	 e (m)	soil type	loading details
Rowley *et al.* (1973, 1975)	2 timber piles	2.67	0.28	0.61	clayey silt	lateral loads varying from 22 to 156 kN.
		2.70	0.261	0.51		
	3 steel pipe piles	2.62	0.274	0.53		
		2.45	0.274	0.37		
		2.45	0.274	0.42		
Nixon (1984)	3 solid model steel piles	0.203	0.0127	0.0754	ice	lateral loads varying from 0.177 to 0.376 kN.
Domaschuk *et al.* (1988)	square steel tube pile	1.80	0.15	0.10	sand	lateral loads varying from 35 to 120 kN.
Foriero and Ladanyi (1991).	aluminum tube and steel rod	0.437	0.022 and 0.021	0.203	sand	lateral loads varying from 157 to 942 N.

L = length of pile below ground level; b = diameter/width of pile;
e = height of load application above ground level

In the early 1980's, plans were made to set up a controlled experimental facility to study pipeline-frozen soil interaction. This resulted in an experimental set-up at Caen, France that closely mimics anticipated field conditions and provides a wealth of experimental data. The details of the experimental data are available through numerous reports (Dallimore and Crawford, 1985; Geotechnical Sciences Laboratories, 1986, 1988, 1989).

The field case studies briefly described above provide an opportunity to validate any proposed solution strategy. In this chapter, we make use of a model (chapter 3) based on a beam on a Winkler creeping foundation to simulate field observation of pile head displacements with time and changing load levels and a pipeline subjected to differential frost heave.

Brief review of previous work

The attempts at replicating the behaviour of laterally load piles embedded in a creeping medium have been few (Neukirchner and Nixon, 1987; Foriero and Ladanyi, 1991) and the results have been partially successful. By this we mean that only the pile head displacement rate rather than both pile head displacement and displacement rate have been compared. These comparisons have been performed for only one specific load step, when often, the pile field load tests involved several incremental load steps.

Rowley *et al.* (1975) proposed a solution based on p-y curves using a time dependent reduced subgrade modulus, k'_s. Nixon (1984) proposed a solution accounting for the fact that the surrounding medium follows

Norton's creep flow law. The differential equation was solved using finite difference techniques. Neukirchner and Nixon (1987) used the solution presented by Nixon (1984) to simulate the field behaviour of pile load tests reported by Rowley *et al.* (1973, 1975) and Nixon (1984). Pile head displacement rates were compared with observed displacement rates while Rowley *et al.* (1973, 1975) acknowledged that determining creep rates from the measured pile head displacement-time history could be subject to considerable error. Moreover, they examined only one steel pile (S-5-L) for one specific lateral load at three distinct temperatures and the model pile tests performed by Nixon (1984).

More recently, Foriero and Ladanyi (1990) have proposed a finite element model where the lateral reaction offered by the frozen soil is based on the Baguelin *et al.* (1977) representation of lateral displacement of a disk in a creeping medium following the Norton-Bailey flow law. Foriero and Ladanyi (1990) compared their solution with the observed behaviour of two timber piles tested at Inuvik, N.W.T. Although the displacement rates seem to compare moderately well (visually), the absolute pile head displacements differ considerably. The more recent work on model test piles reported by Foriero and Ladanyi (1991) adds much needed data on laterally loaded piles. They attempted to fit a power-law expression to describe the stage load-deformation behaviour with time. These curve-fitting procedures demonstrate the limited use of this type of characterization because it is even unable to replicate the displacement time history description within the time frame that it was derived from. The finite element analysis achieved a better representation of the displacement rates but the predicted pile head displacements differed considerably from those observed.

Crowther (1990) presented an analysis of piles tested by Rowley *et al.* (1973, 1975) based on the p-y curve type analysis developed by Matlock (1970) and Reese (1975, 1977) for unfrozen soil. The frozen soil shear strength used in generating p-y curves reflects the influence of duration of the load application and soil temperature. It is interesting to note that shear strength of frozen soil was reduced by the so called *correction factor* to match the pile head displacements at high load steps. Crowther's (1990) approach is essentially based on ultimate resistance of frozen soil which may be valid when the creep exponent, n, is sufficiently high so as to reflect elastic-perfectly plastic behaviour. It must be emphasized that the analysis proposed by Crowther (1990) is quasi-static and does not consider creep behaviour of frozen soils but attempts to evaluate frozen soil strength at discrete time steps. Morin *et al.* (1991) describe creep displacement tests carried out on a rigid bar pulled laterally in ice but no specific lateral load pile tests were performed.

It is apparent from the above brief review that the prediction of pile head displacements has been achieved with only partial success and a solution strategy that replicates all available field and laboratory data is warranted. Since only pile head displacements are monitored with time, excessive liberty exists in selecting frozen soil geomechanical properties to match observed behaviour. Effectively this means that we should be even more stringent in comparing observed and predicted behaviour than we would otherwise be. As we shall see, this is not the case for the pipeline field study where stress measurements were accompanied by vertical displacements along the pipeline.

Nixon *et al.* (1983) attempted to solve the problem of a pipeline subjected to frost heave where the problem was simplified to that of plane strain conditions and the free field frost heave was applied over a predetermined section of the frost susceptible soil. Nixon *et al.* (1983) studied attenuation specifically at the interface of the frost and non-frost susceptible soils. However, the pipeline was considered as a passive component of the whole system and hence its interaction effects were not studied. Frost heave attenuation was studied by varying elastic moduli, permafrost thickness and half-widths. Though the study was based on specific material properties and geometry of the discontinuous permafrost, it was found that the free field frost heave was significantly attenuated at the interface of the discontinuous permafrost. The frost heave data from Caen indeed shows that the attenuation is in the order of 50 to 60%. Selvadurai (1988) analyzed the elastic behaviour of an embedded pipeline at shallow depth using the thermo-elastic analogy. Frozen soil hardly behaves as an elastic material and hence the application of this analysis is limited.

Ladanyi and Lemaire (1984) attempted to back-analyze the Caen experiments using a simplified model based on the elastic Winkler foundation that accounted for free field frost heave in an idealized manner. The proposed procedure did not attempt to simulate observed behaviour over any particular period of time but it rather attempted to evaluate the reduced foundation subgrade modulus, k_s' at a specific time that would match the measured stresses.

Simulation of laterally loaded piles in frozen soil

The replication of experimental pile load test data can be a difficult and challenging task. It has become customary to monitor pile head displacements only without any accompanying stress measurements. Since the pile head displacement response is a result of the interaction between many distinct parameters, any one parameter can be arbitrarily manipulated to match the observed behaviour. The arbitrary manipulation of any parameter would certainly reduce any credibility in the proposed model. Consequently certain guidelines are required for a judicious selection of the different parameters and these were established prior to the initiation of the simulation. These guidelines are:

- the field elastic and creep geomechanical data should be varied to a minimum.

- the pile elastic properties for timber and steel tubular piles should be varied only within the anticipated range.

- once an elastic response for the first load step has been established and is acceptably matched with experimentally observed data, then neither pile nor soil data can be altered for subsequent load steps.

The signatures of the pile head displacements with time for all the pile heads are similar and can be conveniently separated into three distinct phases. They are: the elastic or instantaneous response, the statical transient creep response and the steady state creep response (Figure 4.1). The

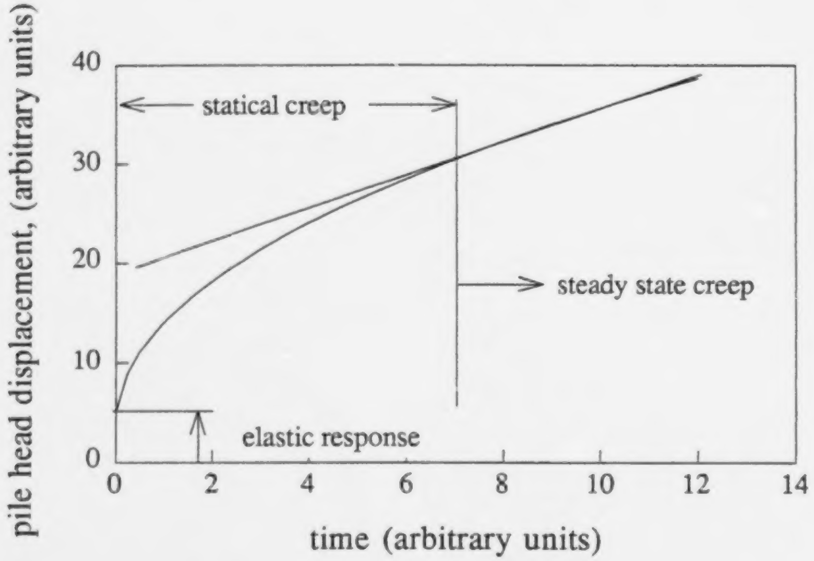

(a) variation of pile head displacement with time

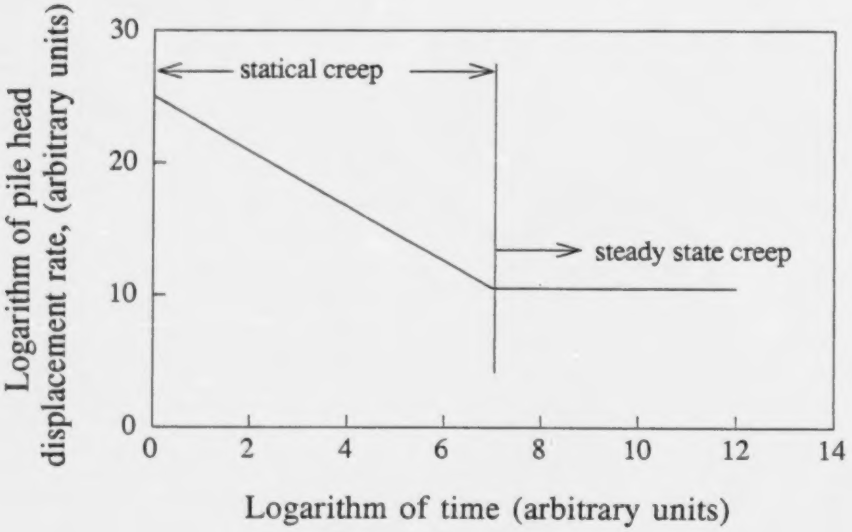

(b) variation of pile head displacement rate with time

Figure 4.1. Typical signature of pile head displacement and displacement rate for laterally loaded pile in frozen creeping medium.

distinction between primary material creep and statical structural creep response has been made previously in chapter 3.

The success of matching observed and predicted responses hinges on obtaining a satisfactory elastic or instantaneous response. This statement is in accordance with the *correspondence principle* for evaluating steady state creep response of structures. As we shall see, the differences in predicted and observed responses for all the field and laboratory tests analyzed in this chapter are primarily due to lack of consistent elastic response. Almost always the elastic response increases at higher load levels which we are unable to account for satisfactorily on the sole basis of the elastic properties of the structure and the surrounding medium. While the structural properties for piles are generally known with certainty, the same cannot be said for frozen soil properties. Another problem that appears is how to translate elastic continuum properties (E, ν) to that of the Winkler subgrade foundation modulus, i.e. k_s'. Vesic (1961) and Biot (1937) have proposed a solution based on comparison of analytical solutions but these estimates can differ by as much as 30 to 40%. In the present analysis, we chose not to vary the available elastic and creep properties of frozen soil for prediction purposes but instead adjust only the flexural stiffnesses of piles so that an acceptable elastic response is obtained. The elastic response is primarily dependent on the characteristic length, β, and is defined as:

$$\beta^4 = k_s'/4EI \qquad [4.1]$$

where the foundation stiffness, k_s', is given by $k_s' = bk_s$, where b is the pipe diameter and EI is the pipe flexural stiffness. Thus the sole adjustment of the flexural stiffness, EI, is tantamount to adjustment of the characteristic length, β, or the ratio of soil medium to beam stiffnesses. The lateral displacement profile is then proportional to the following function:

[4.2] $$w \propto e^{-\beta x} \cos\beta x$$

Pile load tests at Inuvik, N.W.T.

Geotechnical properties

Though the pile load tests were carried out at a single site, vertical homogeneity of soil is not guaranteed and for prediction we shall assume that the soil properties (Table 4.2) do not change significantly. In fact, soil investigation at the Inuvik site indicates that the soil type changes at a depth of 1.5 m from clayey to peat in ice matrix. The pressuremeter tests were also carried out at this depth and consequently uncertainty exists as to whether the test reflects the properties of the clayey silt or peat. On the other hand the data is considerably more reliable than that from uniaxial tests since the pressuremeter closely resembles the deformational mode of a pile under lateral load. Also, a considerable ground temperature variation was measured during the test period which undoubtedly affects the creep modulus, B. The Norton-Bailey type creep flow law was adjusted to the pressuremeter data, i.e.

[4.3] $$\varepsilon = \dot{\varepsilon}_o \left(\sigma/\sigma_o\right)^n t^s = B\sigma^n t^s$$

where n and s are exponents and $\dot{\varepsilon}_o$ and σ_o are proof strain rate and proof stress respectively. In the present analysis only average suggested values were used though a range of parameters were reported by Rowley *et al.* (1975).

Table 4.2. Geotechnical properties for clayey silt at Inuvik, N.W.T.

Properties	**clayey silt**
Soil properties	
soil classification	SP
dry density (laboratory), γ kN/m^3	18.15
dry density (field), γ kN/m^3	18.52
range of void ratios (laboratory), e	0.40 - 0.44
Elastic properties	
Poisson's ratio (assumed)	0.3
Elastic modulus, E_s MPa	$54 < E_s < 88$
Tensile strength, T_s MPa	$0.64 < T_s < 0.88$
Cohesion, c, (for $\phi = 0$), MPa	$0.69 < c < 1.18$
Creep properties	
proof strain rate, $\dot{\varepsilon}_o$ min^{-1}	10^{-5}
proof stress, σ_o MPa	0.31
creep exponent, n	$3.00 < n < 3.89$
time creep exponent, s	$0.85 < s < 0.87$
creep coefficient, B, kPa^{-n} year^{-1}	2×10^{-8}

Comparison of predicted and observed behaviour for timber piles T-2-L and T-3-L

The displacement histories for the two timber piles are very similar qualitatively but several notable differences exist:

- elastic response forms a small proportion of the total response.

- when the magnitude of the load is small, the steady state pile response is attained fairly rapidly. Hence, pile T-3-L can be classified as a long term test while pile T-2-L is a short term test.

- when the lateral load is increased beyond 133.8 kN (15 t), an unidentified effect seems to kick in and results in a relatively long statical creep response for pile T-2-L and failure in the case of pile T-3-L.

The above observed phenomena are perhaps related to the fact that Rowley *et al.* (1975) found that the elastic or instantaneous response was non-linear rather than linearly dependent on the magnitude of the applied load. It may be that the entrapped moisture within the timber piles led the pile itself to creep in addition to the surrounding creeping medium. For the present analyses we assume that the timber piles behave elastically but there is evidence to suggest that the cited explanation is valid, as we shall discuss later.

The first step in the simulation procedure was to establish a good match in the elastic response for the first load step. It is well known that the elastic modulus of timber (Götz *et al.*, 1989) can vary widely from one specimen to another and often with samples from the same species. The elastic modulus of timber is found to be influenced by the moisture content and the elastic modulus can be as high as 3 to 5 times the lowest value. If indeed there was significant moisture within the pile as suggested above then there is sufficient reason to believe that the elastic modulus of the ice-wood matrix would be somewhat higher. Consequently, timber pile flexural stiffnesses (EI) were adjusted to 4 and 2 times the value indicated by Rowley *et al.* (1973) in order to match the predicted and observed elastic responses for piles T-2-L and T-3-L respectively. This variation is within the expected range for different species of timber as indicated by (Götz *et al.*, 1989). Only substantially more testing can probably clarify this point. Observed and predicted pile head displacement time histories for piles T-2-L and T-3-L are shown in Figures 4.2 and 4.3. The simulation is in good agreement for the two piles as long as the load is below 133.8 kN. The inability of the model to represent the observed behaviour at higher load levels is probably due to the material non-linearity in the pile itself as explained earlier. Though the steady state response for all load steps for the two piles compares well, the absolute pile head displacements for pile T-3-L corresponding to the two intermediate loading steps differ significantly.

Comparison of predicted and observed behaviour for steel tubular piles S-4-L and S-5-L

Though Rowley *et al.* (1973, 1975) seem to have carried out three load tests on steel tubular piles, pile displacement histories for only two of them are available. The displacement histories for the two steel piles are very similar qualitatively but several notable differences are:

- the first pile, S-4-L, load test is a short term load test in the sense that

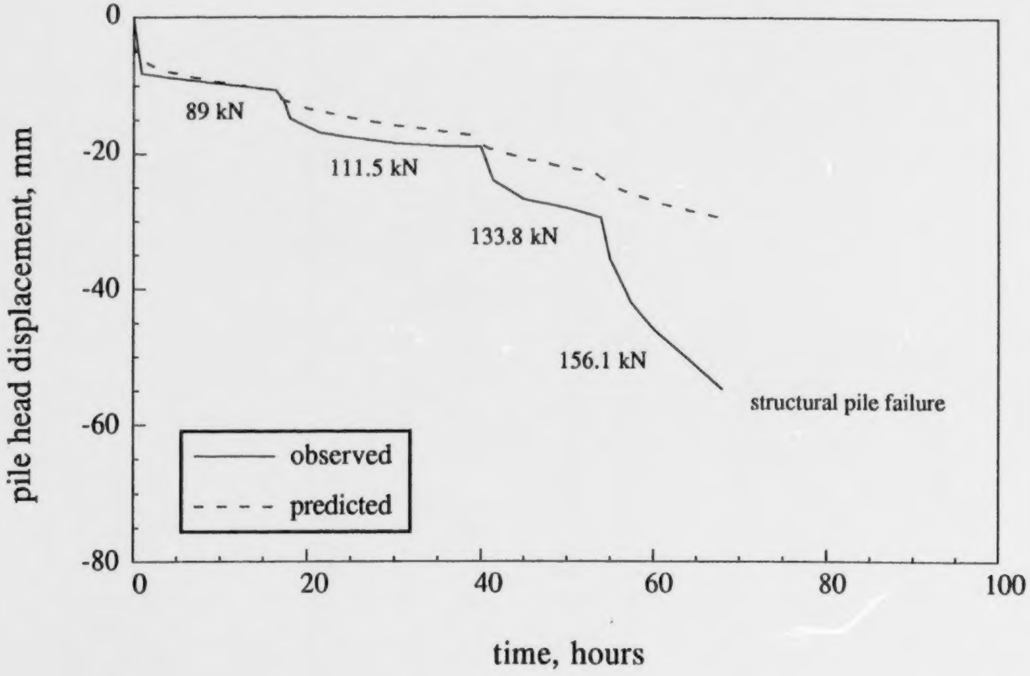

Figure 4.2. Comparison of predicted and observed pile head displacement time history for timber pile T-2-L.at Inuvik, N.W.T.

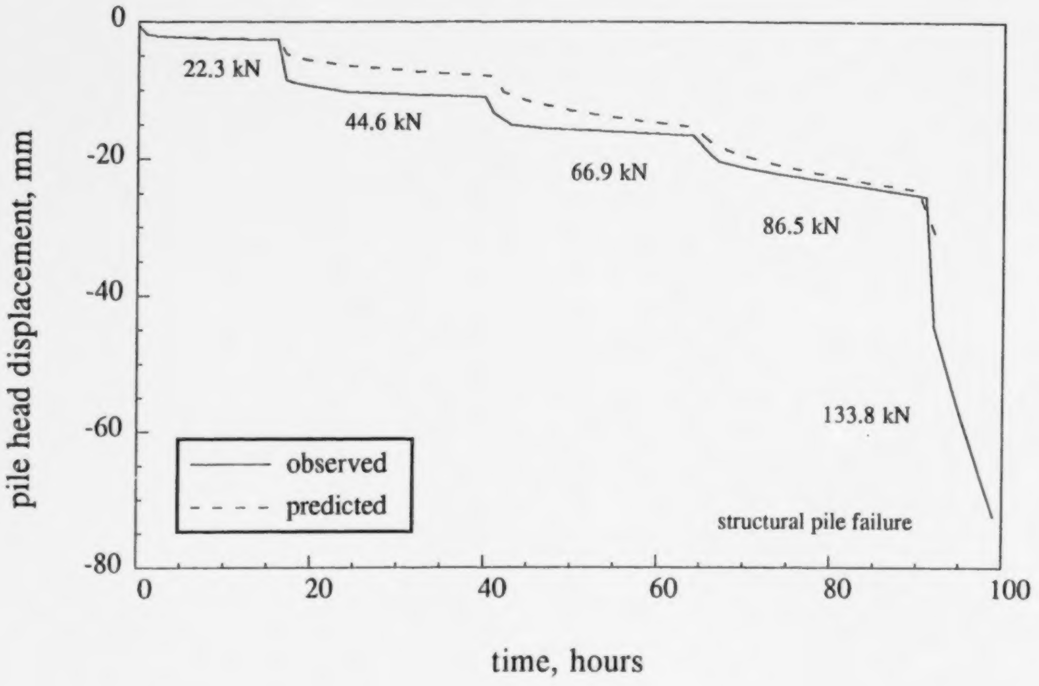

Figure 4.3. Comparison of predicted and observed pile head displacement time history for timber pile T-3-L at Inuvik, N.W.T.

sufficient time was not permitted to elapse to obtain a steady state response.

- the elastic response of the second pile, S-5-L, load test is clearly evident for the first three load steps but the pile fails to respond in a similar fashion for higher loads i.e > 356 kN (40 t).

- though piles S-4-L and S-5-L are similar in all structural and geotechnical aspects, the elastic response of pile S-4-L is such that it was much stiffer than pile S-5-L. This could either occur as a consequence of the stiffer surrounding medium or increased pile structural stiffness due to infilling with moist sand. But then why would pile S-5-L not respond equally to either of these effects?

The simulation was carried out along the same lines as for timber piles. In order to match the much stiffer elastic response of pile S-4-L for the first step loading, the expected pile flexural stiffness (EI) had to be increased by 20 times and the elastic soil modulus by 10. This exaggerated increase in pile flexural stiffness cannot be explained by material properties or infilling of the tubular piles with moist sand. The predicted response of pile S-5-L was obtained using the geotechnical properties listed in Table 4.2 and no change in the properties was required. The predicted and observed lateral pile responses are shown in Figures 4.4 and 4.5. The prediction thus obtained for the two steel piles is comparable with the observed response for load levels till 178 kN, after which it differs significantly.

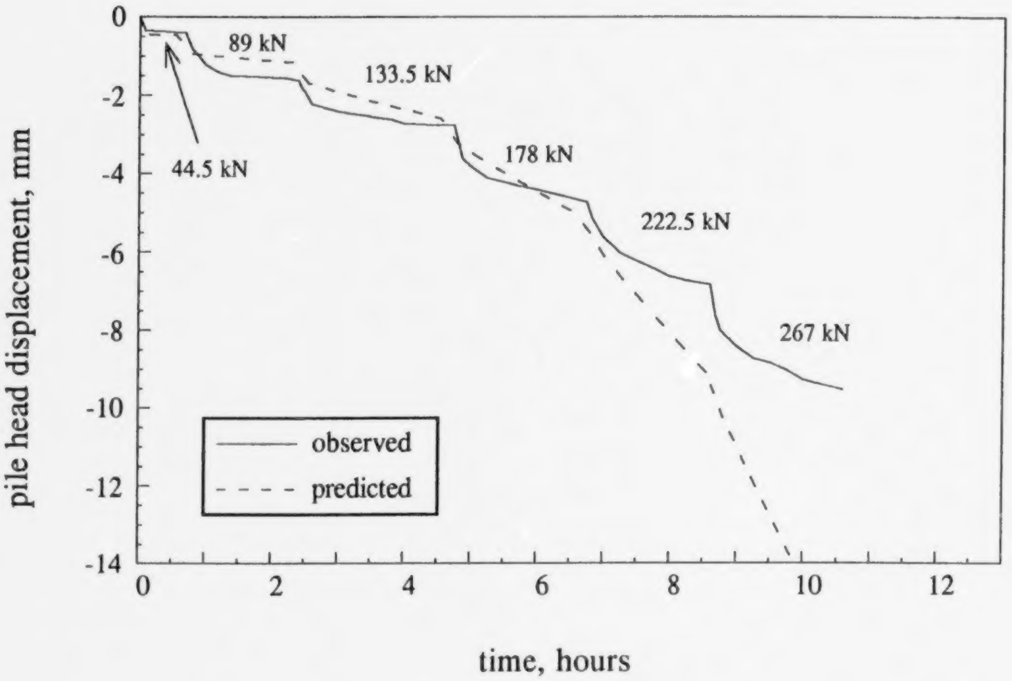

Figure 4.4. Comparison of predicted and observed pile head displacement time history for steel tubular pile S-4-L at Inuvik, N.W.T.

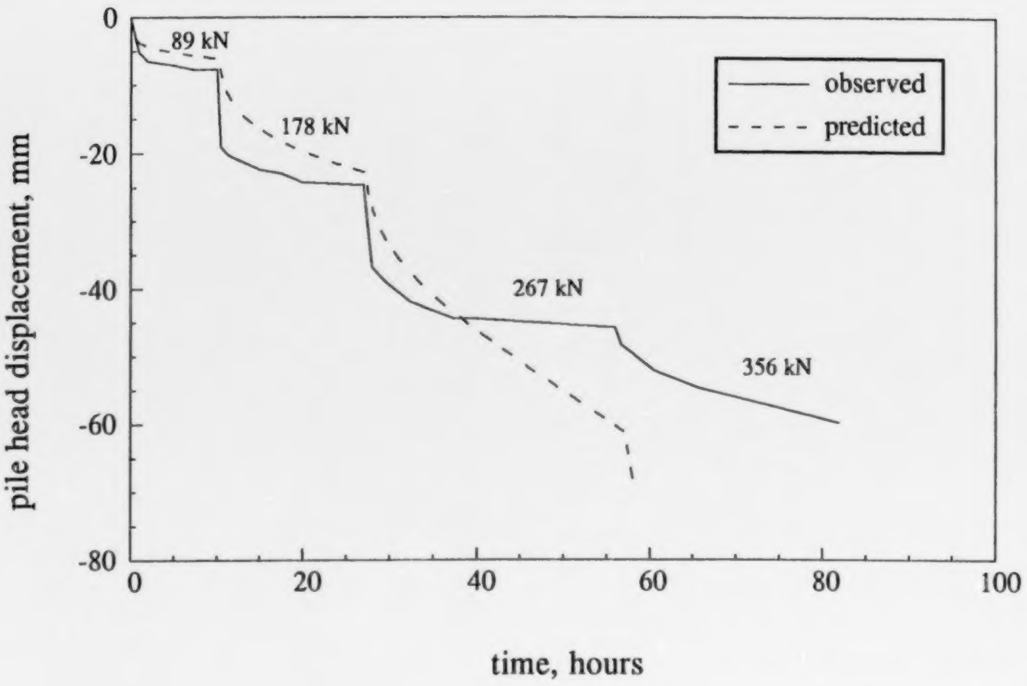

Figure 4.5. Comparison of predicted and observed pile head displacement time history for steel tubular pile S-5-L at Inuvik, N.W.T.

Model solid steel piles in ice (Nixon, 1984)

Ice properties

The elastic or creep properties were not determined for samples of ice that Nixon (1984) used to test the steel model piles. The ice was produced by seeding snow crystals and it was grown in layers of 25 mm. Morgenstern *et al.* (1980) carried out an extensive review of the creep properties of ice which can be used for the present analyses. These properties are listed in Table 4.3.

Comparison of predicted and observed behaviour for steel model piles in ice.

The three model pile tests were essentially the same except that each was subjected to a different lateral load. The use of the largest possible value for elastic modulus for ice listed in Table 4.3 resulted in an elastic pile head displacement larger than that observed. If we accept the ice properties as indicated in Table 4.3, then, in order to match the observed elastic displacement we are left with the only alternative of increasing the flexural stiffness. We found that the flexural stiffness (EI) would have to be approximately 3 to 4 times larger than that obtained using given elastic properties if a good match between the predicted and observed elastic pile head displacements is to be attained. While the increase in flexural stiffness for timber piles could be substantiated as explained earlier, we found no convincing arguments for the suggested values for model steel piles. In fact, there is no experimental evidence suggesting that the elastic modulus

Table 4.3. Elastic and creep properties for ice.

Properties	ice
Elastic properties	
Poisson's ratio (assumed)	0.3
Elastic modulus, E_s, GPa	8.93
Creep properties	
proof strain rate, $\dot{\varepsilon}_o$ min^{-1}	10^{-5}
proof stress, σ_o MPa	0.31
creep coefficient, B, kPa^{-3}, yr^{-1}	$6.1 \times 10^{-8} / (1 - T)$
creep exponent, n	3.00

of steel varies significantly within the range of temperatures under consideration here. Since the pile head displacements were monitored at the point of load application, simple static structural analysis indicates that surface pile displacements undergo an amplification of about 3. Hence, any minor error at the surface is magnified considerably and for this reason the cited value was accepted for the present analyses. The comparisons between observed and predicted pile head displacements are shown in Figure 4.6. The match for displacement and displacement rates for pile load test No. 2 is very good but only moderately comparable for pile load test No. 3. Since pile load test No. 1 was not of a sufficient long duration, it is difficult to assess the comparison. Nonetheless, the pile displacement rates (Figure 4.7) are in good comparison with those obtained by Neukirchner and Nixon (1987). The pile head displacement rate predictions are slightly closer to those measured experimentally than those predicted by Neukirchner and Nixon (1987).

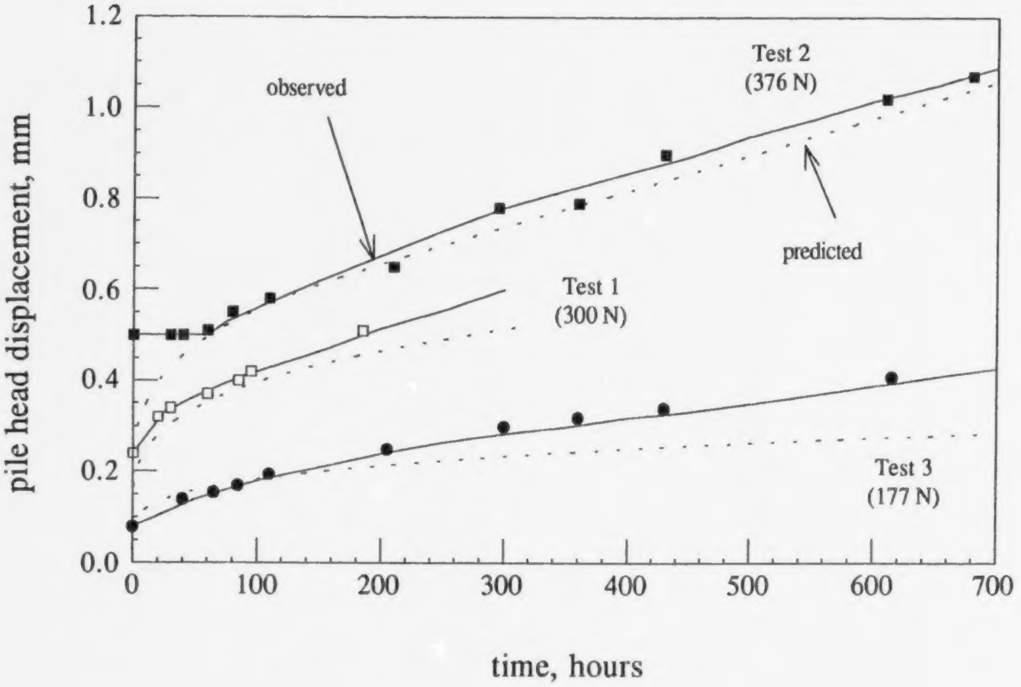

Figure 4.6. Comparison of predicted and observed pile head displacement time history for steel model piles in ice.

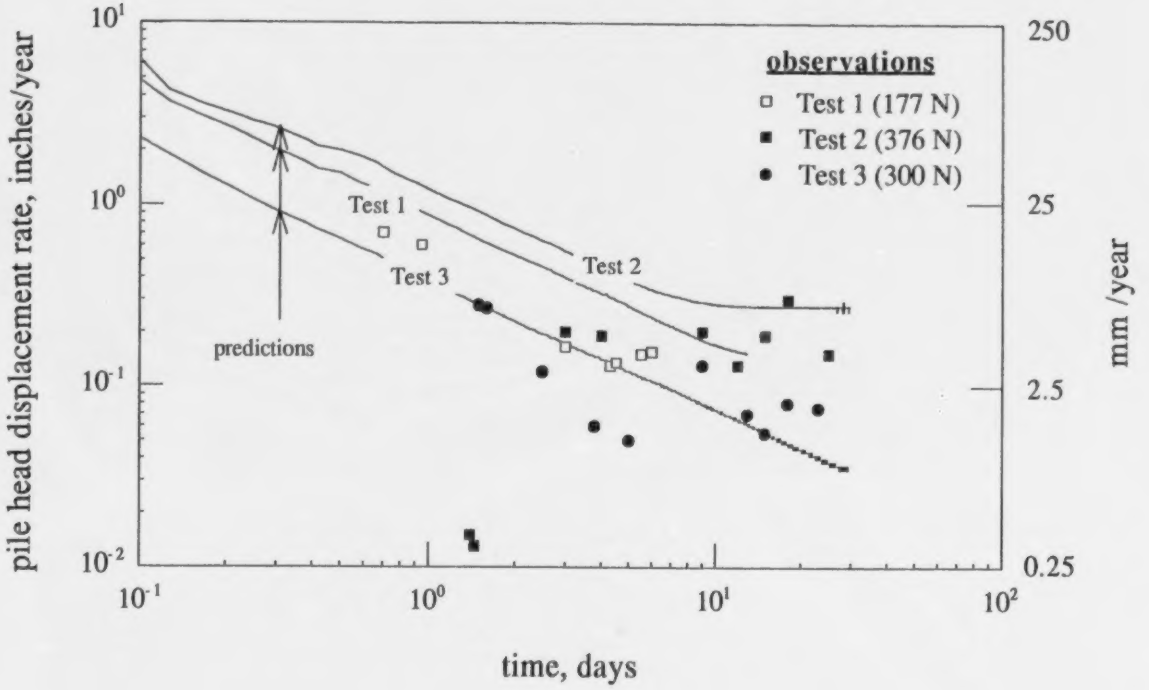

Figure 4.7. Comparison of predicted and observed pile head displacement rates time history for model test piles in ice.

Model aluminium and steel piles in sand (Foriero and Ladanyi, 1991)

Geotechnical properties

No tests were performed to determine the elastic or creep properties though the sand used was similar to that described by Ladanyi and Eckardt (1983). Ladanyi and Eckardt (1983) found the variation in the creep properties (i.e. n and B values) to be dependent on the particular interpreting techniques and substantial variations could result. A review of the available data on creep for different soil types indicates that even within the same soil type the variations in creep properties can be quite significant and especially so for sand. However our review of existing data indicated that there was no evidence that the creep exponent n could be as low as 1.2 as inferred by Foriero and Ladanyi (1991). Indeed data from Ladanyi and Eckardt (1983) indicates that the value of n lies between 1.8 and 3.6 and that of B lies between 8.68×10^{-7} to 1.86×10^{-9} $\mathrm{kPa}^{-n}\ \mathrm{year}^{-1}$. We chose a value of 3 for n since other available data on sands confirmed the range of possible variation and also since this value has been widely accepted for ice-rich soils.

The value suggested by Foriero and Ladanyi (1991) for the soil subgrade modulus, k_s', is 310 MPa which is equivalent to an elastic modulus, E_s, of 160 MPa (using Biot's (1937) relation with a Poisson's ratio of 0.3). This is considerably more than that for polycrystalline ice (Table 4.3). Sego *et al.* (1982) determined the secant elastic modulus for frozen sand samples with different degrees of salinity. They found that the elastic modulus was dependent on the strain rate and for samples with zero salinity the elastic modulus was in the order of 5 to 20 MPa for an axial strain rate of 10^{-3} %/hour. This range of values is also close to that obtained for SNEC sand discussed later in relation with the pipeline response subjected to frost heave. The final selected value for elastic modulus was 8 MPa for the analysis of the two model pile tests and the selection of this particular value will be discussed in the next section. All elastic and creep properties have been summarised in Table 4.4.

Table 4.4. Assumed elastic and creep properties for sand.

Properties	**sand**
Elastic properties	
Poisson's ratio (assumed)	0.3
Elastic modulus, E_s, MPa	8.00
Creep properties	
creep coefficient, B, kPa^{-3}, yr^{-1}	1.3×10^{-6}
creep exponent, n	3.00

Comparison of predicted and observed behaviour for model piles 1-A1 and 16-S1

Foriero and Ladanyi (1991) performed 16 lateral stage-load tests on aluminium and steel piles embedded in sand. The pile installation procedure followed was similar to that usually used in the field, i.e. the annulus between the pile and the predrilled hole in the frozen ground was filled with a mixture of sand-slurry. It should be mentioned that the influence of using a sand-water slurry installation on pile behaviour was not discussed by Foriero and Ladanyi (1991).

The displacement-time signatures for the stage-load tests (Figures 4.8 and 4.9) are very similar and typical of what would be expected as discussed earlier. In particular we note:

- the pile displacement history for pile 1-A1 shows that little creep displacement took place.

- the elastic response is not consistent with the stage loads. i.e. the plot of load versus net elastic displacement shows that there is significant displacement even at zero load. This is evident for both tests but better consistency is found for pile test 16-S1. We suspect that if the stage-loads are not applied slowly enough then the elastic response can be increased due to dynamic amplification. This demonstrates the need for applying loads very slowly indeed.

- the analytical power law expressions used to fit experimental data demonstrates its limited use because the results from 16 pile tests do not indicate any trends that can prove useful in practice. We also note that the analytical expressions fail to trace the observed behaviour for higher load levels.

As mentioned earlier the key to matching displacements is dependent on the elastic response while the matching of displacement rates is influenced by the creep properties. Since slightly better net elastic responses were

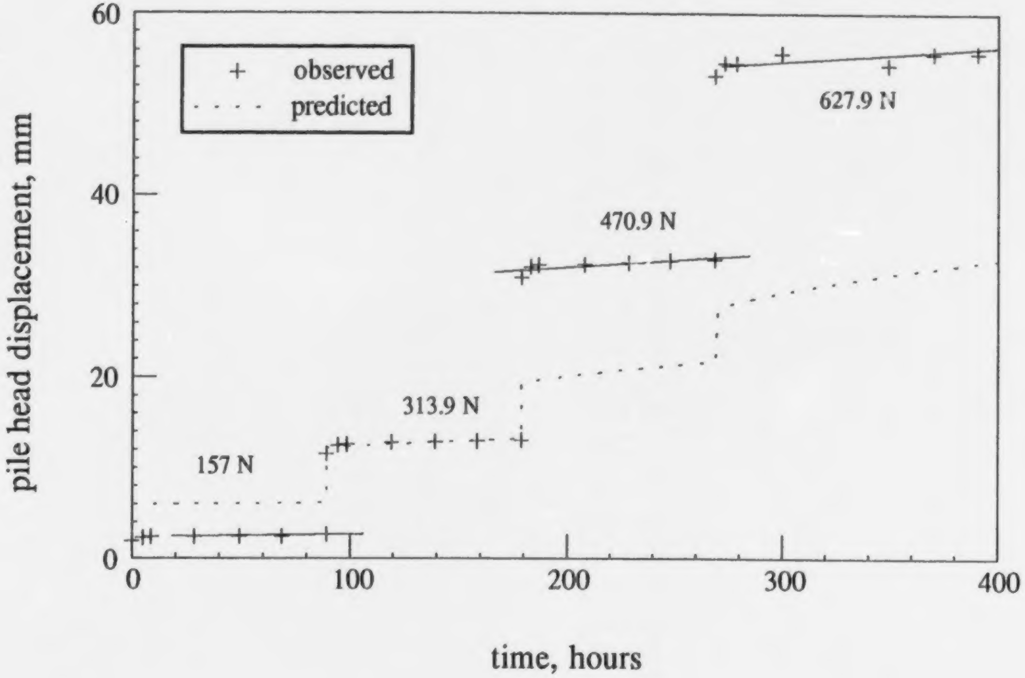

Figure 4.8. Comparison of predicted and observed pile head displacement time history for aluminium pile 1-A1 (with slurry).

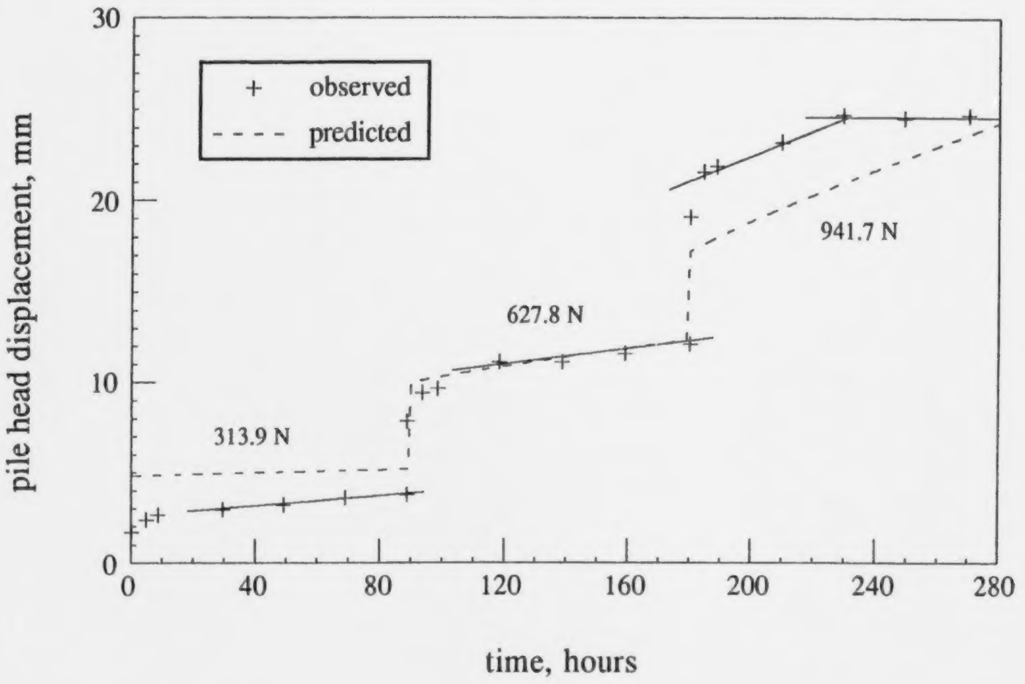

Figure 4.9. Comparison of predicted and observed pile head displacement time history for steel rod pile 16-S1 (no slurry).

observed for pile test 16-S1 an elastic modulus, E_s, was selected that best traced the observed elastic response for the second stage load.

The value of B was obtained by trial and error so that the creep displacement observed for pile test 16-S1 matched that with the predicted response for the second stage load. The second stage load response for pile 16-S1 was used to calibrate the elastic and creep properties for frozen sand because it seemed to exhibit behaviour in line with criteria for the analysis of lateral pile tests. Also the steady state response was clearly evident for this load level. A direct consequence of the selected elastic modulus for frozen sand is that the non-dimensional characteristic length, βL for both model piles is in the order of 2 as opposed to 15 to 20 as suggested by Foriero and Ladanyi (1991). Consequently the piles would be classified as short piles and not as long piles.

The elastic response for each pile is over estimated for the first load level while it is underestimated for the third and fourth load levels. The predicted steady state lateral displacements (Figures 4.8 and 4.9) are comparable to those observed. The experimental observations for pile 16-S1 seem to indicate that a steady state response at the high load levels was not achieved.

Simulation of pipeline subjected to differential frost heave

As indicated earlier, the experimental pipeline facility at Caen, France is the only field study (at least where experimental data is publicly available) where frost heave and corresponding stresses induced in the pipeline have been monitored over a significant period of time and freezing periods. For ease of reference the vertical displacement and stress profiles are reproduced in Figures 4.10 and 4.11 for the first and the second freeze periods respectively. A look at a typical observed vertical displacement profile of the pipeline in sand indicates that the pipeline beyond 4 m undergoes minor differential movement. This probably reflects on the relative stiffnesses of the pipeline and the surrounding frozen sand. In contrast, the portion of the pipeline embedded in silt shows significant rotation at the far end.

The observed stress history profiles (Figures 4.10 and 4.11) reveal a near zero stress state at the interface between the sand and silt. This fact, combined with the observation that the stress wave is nearly anti-symmetrical on either side of the sand/silt interface, suggests that near surface effects are minimal. Meanwhile, the stress wave for the pipeline in sand is half sinusoid and that in the silt is a distorted full sinusoid. The stress wave for the portion of the pipeline in silt steadily approaches that of a distorted sinusoidal wave form but with significant stress in the pipeline at the far-end as compared to stress at the homologous point in the pipeline embedded in sand. This is especially true for larger time periods and in second, third and fourth freeze periods. We also note that the peak stresses occur at approximately 2 - 2.2 m and 1 - 1.5 m in sand and silt respectively from the sand/silt interface. It is to be noted that the position of peak stress is not stationary but steadily propagates with time towards the far ends of sand and silt respectively. The steady propagation of stress waves towards the free end may be related to the continually changing elastic and creep properties of the surrounding solids due to the steady advancement of the

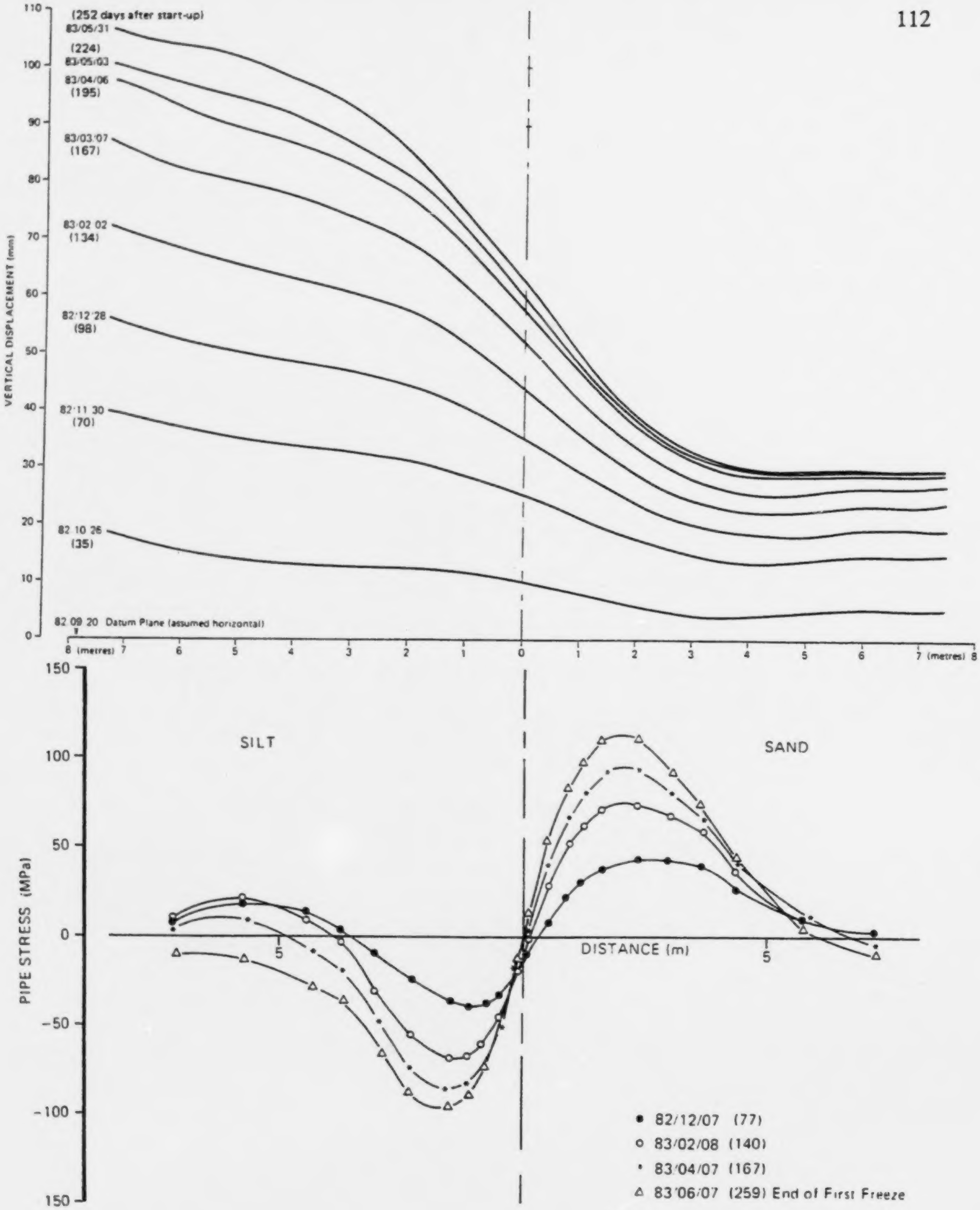

Figure 4.10. Vertical displacement and stress wave history profiles during 1st freeze period for pipeline at Caen, France (after Dallimore and Crawford, 1984).

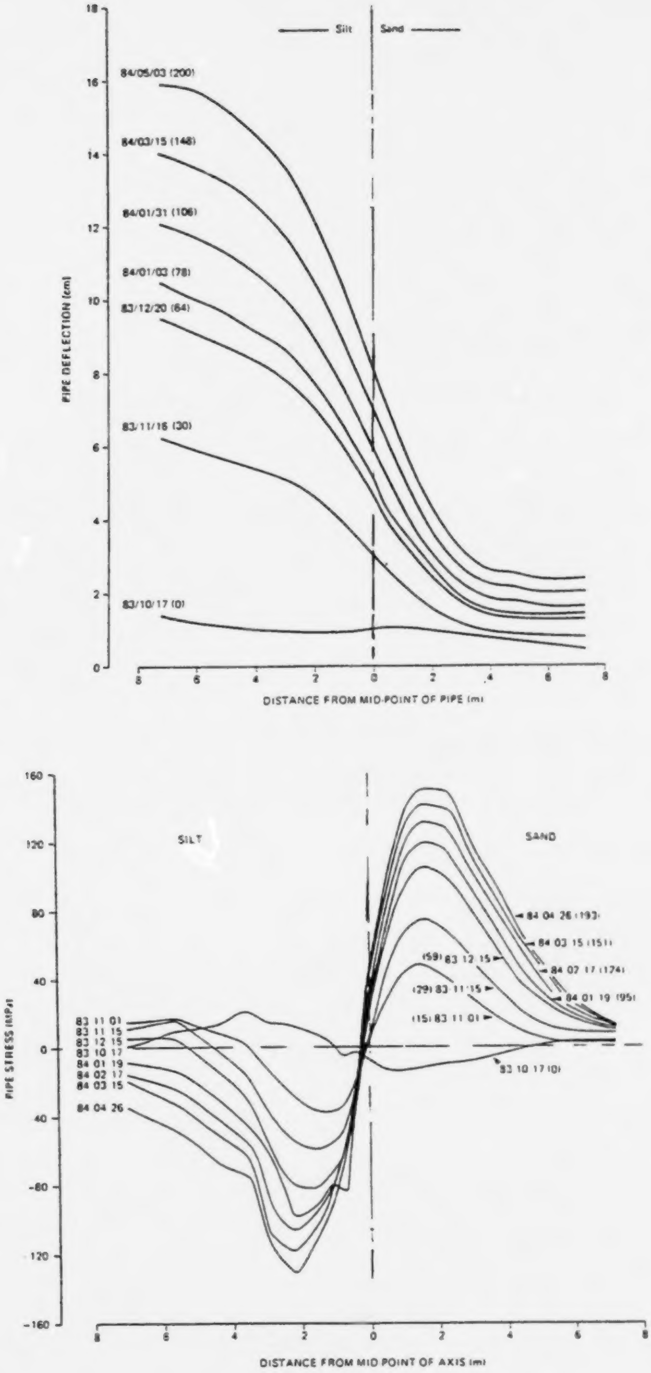

Figure 4.11. Vertical displacement and stress wave history profiles during 2nd freeze period for pipeline at Caen, France (after Dallimore and Crawford, 1984).

freezing front.

The above observations are found to be equally valid for the third and fourth reported freeze periods. From available data for the pipeline stresses it appears that, due to a probable malfunction of the strain gauges on the pipeline embedded in silt, the stresses beyond 4.25 m were not registered during the third and fourth freeze periods.

Idealized vertical displacement and stress wave profiles

The idealized behaviour of a beam embedded in a creeping medium subjected to an end load was studied in the previous chapter. Various approximate solutions were obtained based on the *correspondence principle* which states that when a viscoelastic system is subjected to a constant load or displacement, then displacements or stresses depend on time and are the same as that in an elastic system except that the elastic material properties are replaced by viscoelastic parameters. Thus, as we saw in the analysis of piles, it becomes very important to be able to predict elastic response with certain exactitude and especially in terms of general trends. Consequently, a close examination of idealized elastic responses as a function of the characteristic length, β, permits an easy identification of behavioural trends noted above and the choice of elastic frozen soil parameters is made rather easy by visual comparison. The vertical displacement profile is given by [4.2] and stress wave profiles are then proportional to the following function:

[4.4] $$\sigma \propto e^{-\beta x} \sin \beta x$$

The variation of vertical displacement and stress as a function of the characteristic length, β, is shown in Figure 4.12. If we require a response with the special characteristics noted earlier, it becomes evident that β should have values close to 0.6 and 0.25 for the portions of the pipeline embedded in sand and silt respectively. These values would be in accordance with the fact that sand is found to be stiffer than silt. For a β value of 0.25 for silt, the stress wave only resembles the observed stress wave form for higher time periods and it could be suggested that the initial silt stiffness is higher than that of sand. However, there is evidence available against this possible argument. We recognize that the pipeline structural properties (E and I) can be established accurately and hence the only uncertainty lies with the soil properties. Significant observed stress at the far end of the pipeline in silt suggests possible restraint but as we shall see later this can only account for stresses developed for higher time periods. On the other hand, significant observed negative rotation at the far end of the pipeline in silt is contrary to the mentioned restraint. These arguments lead us to conclude that within the silt zone itself there seems to exist two lateral sub-zones of silt with different frost heave characteristics or that because of the low stiffness of silt the end effects play a major role in the interaction.

The rate of increase of flexural stresses in the pipeline is influenced by the value of the creep exponent, n. A large value necessarily means that the creep rate will be faster and hence the flexural stresses in the pipeline will be much higher than those expected for a smaller value of the creep exponent during the same time span. However, as n gets larger than three, the response is not significantly different as shown by approximate methods

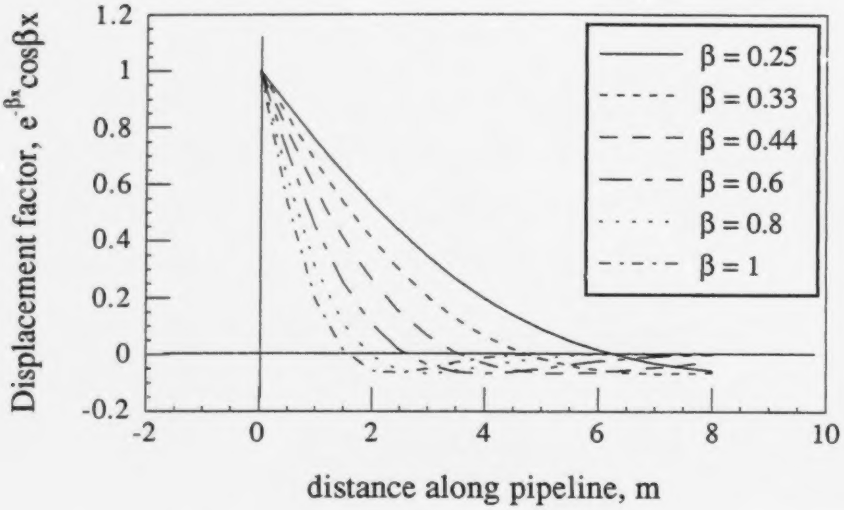

(a) vertical displacement profiles

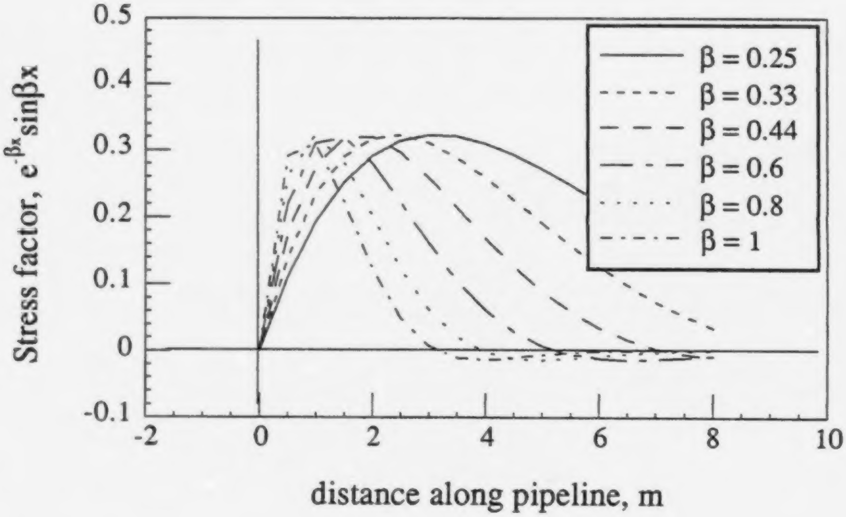

(b) stress wave profiles

Figure 4.12. Vertical displacement and stress factor profiles for a semi-infinite beam on elastic foundations as a function of characteristic length β.

developed in chapter 3.

Consequently, assuming all other pipe and soil properties are known, it becomes a relatively simple task to simulate observed trends by varying the elastic soil modulus and the creep exponent, n, within the anticipated range. This strategy proves particularly useful when reliable geomechanical data is lacking.

Geotechnical properties

Numerous samples of SNEC sand and Caen silt have been tested (Geotechnical Sciences Laboratories, 1986) to determine elastic properties as well as creep properties. A total of 22 constant load and constant displacement rate tests were carried out on laboratory prepared samples. The stress-strain rate data were fitted to an empirical approximation as proposed by Ladanyi (1972). This expression is given by:

$$\varepsilon = \varepsilon_e(\sigma/\sigma_e)^m + \dot{\varepsilon}_o(\sigma/\sigma_o)^n t \tag{4.5a}$$

or

$$\varepsilon = \varepsilon_e(\sigma/\sigma_e)^m + B\sigma^n t \tag{4.5b}$$

where the first term corresponds to the elastic or instantaneous response and the second term corresponds to the creep response; m and n are the elastic and creep exponents, ε_e, $\dot{\varepsilon}_o$ are the proof elastic strain and creep strain rates respectively and σ_e, σ_o are proof stresses. The constant B involves the proof strain rate, proof stress and the creep exponent, n.

The data for SNEC sand and Caen silt is summarized in Table 4.5. Since

Table 4.5. Geotechnical properties for sand and silt at Caen, France.

Properties	sand	silt
Soil properties		
soil classification	SP	ML
dry density (laboratory), kN/m^3	18.15	16.68
dry density (field)	18.52	16.29
range of void ratios (laboratory)	0.40-0.44	0.60-0.63
Elastic properties		
Poisson's ratio (assumed)	0.3	0.3
proof strain, ε_e	0.001	0.001
proof stress, σ_e kPa	170	140
exponent, m	1.43	2.40
Elastic frozen soil modulus, E_s, kPa	2820	960
Creep properties		
proof strain rate, $\dot{\varepsilon}_o$ min^{-1}	10^{-6}	10^{-8}
proof stress, σ_o kPa	900	280
creep exponent, n	5.6	10.6
creep coefficient, B, kPa^{-n} year^{-1}	1.503×10^{-17}	6.036×10^{-29}

the laboratory tests were carried out at -2 °C, their use for the simulation of the second freeze period will be limited because of the lower operating temperature at -5°C. Higher sand dry densities for both laboratory and field samples than that for silt is in accordance with the higher sand stiffnesses mentioned earlier. Another observation that supports this fact is that stresses induced in the pipeline embedded in sand are higher than those induced in the pipeline embedded in silt. Independent dynamic elastic moduli for a range of sands and silts (Kaplar, 1969) confirms that sand is 30 to 60% stiffer than silt. The elastic modulus, E_s, as indicated in [4.5] is stress dependent and can vary considerably as shown in Figure 4.13. In fact, though the measured stress in the soil near the pipeline was in the order of 50 kPa, the laboratory investigations were performed within the 200 - 1300 kPa stress range because of equipment limitations. Ladanyi and Lemaire (1984) found that an elastic modulus of 2.8 MPa (corresponds to their value of k_s' of 1.2 MPa and assuming a Poisson's ratio of 0.3) matched the observed response. Figure 4.11 also serves to illustrate that for the stress range of interest, the expression given by [4.5] in fact predicts a higher stiffness for silt than sand. We note that the value of elastic modulus, E_s used by Ladanyi and Lemaire (1984) is orders of magnitude lower than that predicted by [4.5]. For the present study, a trial and error procedure also established that the elastic modulus for sand within that range adequately represented the observed behaviour. The pertinent question then to be posed is: why such a difference in the elastic modulus?

We believe that the elastic moduli given by expressions like [4.5] or those given by dynamic test methods primarily reflect the compressional mode of displacement rather than the tensile mode that would be of most relevance when the pipeline is subjected to uplift. This highlights the importance of obtaining mechanical properties of creeping media that adequately represent the possible modes of displacement. The creep exponent, n, for both sand and silt is unexpectedly high. McRoberts *et al.* (1978) have reported creep test data on undisturbed samples of ice-rich silt. Nixon and McRoberts (1976) suggested that the creep exponent, n, could be

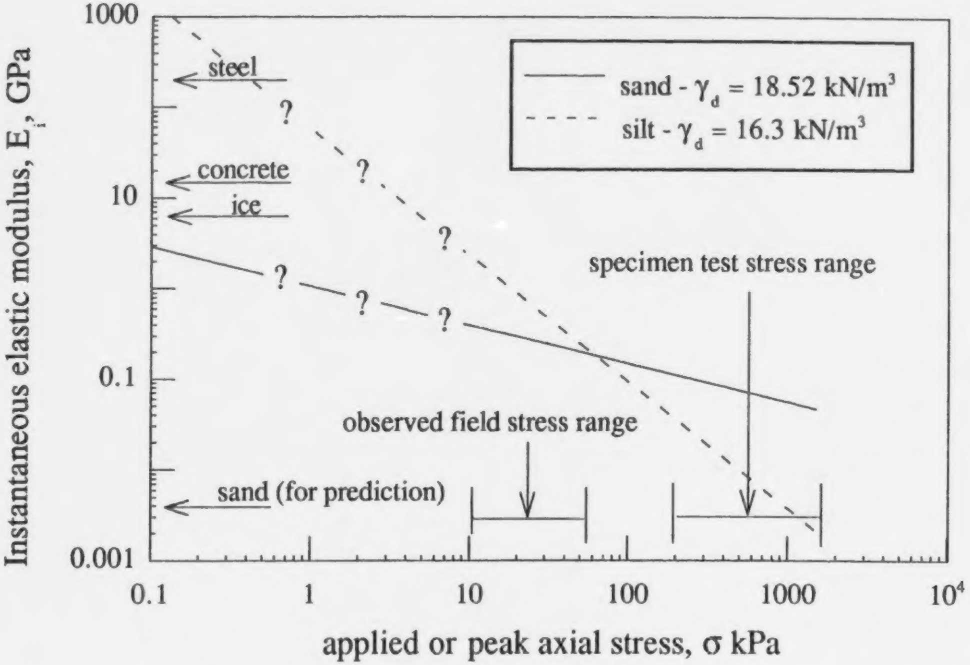

Figure 4.13. Instantaneous elastic modulus for sand and silt at Caen from constant load and constant displacement rate tests.

related to the temperature by an empirically obtained power relation. The particular relation suggested for ice-rich silt samples from Norman Wells, N.W.T. is:

$$\dot{\varepsilon} = \frac{1.6\text{x}10^{-7}\sigma^{3}}{(1-\text{T})^{1.8}} + \frac{1.5\text{x}10^{-14}\sigma^{6}}{(1-\text{T})^{1.8}} \qquad [4.6]$$

However, a careful review by Weaver (1979) concludes that sufficient data does not exist to indicate that the creep exponent varies significantly from 3. The creep coefficient, B, has been found (Morgenstern *et al.*, 1980) to vary significantly with temperature for both ice and ice-rich silt. Since the laboratory tests on soil samples were carried out at one specific temperature and due to the fact that the frost heave was steadily imposed as chilled air passed through the pipeline, the simulations should only be expected to trace observed trends. The comparison of creep test data for Caen silt and SNEC sand with that reported by McRoberts *et al.* (1978) indeed confirms that the flow law for ice is an upper bound for ice-rich soils.

Frost heave

The free field frost heave rate can be readily estimated as suggested by Konrad and Morgenstern (1984). As expected the Caen silt heaves considerably more than SNEC sand and the free field heave is attenuated at the sand/silt interface because of the restraining effects of the much stiffer sand. The amount of frost heave is considerably larger during the second freeze period than that observed during the first freeze period (Figures

4.14 and 4.15). The amount and mode of attenuation is closely related to the geometry and mechanical properties of the two adjacent media as discussed earlier. In the present study we do not attempt to identify the mechanism of attenuation though this has been studied previously (Nixon *et al.*, 1983). Instead, we propose to impose prescribed displacements corresponding to the observed differential frost heave rate on the pipeline at the sand/silt interface.

Comparison of vertical displacement and stress history

The simulation of the pipeline was carried out individually for each portion of the pipeline embedded in sand and silt using the corresponding mechanical properties for each soil type. The pipeline was discretized into beam finite elements and the surrounding medium was represented by truss springs with creeping material characterization as explained in chapter 3. The pipeline was subjected to prescribed vertical displacements which were obtained by subtracting free field heave in sand and silt respectively from the heave at the sand/silt interface. This procedure essentially extracts the rigid body mode of movement which does not contribute to any stresses in the pipeline. We also assume that the frost heave rate is not significantly influenced by the differential movement of the pipeline. The differential frost heave rates calculated using the aforementioned procedure are shown in Figures 4.14 and 4.15. The free field frost heave rate used for silt was that determined by Nixon (1985) while that for sand was estimated from the observed vertical displacement of the pipeline at the far end.

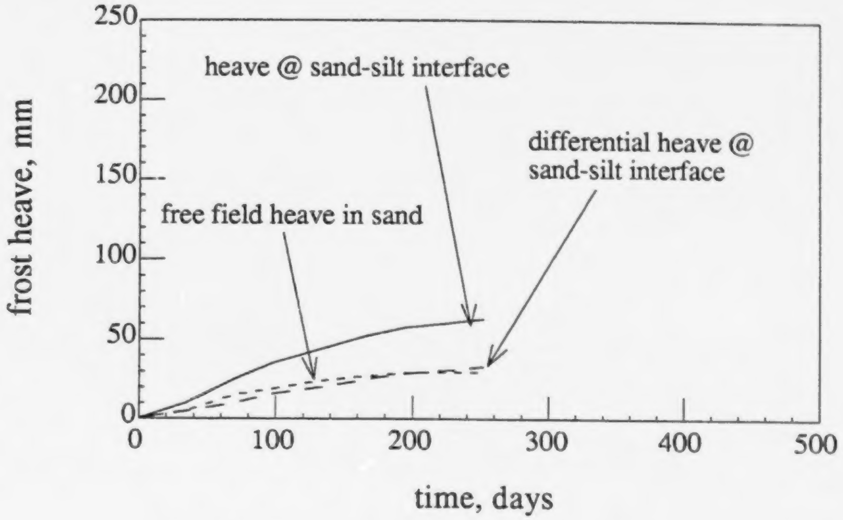

(a) frost heave in sand during 1st freeze period

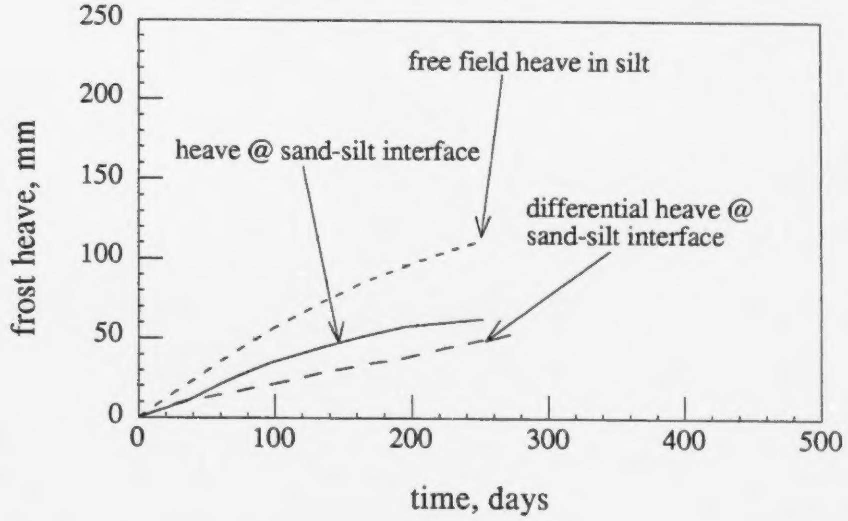

(b) frost heave in silt during 1st freeze period

Figure 4.14. Frost heave in sand and silt during 1st freeze period at Caen, France.

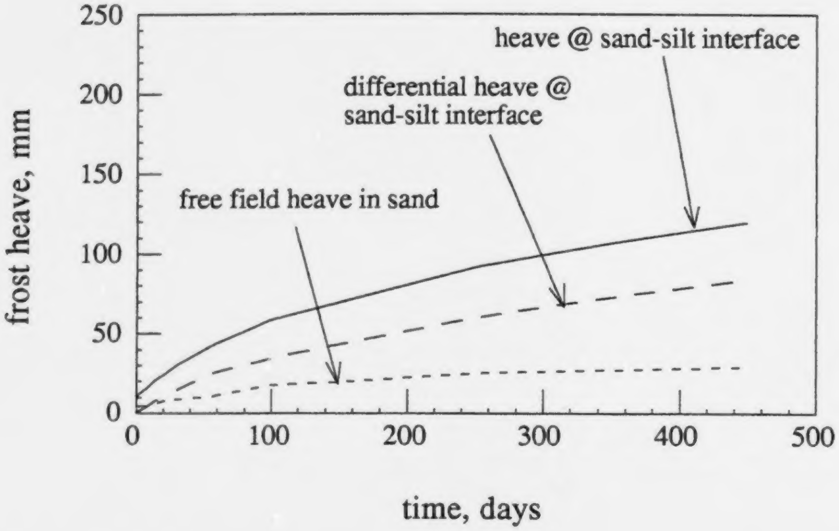

(a) frost heave in sand during 2nd freeze period

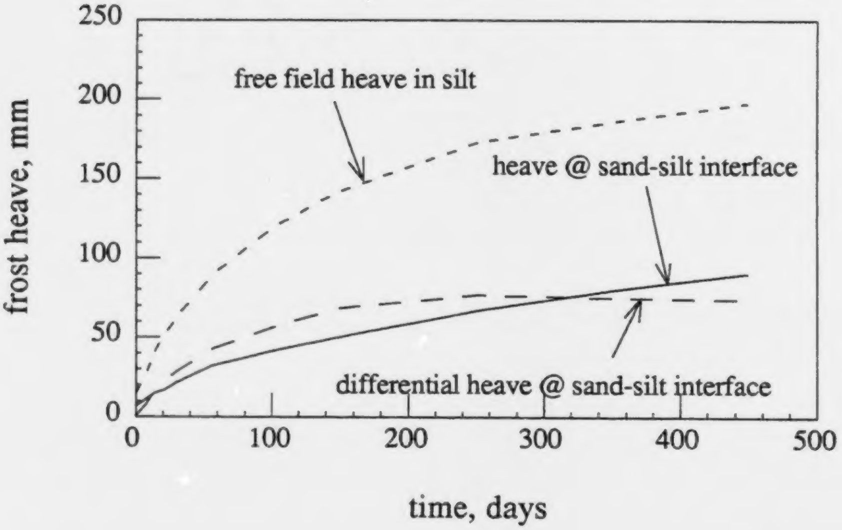

(b) frost heave in silt during 2nd freeze period

Figure 4.15. Frost heave in sand and silt during 2nd freeze period at Caen, France.

At the Caen experimental facility, the advance of the frozen front took place by maintaining the temperature of the pipeline at -2°C and -5°C during the first and second freeze periods respectively. As expected, the frost bulb penetration was greater during the second period than during the first freeze period. Frost front advance data indicates that the steady state conditions were observed after about 100 days. The soil characteristics are continually changing during the transient phase when many complex processes are simultaneously taking place as the soil is being steadily frozen. One such important process is the migration of moisture associated with frost heave. Shen and Ladanyi (1987) have analyzed this aspect of the problem in two dimensions and they find that the hoop stress induced as a result is in the order of 1.5 MPa, which is relatively insignificant in comparison with the flexural stresses. In the present analysis we assume that the frost bulb advance took place instantaneously and that the soil properties given in Table 4.5 adequately represent the situation for the first freeze period at the end of the transient response. A more realistic approach would be to represent material properties for each specific temperature. Furthermore, the laboratory testing of samples was carried out at -2°C and consequently the use of the same values for the second freeze period introduces additional uncertainty in the predicted response. Besides the definite alternate operating conditions of the pipeline at -5°C, the freezing and thawing and subsequent refreezing of surrounding sand and silt substantially changes the soil structure and hence the creep properties. Therefore, the simulation corresponding to the second freeze period involves considerable simplifications and our goal was to account for 90-95% of the stresses that can arise as a consequence of differential frost heave using a relatively simple method of analysis. For the second freeze period we neglected the fact that the pipeline was deformed and had minor locked-in stresses after the thaw of the first freeze cycle.

The simulation of the pipeline portion embedded in sand during the first freeze period was a straight forward procedure. The elastic modulus, E_s (= 2820 kPa), used was as essentially proposed by Ladanyi and Lemaire (1984) and it was within the expected range as we saw for the idealized behaviour (Figure 4.12). The final vertical displacement profile was obtained by adding the free field frost heave rate as shown in Figure 4.16a. Similarly the stress wave histories are shown in Figure 4.16b. The analysis for the second freeze period (Figure 4.17) resulted in lower predicted stresses than that measured for the initial time intervals but the stresses were grossly overestimated for the higher time intervals. Since insufficient laboratory or field data exists on geomechanical properties, we believe that at present extra effort is not warranted for a better match of field history.

It was expected that the simulation of vertical displacement stress wave histories for the portion of pipeline embedded in silt would be much more challenging because of the observed behavioural characteristics discussed earlier. A first attempt was made along the same lines as that for sand except that the elastic modulus was reduced by 70%, i.e. E_s = 960 kPa. While significant end rotation was obtained it was still significantly less than that observed and the stress wave was essentially half sinusoidal, i.e with zero end stresses. In an attempt to attract more stress towards the free end, total rotational restraint was imposed at the far end. While this boundary condition attracted significant stress towards the far end, the rotational restraint is contrary to the observed end rotation. On the other

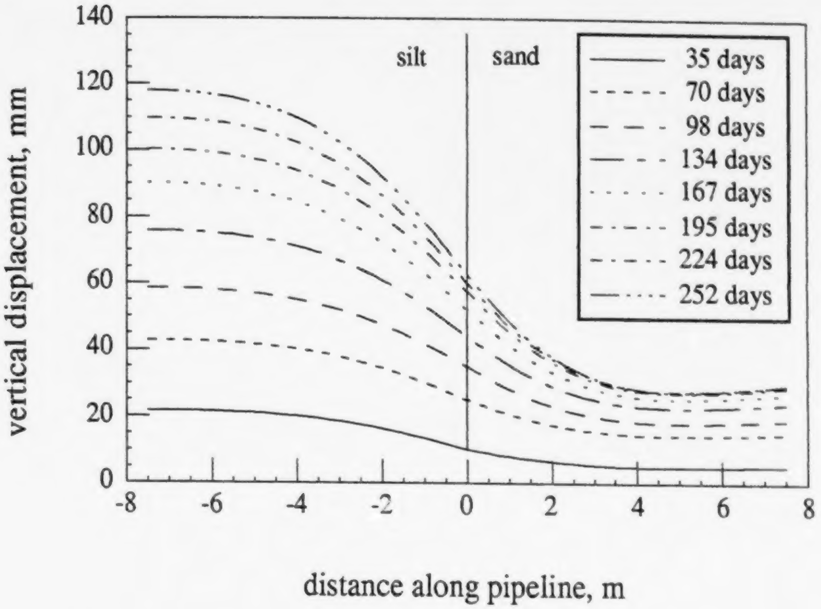

(a) predicted vertical displacement profiles during 1st freeze period

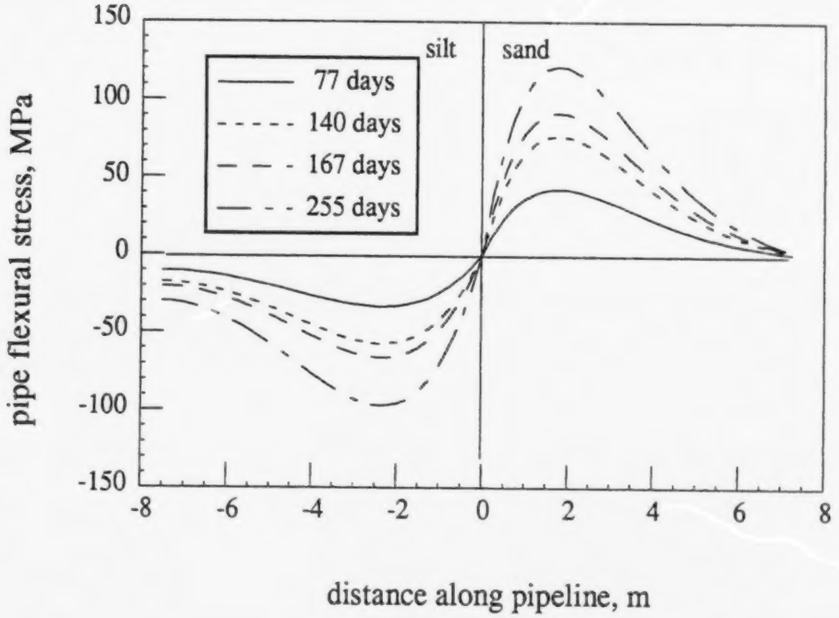

(b) predicted stress history profiles during 1st freeze period

Figure 4.16. Predicted vertical displacement and stress history profiles during 1st freeze period (fixed/ free conditions) for pipeline at Caen, France.

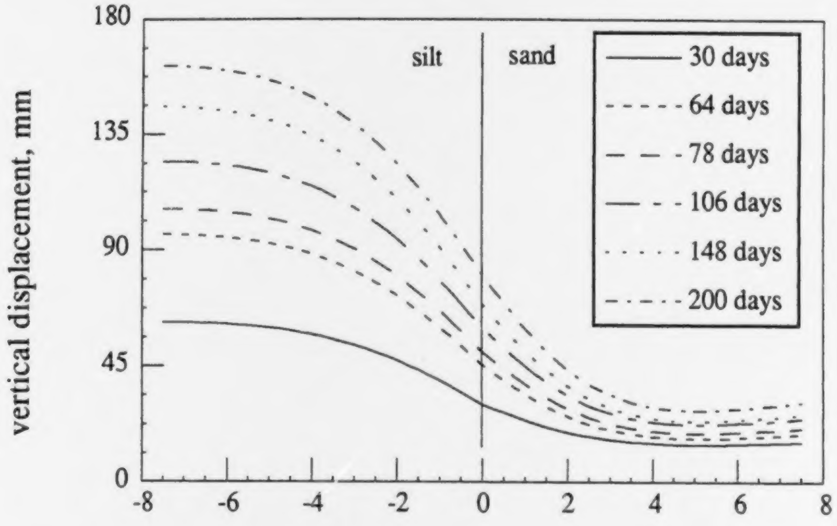

(a) predicted vertical displacement profiles during 2nd freeze period

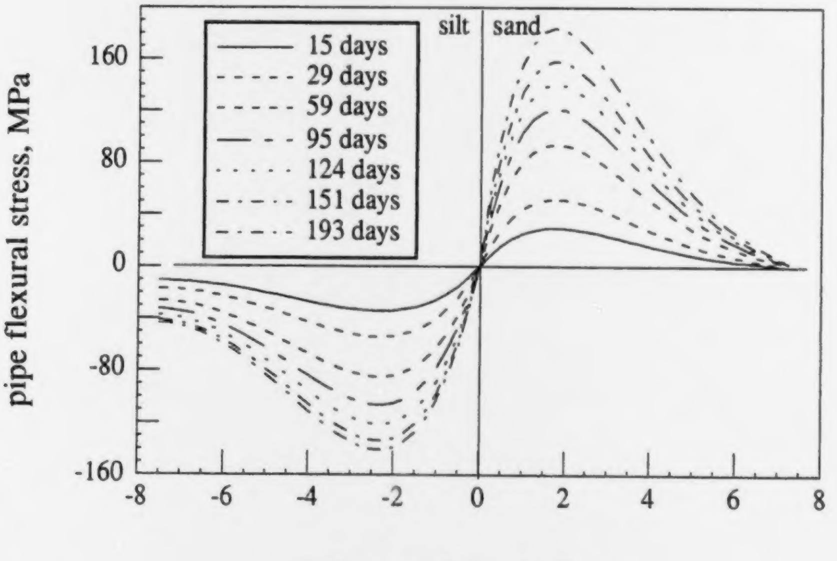

(b) predicted stress history profiles during 2nd freeze period

Figure 4.17. Predicted vertical displacement and stress history profiles during 2nd freeze period (fixed/free conditions) for pipeline at Caen, France.

hand, a significant increase in the peak stress was observed and the stress wave was not of the desired form when we imposed the measured prescribed end rotation. This leads us to conclude as discussed earlier that the frost heave characteristics of silt is subdivided into two zones each with its own particularities.

The simulations were carried with the intention of matching magnitudes of observed with predicted stresses. The predicted vertical displacement profile of the pipeline automatically matched the profile for the portion of pipeline embedded in sand but the predicted displacements were higher at the far end than those measured for the portion of pipeline embedded in silt.

Conclusions

The behavioural characteristics of the pile lateral load tests in frozen soil and a pipeline at Caen subjected to frost heave have been critically reviewed. Anomalies in the responses of the field tests have been identified and discussed with possible consequences in reliable predictions. Displacement and stress histories have been simulated using a model based on a Winker model where the discrete springs are characterized by a material model following the Norton-Bailey relationship.

The primary difficulty in the simulations is in obtaining a satisfactory elastic response. Once this has been established the subsequent creep response is comparable with the observed response. The elastic response establishes a footprint of the stress wave in the creep medium as a result of the pile-frozen soil interaction. We found that we had to increase the flexural stiffness of timber piles to obtain comparable elastic responses. While the increase in flexural stiffness of timber piles can explain the difference in elastic response because of entrapped moisture in the wood matrix, a convincing argument could not be found for the short-term steel pile test (S-4-L). A similar increase in flexural stiffness of steel model piles was required to match elastic response. On the other hand, the pile head displacement rates for all piles was comparable to observed responses.

Unexpected behaviour for the portion of the pipeline embedded in silt is identified and several explanations are offered to explain this behaviour. A simple Winkler model based on finite elements is then used to simulate the response of the pipeline subjected to frost heave. While a good match is obtained between predicted vertical displacement and stress wave histories for the portion of pipeline in sand, the simulations fail to trace all the particularities of the response of the pipeline in silt. An attempt has been made to explain the differences. We have identified the need for an analytical procedure to quantify the attenuation of the free field frost heave to serve as a useful input for the analysis of a pipeline subjected to frost heave.

The Winkler model for a beam embedded in a creeping medium has been shown to be sufficiently robust to adequately analyze both piles under lateral loads and pipelines subjected to imposed frost heave movement respectively. The finite element discretization also permits the analysis of a pile embedded in a layered medium.

References

Baguelin, F., Frank, R., and Said, Y.H. 1977. Theoretical study of lateral reaction mechanism of piles. Geotechnique, **27**(3): 405-434.

Biot, M.A. 1937. Bending of an infinite beam on an elastic foundation. Transactions, ASCE Journal of Applied Mechanics, **59** (A1-A7).

Crowther, G.S. 1990. Analysis of laterally loaded piles embedded in layered frozen soil. ASCE Journal of Geotechnical Engineering Division, **116**(7): 1137-1152.

Dallimore, S.R. and Crawford, H. 1985. Experimental observations of differential heaving and thaw settlement around a chilled pipeline. *In* Pipelines and Frost Heave. Proceedings of a seminar held at Centre de Geomorphologie, Caen, France. v + 75p.

Domaschuk, L. Fransson, L. and Shields, D.H. 1988. Interaction between a laterally loaded pile and frozen soil. Proceedings of the Fifth International Conference on Permafrost, Trondheim, Norway. Vol. 2, pp. 1060-1065.

Foriero, A. and Ladanyi, B. 1990. Finite element simulation of behaviour of laterally loaded piles in permafrost. ASCE Journal of Geotechnical Engineering Division, **116**(2): 266-284.

Foriero, A. and Ladanyi, B. 1991. Generalized finite element algorithm for laterally loaded piles in permafrost in comparison with measurements. Canadian Geotechnical Journal, **28**: 523-541.

Geotechnical Sciences Laboratories, Carleton University. 1986. Investigations of frost heave as a cause of pipeline deformation. Internal report - IR 50. Report prepared for Earth Physics Branch, Energy, Mines and Resources Canada, 71p.

Geotechnical Sciences Laboratories, Carleton University. 1988. The third freeze cycle of the Canada-France ground freezing experiment. Internal report - IR 54. Report prepared for Permafrost Research Section, Terrain Sciences Division of Geological Survey of Canada. 78p.

Geotechnical Sciences Laboratories, Carleton University. 1989. Canada-France pipeline-ground freezing experiment. Internal report - IR 58. Report prepared for Permafrost Research Section, Terrain Sciences Division of Geological Survey of Canada. 81p.

Götz, K.H., Hoor, D., Möhler, K. and Natterer, J. 1989. Timber design and construction handbook. McGraw-Hill, New York.

Kaplar, C.W. 1969. Laboratory determination of dynamic moduli of frozen soils and of ice. U.S. Army Cold Regions Research and Engineering Laboratory, Hanover, NH. Technical Report 163. 45p.

Konrad, J.-M. and Morgenstern, N. 1984. Frost heave of chilled pipelines buried in unfrozen soils. Canadian Geotechnical Journal, **21**: 100-115.

Ladanyi, B. 1972. An engineering theory of creep of frozen soils. Canadian Geotechnical Journal, **9**: 63-80.

Ladanyi, B. and Eckardt, H. 1983. Dilatometer testing in thick cylinders of frozen sand. Proceedings of the Fourth International Conference on Permafrost, Fairbanks, Alaska, National Academy Press, Washington, DC., **1**: 677-682.

Ladanyi, B. and Lemaire, G. 1984. Behaviour of a buried pipeline under differential frost heave conditions. Proceedings of Cold Regions Engineering Speciality Conference. Canadian Society of Civil Engineering. Montreal, pp. 161-176.

Matlock, H.M. 1970. Correlation for design of laterally loaded piles in soft clay. Proceeding of the Second Annual Offshore Conference, Houston, Texas. Paper No. 1204, **1**; 577-594.

McRoberts, E.C., Law, T.C. and Murray, T.K. 1978. Creep tests on undisturbed ice-rich silt. Proceedings of the Third International Conference on Permafrost, Edmonton, Alberta. **1**: 539-545.

Morgenstern, N.R., Roggensack, W.D. and Weaver, J.S. 1980. The behaviour of friction piles in ice and ice-rich soils. Canadian Geotechnical Journal, **17**: 405-415.

Morin, P., Shields, D.H., Kenyon, R., Domaschuk, L and Frank, R. 1991. Predicting creep displacements of laterally loaded piles in ice and ice-rich materials. Proceedings of the First International Offshore and Polar Engineering Conference, Edinburgh. pp. 535-542.

Neukirchner, R.J. and Nixon, J.F. 1987. Behaviour of laterally loaded piles in permafrost. ASCE Journal of Geotechnical Engineering Division, **113**(1): 1-14.

Nixon, J.F. 1984. Laterally loaded piles in permafrost. Canadian Geotechnical Journal, **21**(3): 431-438.

Nixon, J.F. 1985. A method for predicting frost heave of buried chilled pipelines. *In* Pipelines and Frost Heave. Proceedings of a seminar held at Centre de Geomorphologie, Caen, France. v + 75p.

Nixon, J.F. and McRoberts, E.D. 1976. A design approach for pile foundations in permafrost. Canadian Geotechnical Journal, **13**: 40-57.

Nixon, J.F., Morgenstern, N.R. and Ressor, S.N. 1983. Frost heave-pipeline interaction using continuum mechanics. Canadian Geotechnical Journal, **20**: 251-261.

Reese, L.C. 1975. Laterally loaded piles. Proceedings of the Seminar Series, Design, Construction and Performance of Deep Foundation, Geotechnical group and Continuing Education Committee, San Francisco Section, ASCE, University of California.

Reese, L.C. 1977. Laterally loaded piles:program documentation. ASCE Journal of Geotechnical Engineering Division, **103**(4): 287-305.

Rowley, R.K., Watson, G.H. and Ladanyi, B. 1973. Vertical and lateral pile load test in permafrost. Proceedings of the Second International Conference of Permafrost, Yakutsk, North American Contribution, pp. 712-721.

Rowley, R.K., Watson, G.H. and Ladanyi, B. 1975. Prediction of pile performance in permafrost under lateral load. Canadian Geotechnical Journal, **12**: 510-523.

Sego, D.C., Shultz, T., Banasch, R. 1982 Strength and deformation behaviour of frozen saline sand. Proceedings, Third International Symposium on Ground Freezing, CRREL, Hanover, NH. pp. 11-17.

Selvadurai, A.P.S. 1988. Mechanics of soil-pipeline interaction. Proceedings of the Annual Conference of The Canadian Society for Civil Engineering, Calgary, **3**: 151-173.

Shen, M. and Ladanyi, B. 1987. Modelling of coupled heat, moisture and stress field in freezing soil. Cold Regions Science and Technology, **14**: 237-246.

Vesic, A.S. 1961. Bending of beams resting on isotropic elastic solid. Proceedings of ASCE, **87**(EM2): 35-51.

Proceedings of ASCE, **87**(EM2): 35-51.

Weaver, J.S. 1979. Pile foundations in permafrost. Ph. D. thesis, University of Alberta, Edmonton. Alberta. 225p.

Nomenclature

The following symbols are used in this chapter:

b = beam width, pipeline or pile diameter
B = creep proportionality constant
e = height of load application above ground level
E = beam (pile or pipeline) elastic modulus
E_s = soil elastic modulus
I = beam moment of inertia
k_s' = foundation subgrade modulus
L = length of pile below ground level
m = elastic exponent for instantaneous response
n, s = creep exponents in Norton-Bailey relation
T = Temperature in Celsius
t = time
w_e = elastic displacement
w = transverse displacement in the z-direction
x = longitudinal coordinate axis
z = axis normal to x-axis

β = elastic characteristic length

$\dot{\varepsilon}_o$ = proof strain rate

γ = soil weight density

ν_s = soil Poisson's ratio

σ, σ_o = stress and proof stress

Chapter 5

UPLIFT OF MODEL STEEL PIPELINES EMBEDDED IN POLYCRYSTALLINE ICE[1]

Introduction

Over the past decade several proposals have been put forward for the construction of a gas pipeline from the arctic to the southern populated areas of North America (ASCE, 1978). These pipelines must be buried because of regulatory requirements which are intended to minimize environmental damage. It has been suggested that by transporting gas at below freezing temperatures (i.e chilled gas) the thawing of permafrost soils would be avoided. The transmission of chilled gas would lead to freezing of unfrozen soils in zones of shallow and discontinuous permafrost. A frozen annulus will develop in a frost susceptible soil around the gas pipeline leading to significant water migration to the freezing front and the formation of ice lenses. Consequently, the induced frost heave will force the pipeline to move upwards. The pipeline will undergo substantial straining which can lead to the formation of wrinkling buckles, specially when the pipeline traverses a transition zone between two soils with different frost susceptibilities or between an unfrozen and previously frozen soil. Ever since the chilled gas pipeline concept was proposed, the effect of frost heave on the performance of pipelines was identified as an important issue that should be addressed. A designer would have to determine the level of strains that can be tolerated in a pipeline before serviceability is seriously hindered and ultimately if structural integrity is to be assured.

---

[1] A version of this chapter is to be submitted for publication to The Canadian Geotechnical Journal: Rajani, B. and Morgenstern, N., 1992. Experimental Response of Steel Model Pipelines embedded in Polycrystalline Ice.

To date, only one experimental pipeline facility has been setup (Caen, France) that attempts to monitor the development of strains in the pipeline as frost heave develops. A lot of economical and experimental effort has been devoted to obtain this unique set of data and indeed the data can be very useful in the validation of models on frost heave, frozen soil-pipeline interaction, etc. The details of the experimental data are available through numerous reports (Dallimore and Crawford, 1985; Geotechnical Sciences Laboratories, 1986, 1988, 1989).

The pipeline (0.273 m x 0.0048 m) tested at Caen never experienced strains beyond the elastic strain limit. The pipeline underwent four freeze-thaw cycles and since the response of the pipeline during each cycle was slightly different, the interpretation of the responses led us to infer that factors such as homogeneity of creep soil properties need to be addressed as discussed previously in chapter 4. A major source of uncertainty in the field experimental studies as those performed at Caen, France, is in the geomechanical (both elastic and creep) properties. As indicated in chapter 3, the elastic and creep properties are crucial to the reliable prediction of stresses in the pipeline. The elastic moduli obtained from test samples on sand and silt were unusually high as discussed in chapter 4. In addition, the reported creep exponent, n, in the Norton creep flow law for silt is presumed to be on the high side. Small scale laboratory model testing, where careful control can be exercised over the different aspects of the frozen soil-pipeline interaction, is warranted and the results would serve to complement some of the observations at the Caen experimental facility. It would also lead to a better understanding of the frozen soil pipeline interaction problem. These tests are also intended to validate findings of chapter 3 on the behaviour of an embedded beam in a creeping medium. Another objective of carrying out these tests was to develop sufficient resistance to uplift in the model pipelines so that portions of the pipeline would strain beyond the elastic limit and well beyond the currently accepted strain limits. These arguments provided a basis for carrying out scaled laboratory testing of model pipelines in polycrystalline ice.

Nixon (1984) performed experiments on solid model piles embedded in polycrystalline ice but several aspects such as shallow embedment, imposed displacements or the implications of a thin tubular section (i.e radius thickness ratio) were not addressed. More recently, Foriero and Ladanyi (1991) have performed lateral load tests on aluminium (tubular) and steel (solid) model piles embedded in frozen sand but again aspects of particular interest to pipelines were not studied. These aspects would not normally be of major concern for the design of laterally loaded piles.

In a realistic scenario, frost penetration would proceed on the commencement of transportation of chilled gas and frost heave in the frost susceptible soil would develop subsequently. It is reasonable to assume that the frost advance takes place in a relatively short period of time while the development of frost heave is a much slower process. The testing of a model pipeline embedded in polycrystalline ice assumes that the freezing of the surrounding soil in the field takes place instantaneously. This assumption may not be too far from reality since the soil adjacent to the pipeline contributes the most uplift resistance and data available from the Caen facility supports this view.

Equipment design

The experimental setup to study pipeline-polycrystalline ice interaction involves three basic aspects: (i) the proportioning of the model pipelines and of the surrounding polycrystalline ice sample, (ii) the preparation of the ice block sample itself and (iii) the loading arrangement that adequately represents frost heave. Each of these aspects will be described in detail followed by experimental observations of the model pipelines subjected to an end prescribed displacement rate.

A prototype pipeline crossing the zone of discontinuous permafrost would be subjected to high strains in that portion of the pipeline embedded in a previously unfrozen soil. The response of the pipeline subjected to a steady frost heave at the interface of the discontinuous permafrost would have nearly double curvature if the stiffness of the frozen soil were quite high. The experience at the Caen experimental facility (Dallimore and

Crawford, 1985) indicates that the nearly double curvature response exists in spite of the relatively shallow burial of the pipeline. The plane strain study, performed by Nixon *et al.* (1983) of a continuum where one half of the soil was frost susceptible and the pipeline was considered to be passive, indicated that the response had double curvature. These considerations indicate that it would suffice to model only one-half of the pipeline thus leading to a much simplified experimental design.

Proportioning of the model pipeline and polycrystalline ice block sample

Pipeline structural integrity must be assured at all time during the operation of the pipeline. In the present context, we do not consider the effects of internal pressure or the temperature differential since the worst case scenario would be when these conditions are absent. Flexural strains are induced in the pipeline wall as the pipeline is subjected to increasing differential frost heave movement and thus eventually causing wrinkling (local buckling) in the pipeline. Hence, the design criterion in order to contain damage due to rupture and leakage of contents is to limit the compressive strain. Two distinct buckling failure modes (Yun and Kyriakides, 1990) have been found to occur for buried pipelines. One failure mode is when the pipeline buckles as an overall beam (Euler-type buckling) and usually this mode would be expected when the pipeline is stocky (low R/t ratio) and very large axial loads are present. The other failure mode is when the principal action is flexural and the resistance is through shell action (thin-walled pipelines), thus enhancing the formation of local wrinkles. It is the latter approach that is more appropriate in the present context. Several criteria have emerged over the years (Southwell, 1914; Wilson and Newmark, 1933; Bouwkamp and Stephen, 1973; Kennedy *et al.*, 1977; Hall and Newmark, 1978; Langner, 1984; Nyman and Lara, 1986; Gresnigt, 1986) for limiting flexural strain in tubular pipes. It is not the intent here to provide an exhaustive review of the wrinkling strain criterion since a brief review has been recently undertaken by Kim and Velasco (1988). The critical strain is expressed in two general forms:

[5.1] $$\varepsilon_c = 0.605ct/R$$

[5.2] $$\varepsilon_c = (2t/R)^2$$

The first expression corresponds to the form of a theoretical solution based on elastic buckling developed by Southwell (1914). The second expression stems from a best fit of the experimental data (Sherman, 1976; Langner, 1984) that distinguishes failures between whether local buckling was observed or not. The constant 0.605 has been determined by Southwell (1914) for elastic buckling and the constant 'c' was introduced by Wilson and Newmark (1933) to account for experimental deviation. The value of c varies from 1.0 for perfect tubes to 0.25 for manufactured tubes. The lower values of 'c' reflect the importance of initial imperfections present in the geometry of the pipe as shown by Kyriakides *et al.* (1983). It is also important to note that all criteria based on limiting strain were established from experiments on steel tubes performed in air, i.e. with no restraint from the surrounding medium. The different existing criteria based on experimental tests are summarized in Table 5.1. Since the critical strain is predominantly a function of the radius-thickness ratio, the present model pipelines were proportioned so that the model design would be within the range of probable prototype design. For instance, the pipeline at Caen has a R/t ratio of 28.44. Consequently, for the present experiments two model stainless (seamless) steel pipelines with R/t ratios of 21.43 (19.05 mm x 0.89 mm) and 20.40 (25.4 mm x 1.24 mm) were selected. These sizes were readily available in the market and yet of adequate size that permitted the easy installation of resistance strain gauges on the model pipelines.

An important aspect that needed to be addressed was to suitably dimension the box where the model pipelines were to be embedded in the polycrystalline ice block sample. The length of the box was sized in accordance with the stress wave length that would be set up along the pipeline. The elastic modulus of polycrystalline ice is dependent on the rate of loading, porosity, salinity and temperature (Michel, 1978). It can vary as much as 8 to 10 times less than that of pure ice as shown by Michel (1978) and Sinha (1989). Sego (1982) demonstrated that the secant elastic modulus for frozen sand is highly dependent on strain rate and that the reduction can be quite large. We conservatively selected the range of 40 to 50 MPa for the elastic modulus of polycrystalline ice for determining the size of stress wave that would be setup as a result of the prescribed displacement rate. The analysis of a pipeline embedded in a creeping medium discussed in chapter 3 indicated that we would require a pipeline length of approximately 32 to 40 diameters to represent the semi-infinite length of the pipeline. We note that the pipeline at Caen, France, had an approximate length/diameter ratio of 33. The width and the height of the box were based on the premise that, when considering the interaction of two adjacent laterally loaded piles, the interaction effects are disregarded if

Table 5.1. Summary of critical strain criterion for pipelines.

$$\varepsilon_c = 0.605ct/R$$

Reference	Critical strain criteria or constant 'c'	comments
Southwell (1914)	$c = 1$	classical elastic solution.
Wilson and Newmark (1933), Hall and Newmark (1978)	$c = 0.25$ to 0.333	experimentally established; tests performed on 58 tubes: (4") Shelby tubes and other fabricated specimens).
Boukamp and Stephen (1973), Kennedy *et al.* (1977)	$\varepsilon_c = 0.004$ to 0.006	based on 8 tests on large diameter (48") pipes.
Langner (1984), Nyman and Lara (1986)	$c = 0.413$	over 40 6" pipes tested in air and other experimental data.
Gresnigt (1989)	$\varepsilon_c = 0.25t/R - 0.0025$	experimental fit to a data from a range of tests.

the piles are spaced at least 3 to 4 diameters. In order to satisfy this criterion as well as to ensure minimal boundary effects, the box was sized to 0.60 m in width and 0.40 m in height. The box for the sample was manufactured from 18 mm (3/4") thick PVC sheets as shown in Figure 5.1. Table 5.2 compares the principal characteristics of the pipeline at Caen and the model pipelines tested in this study.

Preparation of a polycrystalline ice block sample

The mechanical behaviour of frozen soil has been studied by Sayles (1973), Sayles and Haines (1974), Sego and Morgenstern (1983) and others. It is now widely accepted that ice-rich frozen soil behaves like a creeping material. The frozen-soil surrounding the pipeline subjected to frost heave will be associated with primary and secondary creep phases of straining. The classical studies of Glen (1955) indicate that the flow law of polycrystalline ice is that of the Norton type. The Norton creep relationship rewritten in the generalized form as proposed by Ladanyi (1972) is:

[5.3] $$\frac{\dot{\varepsilon}}{\dot{\varepsilon}_o} = \left(\frac{\sigma}{\sigma_o}\right)^n \quad \text{or} \quad \dot{\varepsilon} = B\sigma^n$$

where $\dot{\varepsilon}$ is the axial strain rate, σ is the axial stress, $\dot{\varepsilon}_o$ and σ_o are proof strain rates and proof stress, B and n are the creep constants. Typically, n is about 3 (Morgenstern *et al.* 1980) for ice or icy silts (McRoberts *et al.* 1978) subjected to low stresses. In search for a dependence of n and B on temperature, Morgenstern *et al.* (1980) found from analyses of available

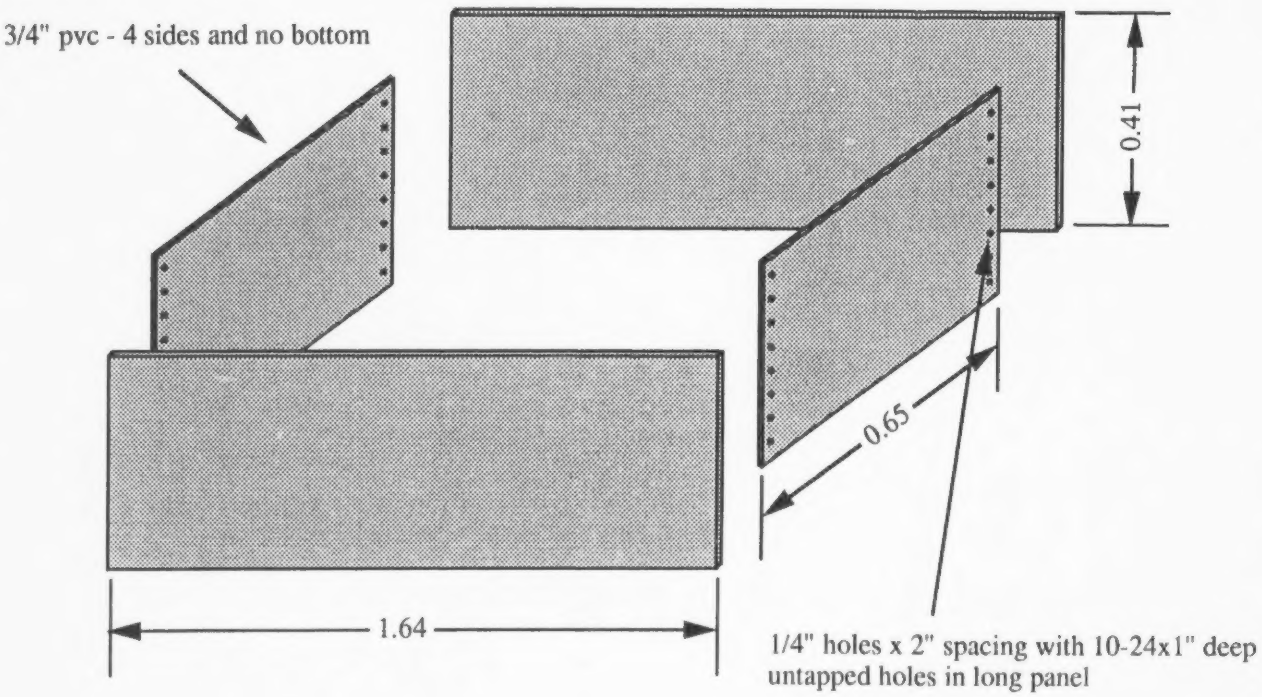
3/4" pvc - 4 sides and no bottom
0.41
0.65
1.64
1/4" holes x 2" spacing with 10-24x1" deep untapped holes in long panel

Note: All dimensions in meters unless otherwise specified and sketch not to scale.

Figure 5.1. Exploded view of PVC box for block sample ice.

Table 5.2. Comparison of prototype and model pipeline characteristics.

Parameter	Prototype at Caen	Model A	Model B
Pipeline structural characteristics			
pipeline diameter, D, m	0.273	0.0381 (1.5")	0.0508 (2")
pipeline thickness, t, mm	4.8	0.889 (0.035")	1.245 (0.049")
Pipeline material	steel	stainless steel 304	stainless steel 304
R/t pipeline ratio	28.44	21.43	20.40
Elastic modulus, E, GPa	210	193	193
Poisson's ratio, ν	0.3	0.3	0.3
Yield strength, σ_y, MPa	240	193	193
Bin size			
half width, m	9.0 (33D)	1.6 (42D)	1.6 (31D)
width, m	8.0 (29D)	0.6 (16D)	0.6 (12D)
height, m	1.7 (6D)	0.4 (10D)	0.4 (8D)
embedment, h, m	0.33 (1.2D)	0.04 (1.05D)	0.06 (1.18D)
Soil/ice characteristics			
elastic modulus, E_s, MPa	2.82 - sand 0.96 - silt	3 - 7 GPa	3 - 7 GPa
dry density, γ, kN/m^3	18.52 - sand 16.29 - silt	8.54	8.46
void ratio, e	0.40 - 0.44 - sand 0.59 - 0.63 - silt	0.06	0.07-0.08
Poisson's ratio, ν	0.3	0.32	0.34
Creeping material	sand/silt	ice	ice
creeping exponent, n	5.6 / 10.6	2.84	2.84

creep data that ice behaves close to a linearly viscous material at temperatures close to 0°C. The constant B is found to be dependent on temperature and soil type. Sego and Morgenstern (1983, 1985) have studied the behaviour of laboratory prepared polycrystalline ice and have indeed confirmed the applicability of the Norton-type power law. In the past, considerable attention has also been paid to the behaviour of polycrystalline ice primarily for glaciology studies as well as laboratory studies related to geotechnical problems. Polycrystalline ice is a good material to work with since control can be exercised over its characteristics (grain size, porosity, etc) in the laboratory. Sego and Morgenstern (1985) studied the indentation of a rigid disk on polycrystalline ice both experimentally and numerically using finite elements and they were able to obtain comparable behaviour.

The preparation of the block sample required the manufacture of ice that is commonly classified as T1 snow ice. The manufacture of polycrystalline ice has been reported by Sego (1980) and Jacka and Lile (1984). The most common technique is to provide snow crystals as seed, saturate the sample with near 0°C deaired water and subsequently freeze the sample unidirectionally. It was desirable to produce snow crystal seeds so that the final ice crystal size in the ice block sample was in the range of 1 to 2 mm since Sego and Morgenstern (1985) had previously studied the experimental indentation of a rigid disk in polycrystalline ice of this type. This meant that the snow crystals had to pass sieve #20 and be retained on sieve #40 as suggested by Sego (1980). However, past experience with the snow manufacturing has involved the production of only small quantities of snow which were usually obtained by scraping accumulated hoar frost on a cold plate in a freezer. Considering that a relatively large quantity (0.384 m^3) of snow crystals had to be manufactured, a first attempt at manufacturing snow was made using a mini-snow gun (Figure 5.2) supplied by Huff (1990). The chilled water channelled through the central nozzle of the gun is essentially atomized by the cold air entering through the annulus. The production was carried out in a cold room at -30°C. It was found that the water flow rate greatly influenced the snow crystal size and basically determined if the snow produced was wet or dry. Chen and Kevorkian (1971) and O'Byrne and Haynes (1973) also found that the air/water ratio had a significant influence on the quality of snow produced. Snow crystals with the desirable size were produced after several trials by adjusting the flow rate to 2 litres/minute and maintaining the air and water pressures at about 276 kPa (40 psi). The air flow rate was not controlled. A slight change in the above parameters determined if the snow was dry or wet and if snow production was possible at all. It is most probable that each particular snow gun would have its own specific set of air/water ratios and pressures to produce the desired quality of snow. The snow crystals were kept in a plastic bag for 72 hours before trial polycrystalline ice samples were prepared using a 0.10 m diameter mould. Trial samples were prepared by mounting the mould containing the snow-water slush on a freezing plate fed by liquid nitrogen. Subsequently, thin sections of polycrystalline ice samples were obtained as described by Sego (1980) to examine the grain size distributions. This method of snow production was abandoned since considerable effort would have to be dedicated to manufacture the quantity of snow required for the ice block sample. Consequently, similar sample moulds were prepared from natural snow and snow collected from an ice rink mechanized scraper from a nearby

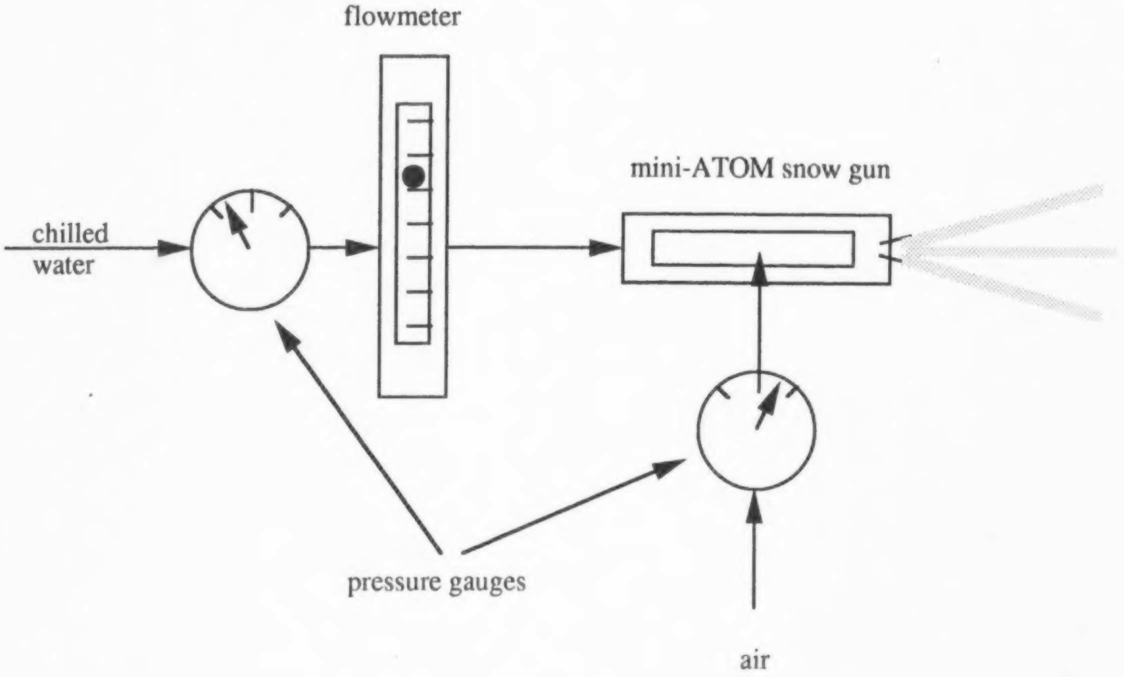
flowmeter
mini-ATOM snow gun
chilled water
pressure gauges
air

Figure 5.2. Schematic diagram for snow production using a mini-snow gun.

recreational facility. Thin sections prepared from these two alternative sources of snow showed no visible differences in polycrystalline ice grain size distribution. Therefore we proceeded to use natural snow because of abundant availability.

The next step was to prepare the polycrystalline ice block sample using the sieved snow crystals as described above. The PVC box was mounted on a loading frame arrangement as shown in Figure 5.3. Lateral struts ensured that the walls did not yield inwards while the vacuum was applied, thus avoiding any disturbance to the sample which could result in additional settling of the snow crystals. The natural snow crystals were sieved and those that passed sieve #20 but were retained on sieve #40 were collected. These pre-sieved snow crystals were rained from a large sieve (#20) positioned on top of the box until the box was filled. The application of a vacuum at the top of the box helped draw cold water at near 0^{o}C into the sample through two copper tubes (6.35 mm) with holes placed at the bottom of the sample box above the freezing plate (Figure 5.1). Normally it took about an hour to saturate the sample with an applied vacuum of 300 mm of mercury. The box was sealed very well using vacuum silicon in order to minimize air entry into the sample.

It was essential to freeze the sample unidirectionally as rapidly as possible to obtain a homogeneous block sample of ice. Snow crystals would otherwise grow beyond the desired size if too much time was allowed to elapse before freezing the snow-water slush. Unidirectional freezing was made possible by positioning the freezing plate at the bottom of the box and by thoroughly insulating the side panels of the box. The freezing plate

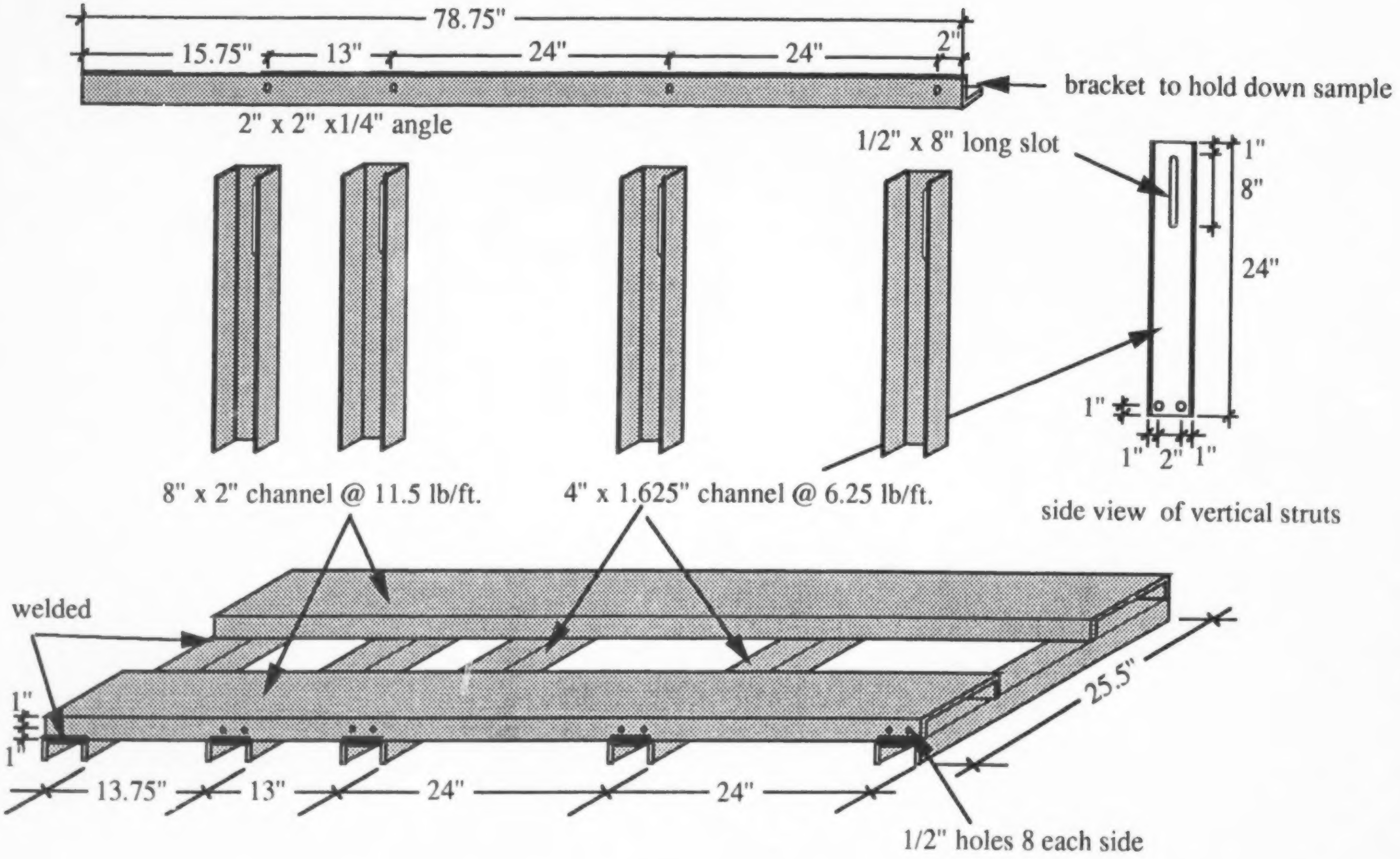
78.75"
15.75"
13"
24"
24"
2"
bracket to hold down sample
2" x 2" x1/4" angle
1/2" x 8" long slot
1"
8"
24"
1"
1"
2"
1"
8" x 2" channel @ 11.5 lb/ft.
4" x 1.625" channel @ 6.25 lb/ft.
side view of vertical struts
welded
1"
1"
25.5"
13.75"
13"
24"
24"
1/2" holes 8 each side

Figure 5.3. Test frame for mounting sample box (not to scale).

consisted of 4 - 6.35 mm copper tubes with holes (1 mm) at 45° sandwiched between two aluminium 12.7 mm plates. The sample was frozen by feeding liquid nitrogen through 6.35 mm copper tubes so that the liquid nitrogen squirted out towards the upper aluminium plate (Figure 5.4). Several spacers between the aluminium plates tied the plates together to avoid their separation as the nitrogen was drawn into the aluminium wafer at a slight pressure. The design of the freezing plate was based on the principle of delivering liquid nitrogen equally throughout the surface of the freezing plates to ensure uniform freezing. It was also found necessary to bolt down the freezing plate to the bottom frame in order to avoid significant warping of the plate during freezing and hence minimize the disturbance of the rained snow particles saturated with near 0°C water. Two layers of insulation were placed between the test frame and the freezing plate to ensure that heat was extracted principally from the snow-water slush. This particular design was adopted after attempting several alternative designs that produced non-uniform freezing. The pipeline was positioned on guides attached to the front and back panels of the sample box so that the polycrystalline ice cover was approximately equal to the external diameter of the pipeline. It normally took four days to freeze the sample and one nitrogen bottle (160 litres) was changed every 24 hours. The final freezing trial was only carried out with the model pipeline placed in the snow-water slush after the several operational problems with the freezing system had been weeded out.

Loading arrangement

It was essential to apply a displacement rate at the pipeline end that

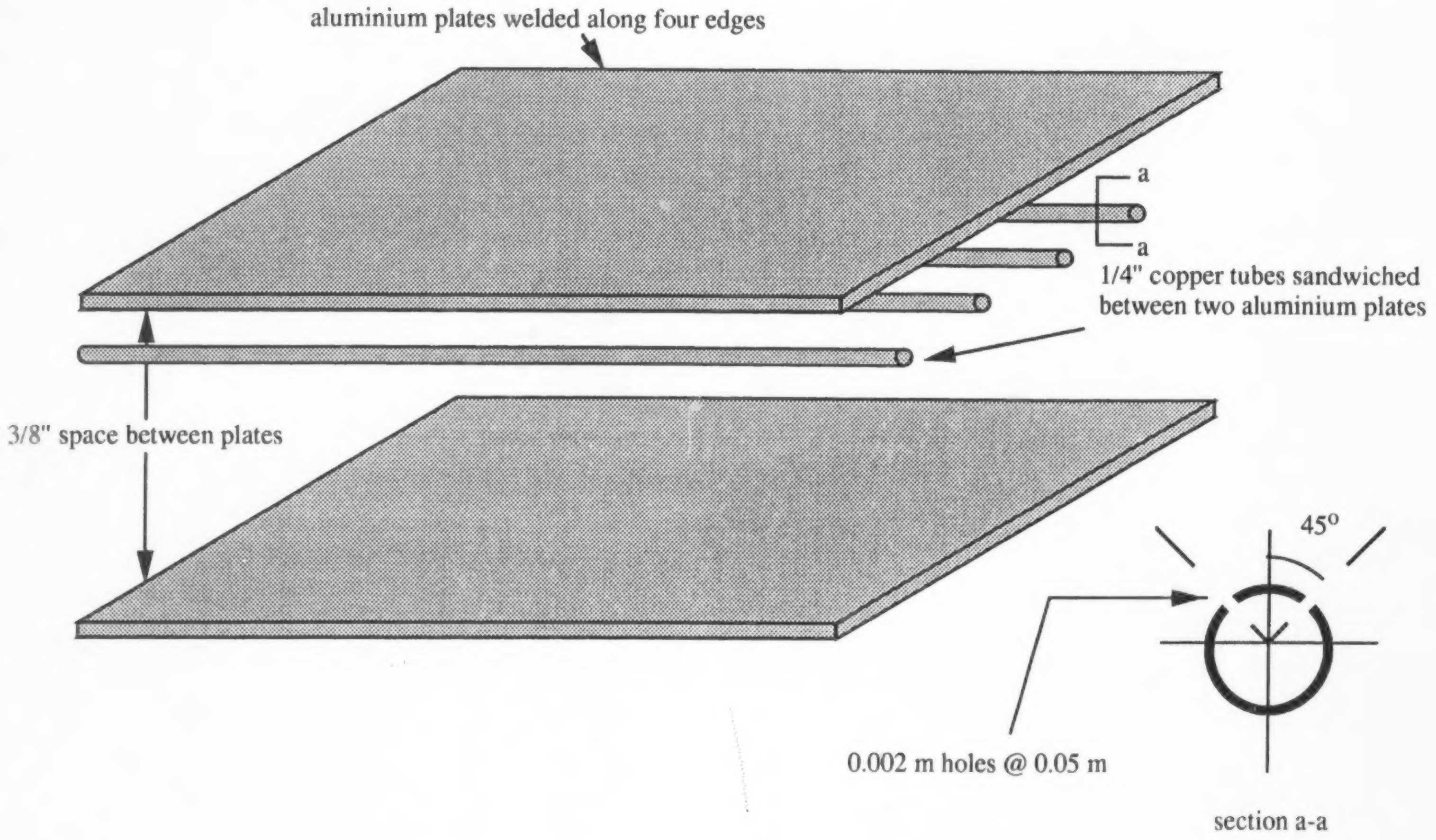
aluminium plates welded along four edges
a
a
1/4" copper tubes sandwiched between two aluminium plates
3/8" space between plates
45°
0.002 m holes @ 0.05 m
section a-a

Figure 5.4. Exploded view of the freezing plate wafer (not to scale).

closely resembled possible field displacement rates as a result of frost heave. At the same time the displacement rate should be slow enough so that strains are in the ductile range of ice deformation The frost heave rate in Caen silt observed at Caen, France, was in the order of 3×10^{-4} mm/minute which is fairly typical for silty soils. Sego (1980) carried out punch tests on polycrystalline ice at typical penetration rates of $3.83 - 18.3 \times 10^{-4}$ mm/minute. Consequently, a Wykeham Farrance 10 kN capacity press was adapted using a slow motor of 24 minutes/revolution to obtain a displacement rate of 1.72×10^{-4} mm/minute. The loading arrangement is shown in Figure 5.5 and Plate 5.1. The horizontal bars (0.025 m x 0.025 m) of the hangar system were not as stiff as initially anticipated for the test on pipeline model A. After completion of the test on pipeline model A, it was observed that the bars had undergone permanent plastic deformation. A calibration test was carried out on the hangar system and it was found that the displacement rate at the pulling end of the pipeline was about one third of that measured at the platen of the Wykeham Farrance machine. This reduced displacement rate was used for the finite element analysis discussed later. As a consequence, much stiffer horizontal bars (0.025 m x 0.050 m) were used for pipeline model B with the intention of reducing the compliance in the loading hangar.

Instrumentation

The model pipelines were instrumented with resistance strain gauges along the length of the pipeline. Strain gauges were located at both top and bottom for the first model pipeline (19.05 mm x 0.89 mm) and a full wheatstone bridge was established between them so as to avoid problems

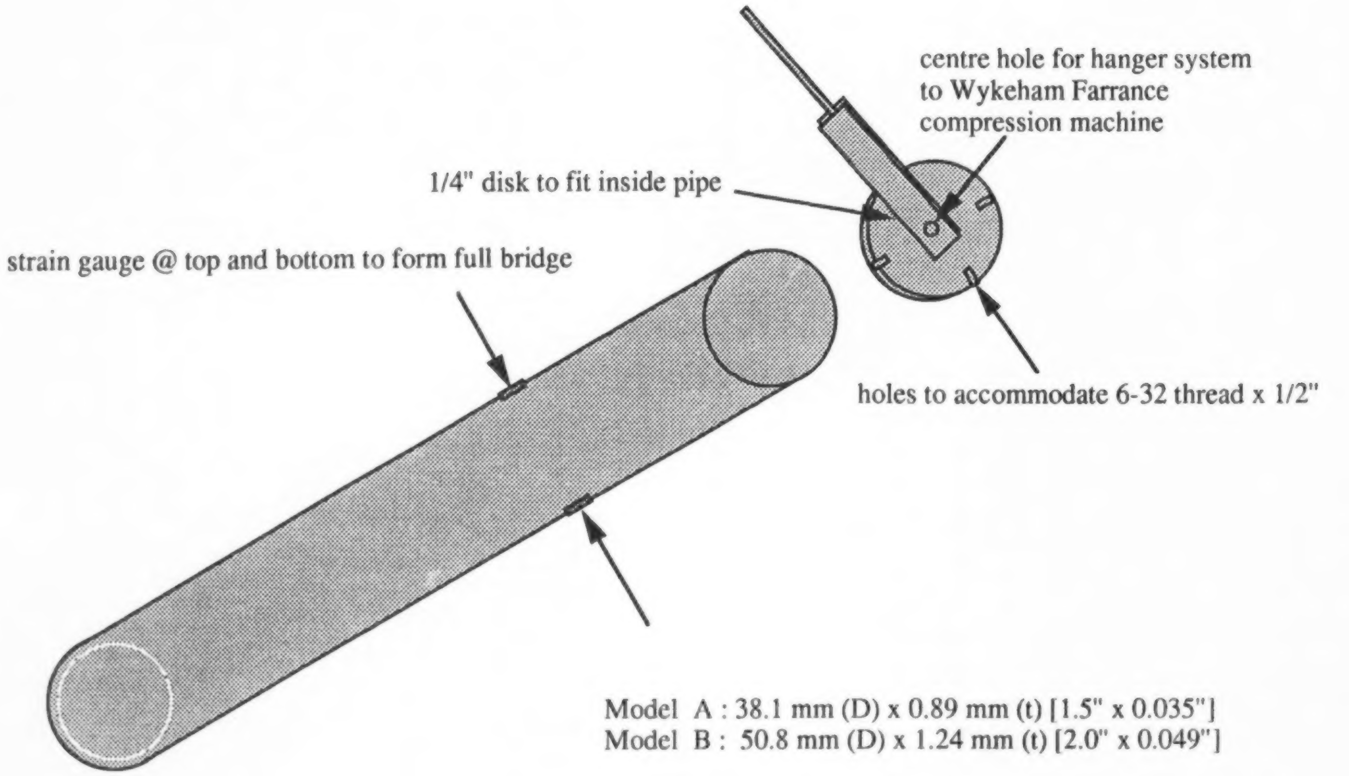
centre hole for hanger system
to Wykeham Farrance
compression machine
1/4" disk to fit inside pipe
strain gauge @ top and bottom to form full bridge
holes to accommodate 6-32 thread x 1/2"
Model A : 38.1 mm (D) x 0.89 mm (t) [1.5" x 0.035"]
Model B : 50.8 mm (D) x 1.24 mm (t) [2.0" x 0.049"]

Figure 5.5. Typical strain gauge arrangement and hanger system for applying displacements.

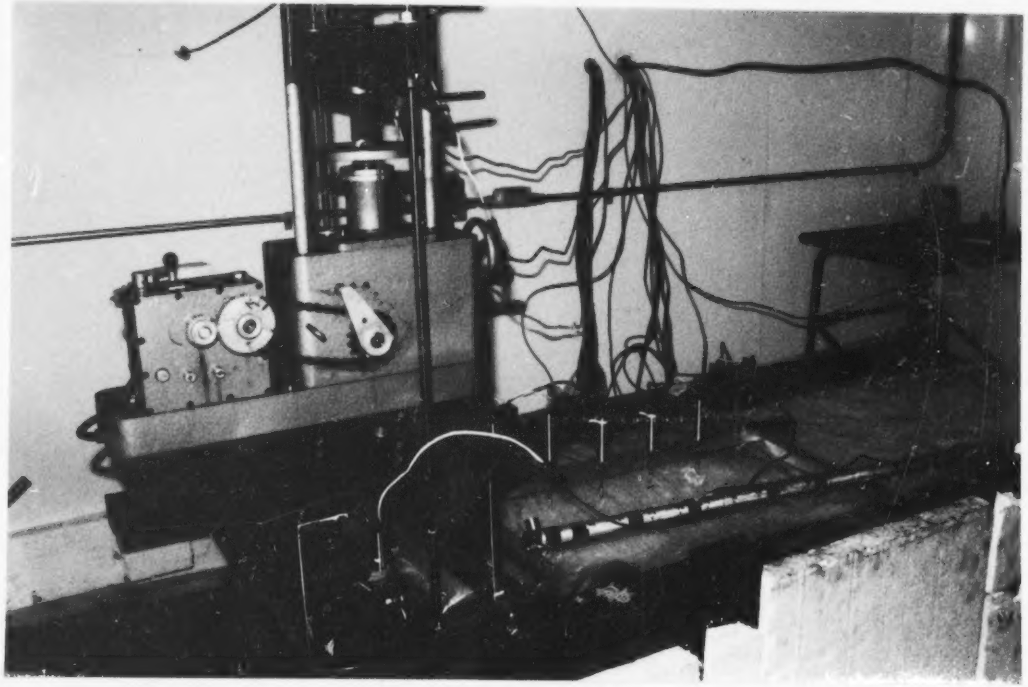

Plate 5.1. General loading arrangement of an embedded model pipeline.

with temperature compensation. Though this approach permitted the use of a reduced number of strain gauges, it was recognized that the true local strain in the pipeline would be difficult to ascertain. Consequently, independent top and bottom strain gauges were used for model pipeline B (25.4 mm x 1.24 mm) in order to remove any possible uncertainty. The strain gauges on the model pipeline A were protected by wrapping the pipe with a heat shrink teflon type material (FIT 221 produced by Alfa Wire Corporation). The teflon material was also chosen to represent some sort of field coatings. Since an adequate size of heat shrink was not available for the model pipeline B, a different wrapping material (Nitto Butyl - 2" self vulcanization rubber tape) was used. The model pipelines were calibrated prior to testing under a cantilever loading arrangement. In addition, the movement of the platen of the compression machine and the corresponding force imposed on the pipeline were monitored by a LVDT (Linear Voltage Displacement Transducer) and a load cell respectively. The displacements along the pipeline close to the loaded end were monitored using closely spaced LVDTs. The LVDTs were placed at the crest of the pipes through holes drilled in the ice block sample A. An alternative procedure was used for pipeline model B where thin tubular stems were attached to the crest of the pipeline prior to freezing. These tubes acted as guides for free movement of the LVDT rods. The Hewlett Packard 24 DCDT LVDTs are capable of measuring displacements to an accuracy of 0.0012 mm. All the data was logged automatically every two hours by a PC for easy retrieval using an electronic spreadsheet.

Elastic and creep properties of polycrystalline ice

Intact core samples of 0.1 m (diameter) x 0.3 m (height) were taken from the ice sample blocks where the pipeline models were tested using a CRREL coring barrel. Thin sections obtained from typical samples (Plate 5.2 and 5.3) examined under polarized light showed near uniformity of crystal size and the background grid (10 mm x 10 mm) permitted a rough estimate of the size of the individual crystals. The thin sections were obtained by the hot-plate method as described by Sego (1980). There were concerns that perhaps the hot-plate may modify the ice crystal structure and therefore thin sections were also obtained using microtome equipment. Plate 5.2 shows that if indeed there were any changes in the ice crystal structure either due to thermal or mechanical stresses they are not readily perceptible to the naked eye. It was difficult to produce very thin sections with the microtome without the risk of cracking as the section got thinner. The rest of the thin sections were prepared using the hot-plate procedure because it was found to be very amenable. The sonic elastic properties were obtained using piezoelectric crystals that detected the arrival of P- and S-waves. The testing procedure used is given in detail by Instanes (1992). Typical value for dynamic elastic moduli were within 3 to 7 GPa range. Typical constant load tests were carried out on 0.10 m (4") samples (typically height diameter ratio was 2) at different loads. The procedure for the constant load creep test was essentially as outlined by Sego (1980), except that a multi-staged loading procedure was applied on most samples. Normally, the load was increased or decreased after considerable deformation at steady state had taken place. Typical axial strain time histories for two of the samples are shown in Figures 5.6 and 5.7 while the axial strain time histories for other samples are included in the Appendix. The strain histories indicate that at low stresses (i.e. < 210 kPa) primary creep had terminated after about 100 to 150 hours. The constant load creep

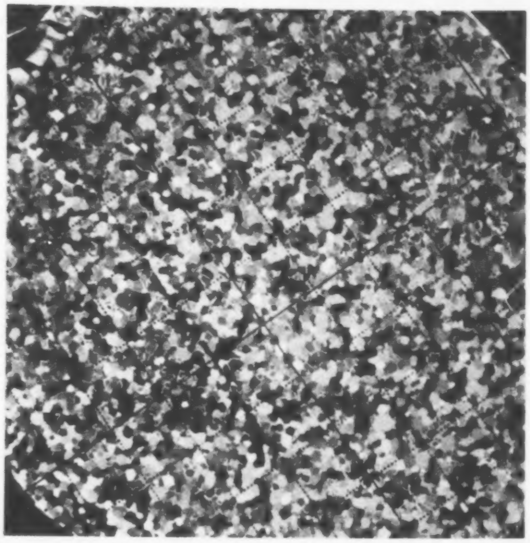

(a) thin section of ice using hot-plate

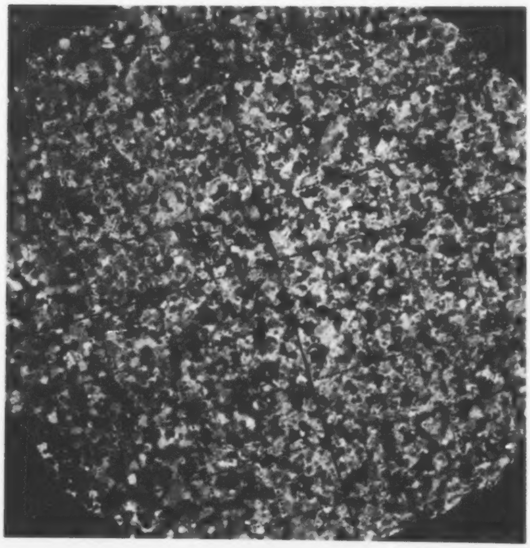

(b) thin section of ice using microtome

Plate 5.2. Thin sections of ice polycrystalline samples from upper 0.10 m of block sample A using the hot-plate and microtome.

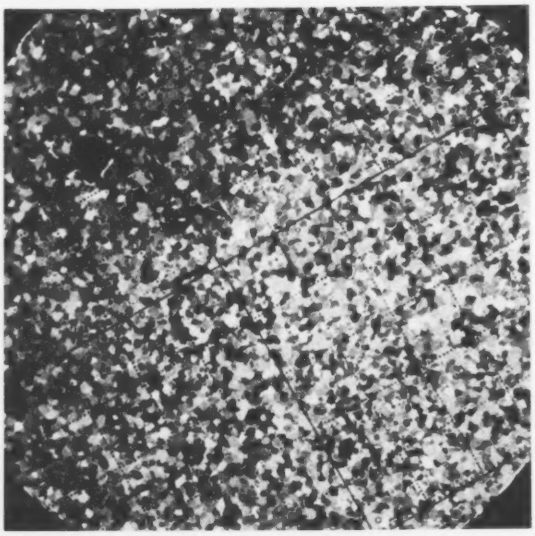

(a) thin section at top of ice block sample using hot-plate

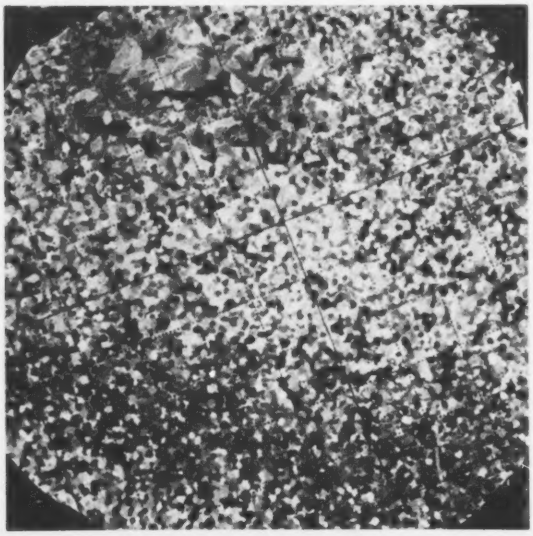

(b) thin section at bottom of ice block sample using hot-plate

Plate 5.3. Thin sections of ice polycrystalline samples from top and bottom block sample B using hot-plate.

test at 400 kPa (Figure 5.A1) shows that the primary and secondary portions of creep were very small and, in fact, tertiary creep approached after approximately 300 hours. The experimental results of the creep multi-staged constant load tests are summarized in Table 5.3. The samples were tested at a temperature as close as possible to that of the pipeline which was essentially at -3^{o}C. The performance of RTDs was found not to be very satisfactory because, though all three test cells were fed from the same bath, the RTD from each sample responded differently. The strain rates were calculated from the steady state response of each sample and were corrected only for temperature as suggested by Sego (1980). Sego's correction formula was used since in the present set of experiments sufficient data on temperature variation was not available to apply an alternative correcting procedure. A grain size correction was not deemed necessary since the ice crystals in present samples were within the 1 mm range and the fact that Sego's (1980) data is normalized with respect to a crystal size of 1 mm. The corrected normalized displacement rates are shown in Figure 5.8 together with data from Sego (1980) and others. Morgenstern *et al.* (1980) have reviewed thoroughly available data on creep properties of ice and they have determined the influence of temperature. The creep test results from the present series of tests on polycrystalline ice were analyzed together with other relevant data shown in Figure 5.8 and the creep constant B and n were obtained. Table 5.4 shows these creep properties together with those obtained by Morgenstern *et al.* (1980). The data from tests on polycrystalline ice reported here serves to confirm that the creep properties of the ice block samples prepared for testing the model pipelines are within the expected range. The creep properties (corrected for temperature) established by

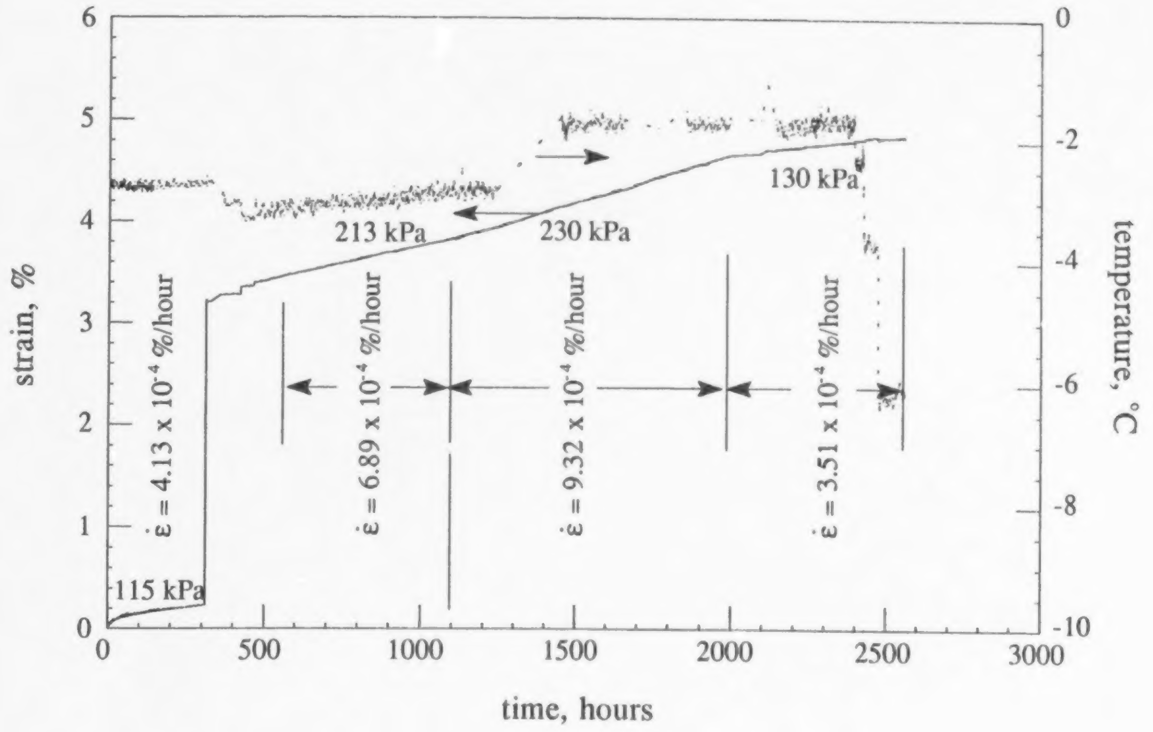

Figure 5.6. Constant load creep test for polycrystalline ice sample T1-10/91.

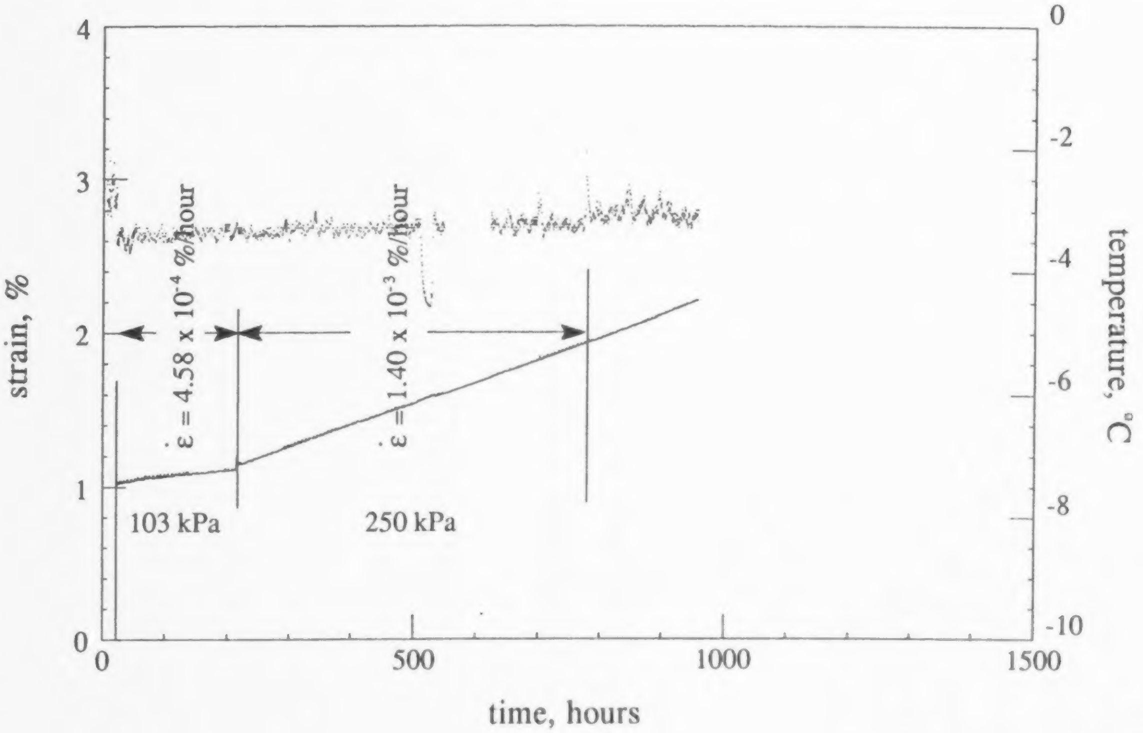

Figure 5.7. Constant load creep test for polycrystalline ice sample B7-02/92.

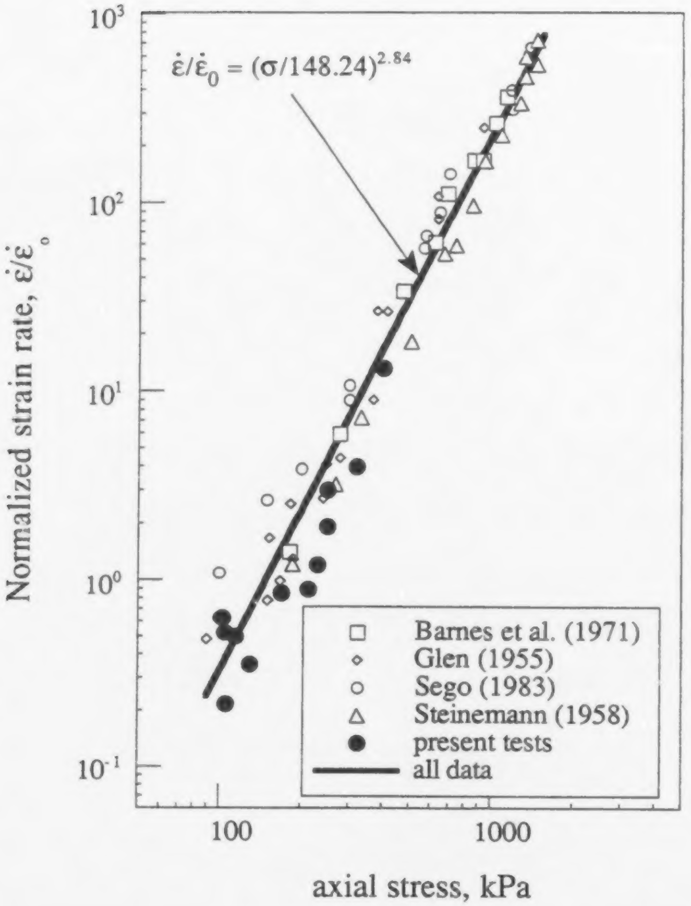

Figure 5.8. Corrected normalized strain rate versus axial stress for polycrystalline ice at -2°C.

Table 5.3. Summary of constant load creep test on samples of polycrystalline ice.

Sample	density Mg/m^3	temperature ^oC	stress kPa	corrected strain rate
T1-10/91	0.876	-2.7 (1.20)	115	0.495
		-3.0 (1.28)	213	0.882
		-3.0 (1.28)	230	1.193
		-2.0 (1.00)	130	0.351
T2-11/91	0.864	-4.3 (1.61)	400	12.98
A4-01/92	0.862	-5.0 (1.77)	106	0.216
		-5.0 (1.77)	250	2.977
		-3.2 (1.33)	320	3.945
B5-01/92	0.848	-3.4 (1.38)	105	0.519
		-4.0 (1.54)	170	0.843
B7-02/92	0.853	-3.3 (1.36)	103	0.622
		-3.3 (1.36)	250	1.903

The values beside test temperatures are correction factors for strain rates normalization at -2°C.

Morgenstern *et al.* (1980) were used in the finite element analyses for predicting strains in the pipeline since these properties were based on an exhaustive review of the data on polycrystalline ice available then.

Structural properties of pipeline steel 304

A 0.3 m long section from each of the model pipelines was instrumented with strain gauges in order to determine the structural

Table 5.4. Creep properties of polycrystalline ice at - 2 °C.

Reference	creep exponent n	creep coefficient B, kPa^{-n} x $year^{-1}$
Morgenstern *et al.* (1980)	3.00	2.03×10^{-8}
present creep tests and others reported by Sego (1980)	2.84	5.98×10^{-8}
parameters used for analysis (- 3 °C)	3.00	1.53×10^{-8}

properties of stainless steel 304. Custom made stems were welded to both ends of the test specimen so that specimens could be tested in the available MTS testing machine. The loading speed was slightly increased at about 2% strain for the first specimen and the tests were prematurely terminated when a weld failure occurred at the stem-specimen connection. The structural steel characteristics determined from the tests (Figure 5.9) are summarized in Table 5.2. The yield stress (σ_y) as defined by CSA Z245.1-1979 is in the 228 - 315 MPa range at a strain of 0.5% (ε_y). Steel 304 maintains stress-strain elastic proportionality till 0.1% (ε_{ep}) axial strain. It is interesting to note that a much lower yield strength was attained by the pipeline model B.

Observation of strain time histories in model pipelines

The displacement and load time histories monitored at the free end of the pipeline models A and B are shown in Figures 5.10a and 5.10b. While

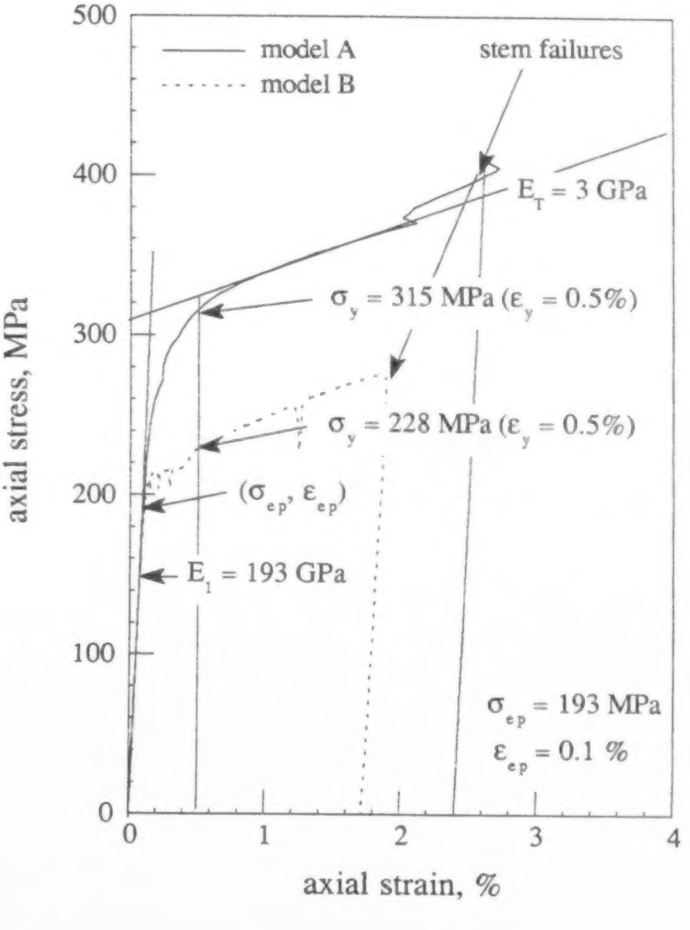

Figure 5.9. Experimental stress-strain characteristics of pipeline models A and B (stainless steel 304).

the pipeline A and B were being steadily displaced, the end load increased for about 1000 hours when it stabilized at load levels of 2744 N and 5600 N respectively. During the test on pipeline model A, the monitoring of the ice temperature (Figures 5.11a and 5.11b) commenced after problems were detected in the refrigeration system. The temperature was monitored by setting a thermistor (RTD) in the ice block sample at a depth of 0.10 m. A gap was noted to develop at the back of the pipeline as it was steadily displaced upwards. The flexural strain time histories for pipeline models A and B are shown in Figures 5.12a and 5.12b.

The deformed shapes of the pipelines obtained from the LVDTs placed at the crest of the pipeline are shown in Figures 5.13a and 5.13b. The deformed shape measured after the completion of the test[2] (pipeline model A) compared well with the last monitored shape and provided additional evidence on the reliability of the LVDTs during the test that lasted for about 90 days.

The flexural strain profile histories developed along the pipeline models A and B for different time intervals are shown in Figures 5.14a and 5.14b. The stress imposed on the ice as a result of the load developed at the end of the pipe (pulling end) can be estimated approximately from statics if a fully plastic moment is assumed to develop at the point of maximum strain. This approach gives an estimate of the average resistance due to uplift of the pipeline. The average reaction intensity calculated in this manner for

---

[2] Test for pipeline model B had not been terminated at the time of the completion of this thesis. The final data will be published in the paper referred to in footnote 1 on page 138.

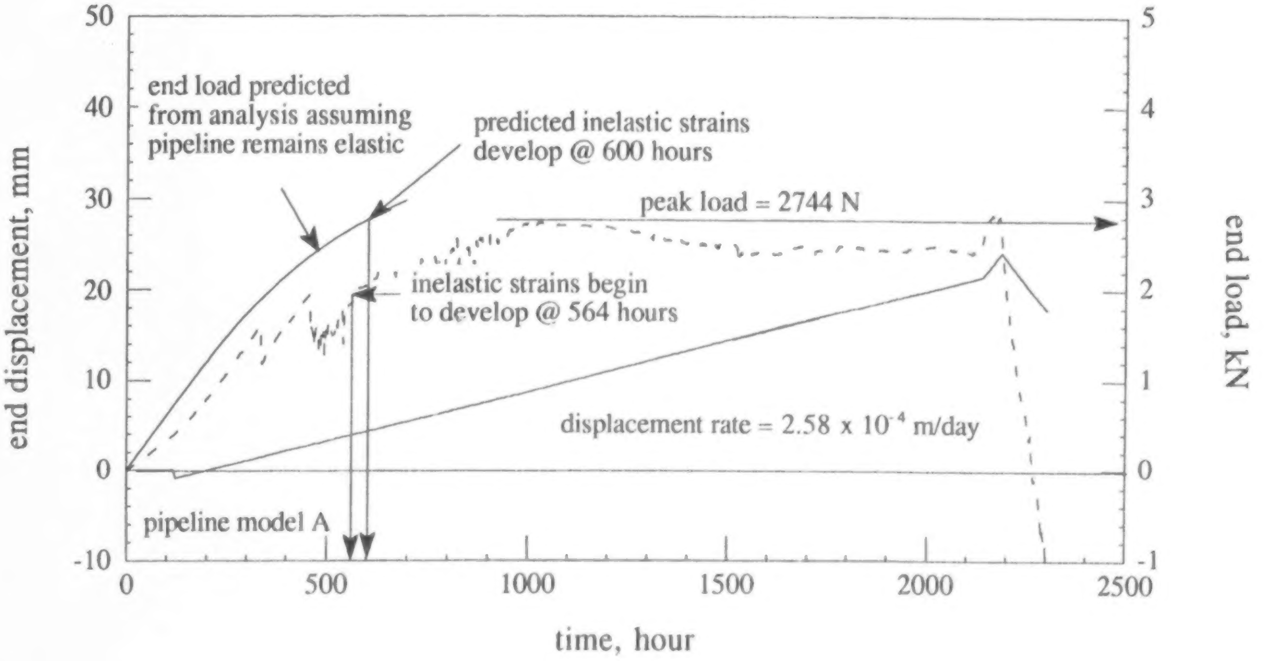

Figure 5.10a. End displacement and load time histories for pipeline model A.

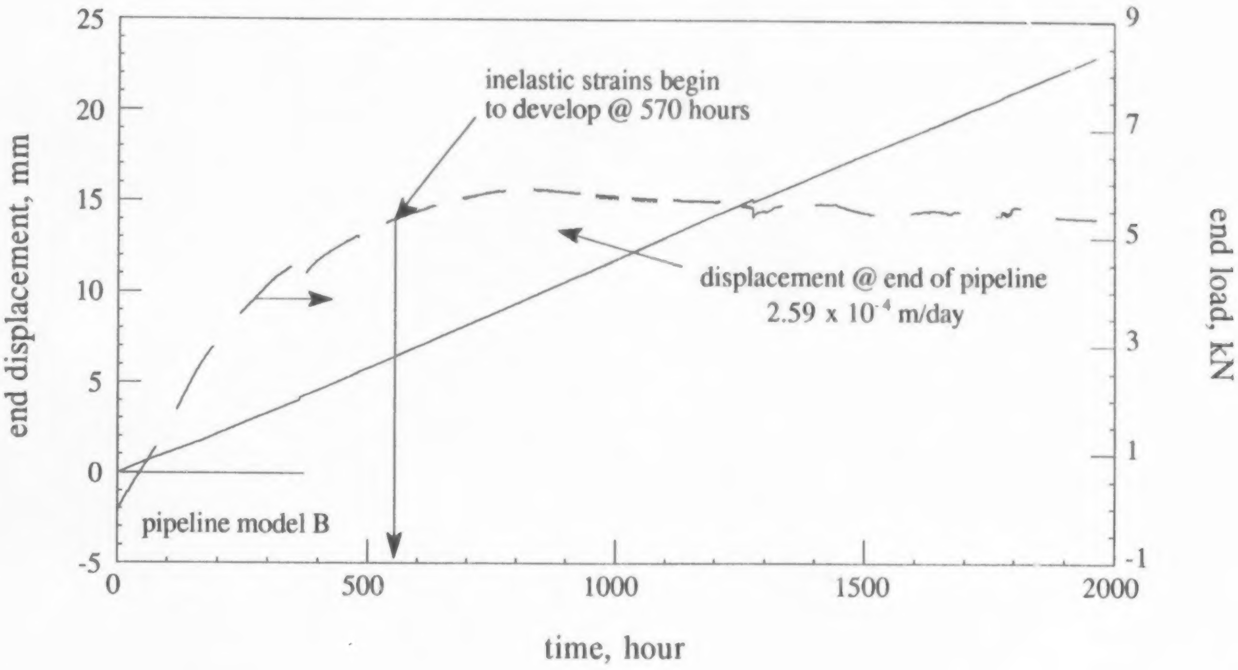

Figure 5.10b. End displacement and load time histories for pipeline model B.

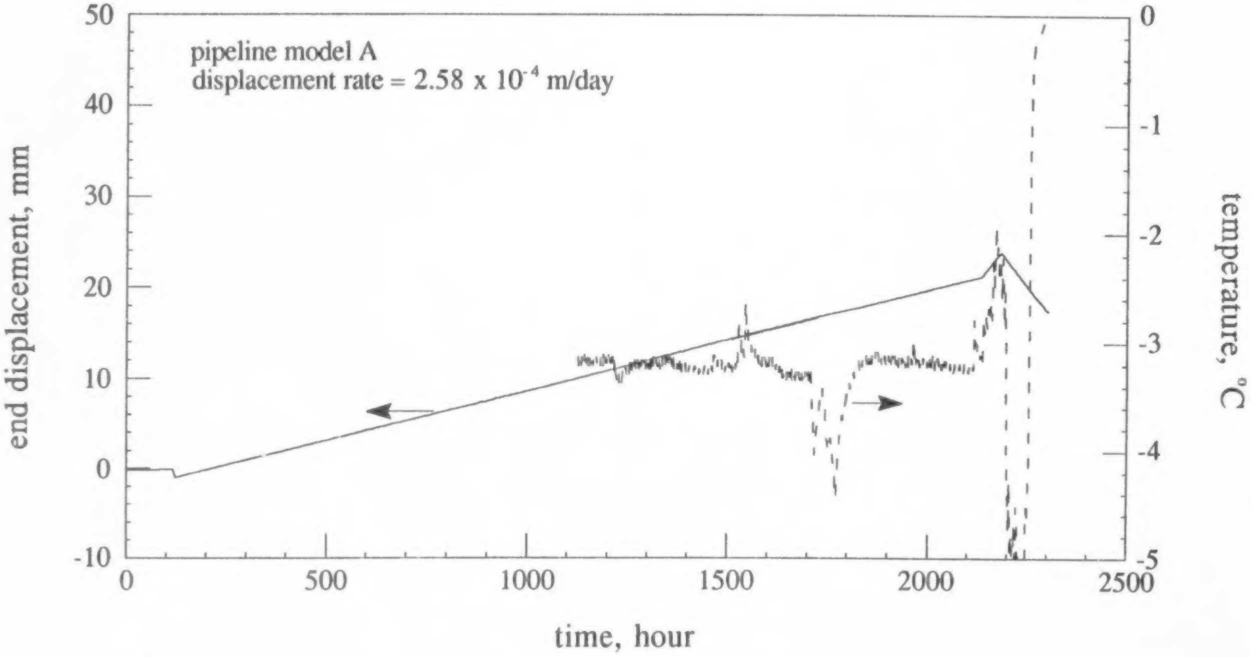

Figure 5.11a. End displacement and temperature time histories for pipeline model A.

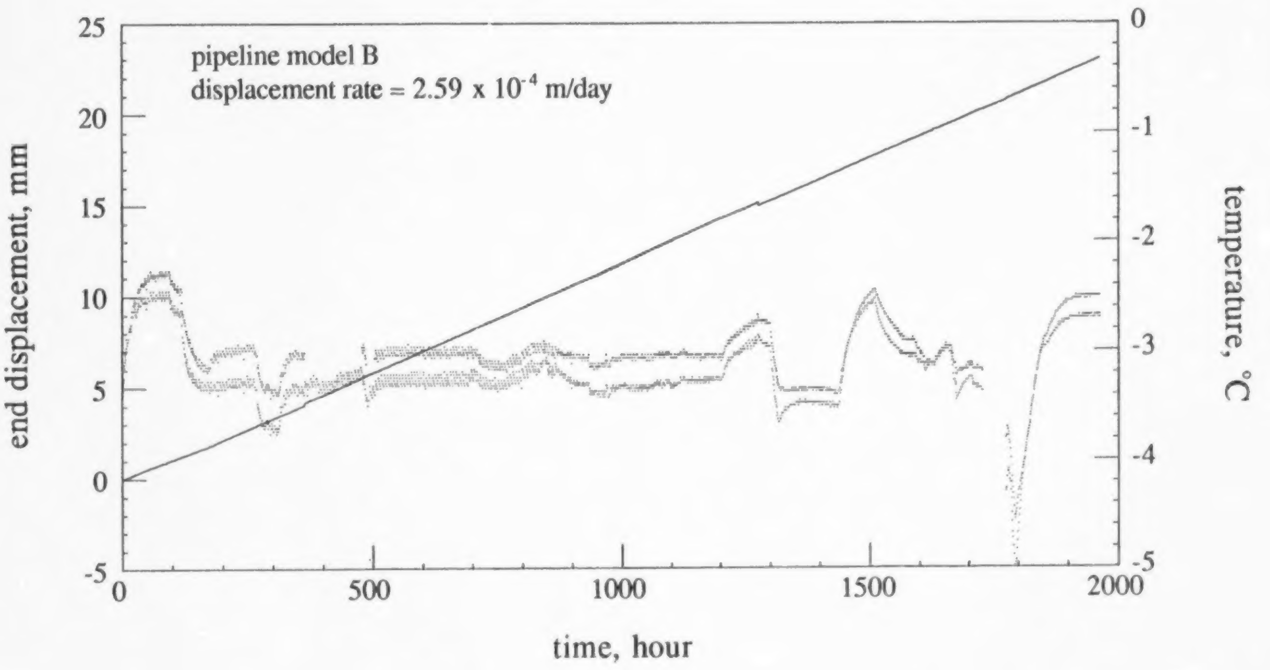

Figure 5.11b. End displacement and temperature time histories for pipeline model B.

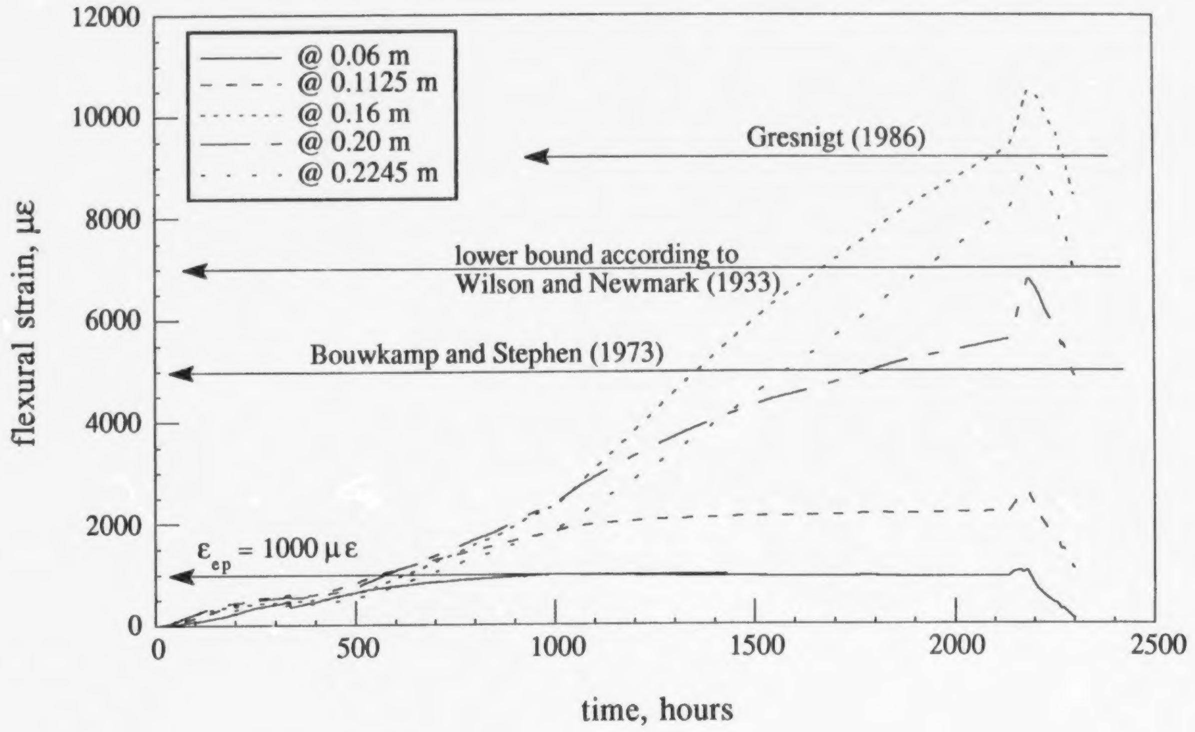

Figure 5.12a. Strain time histories for points in the immediate vicinity of peak strains for pipeline model A.

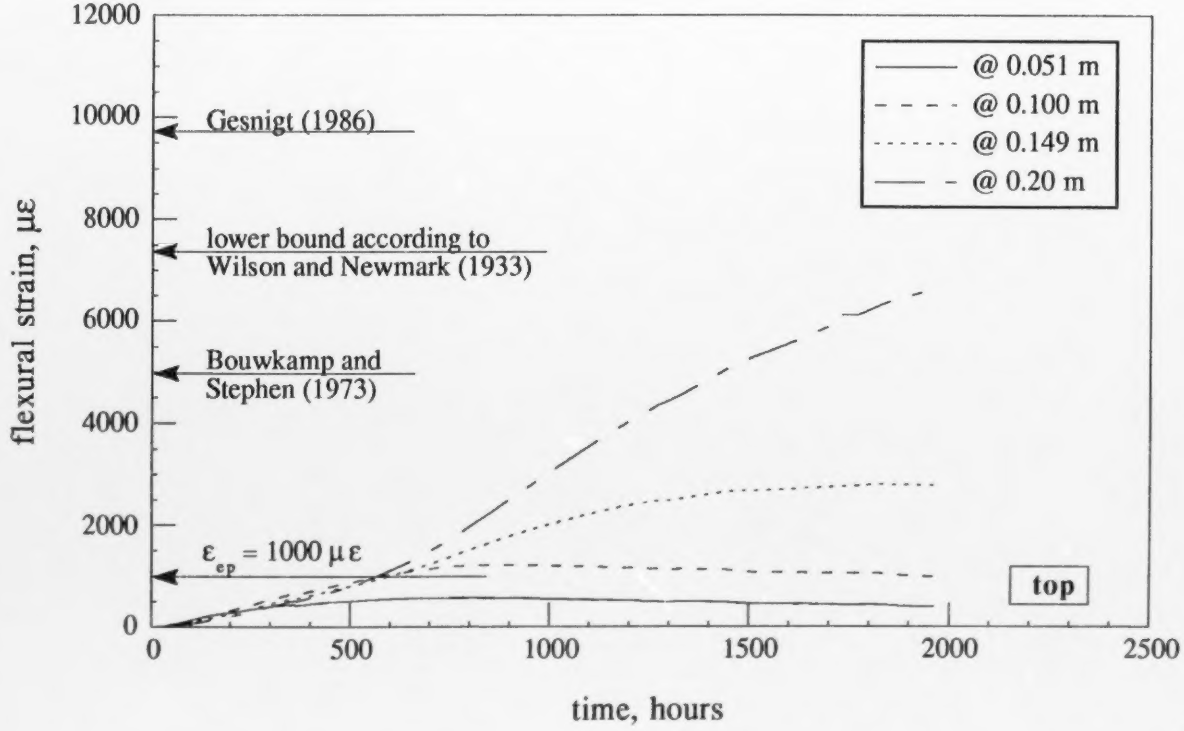

Figure 5.12b. Strain time histories for points in the immediate vicinity of peak strains for pipeline model B.

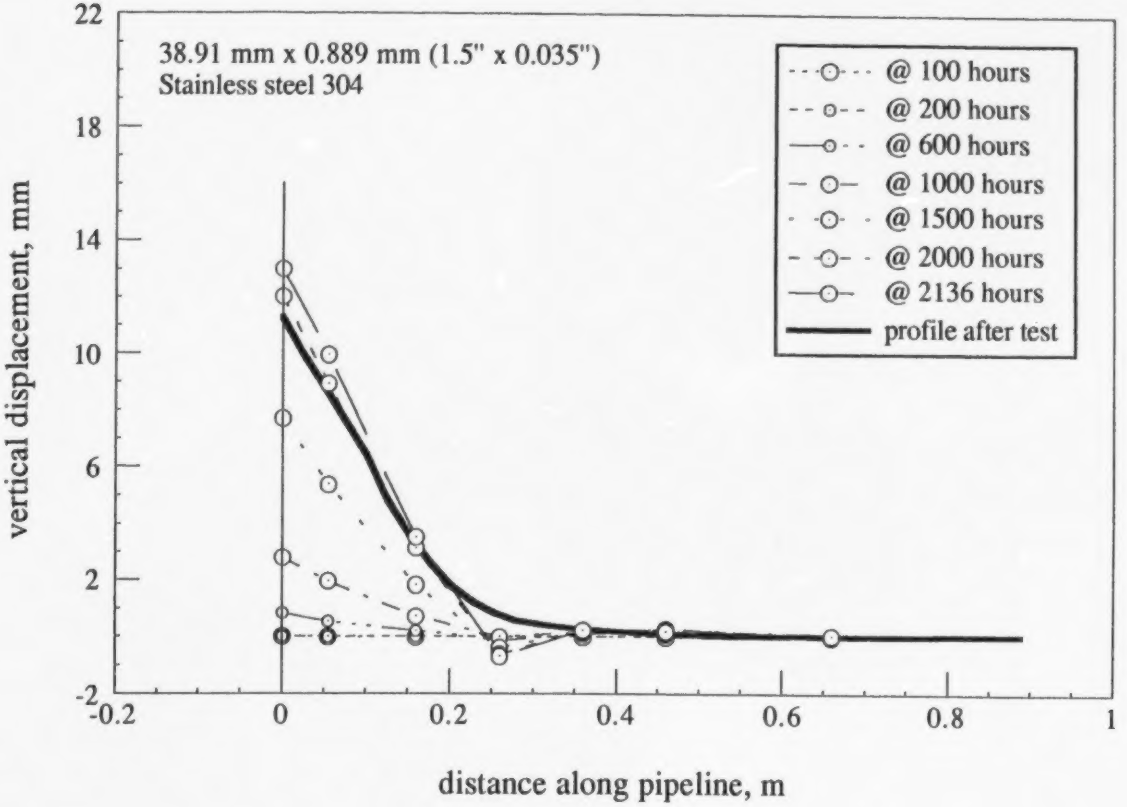

Figure 5.13a. Vertical displacement profile histories for pipeline model A.

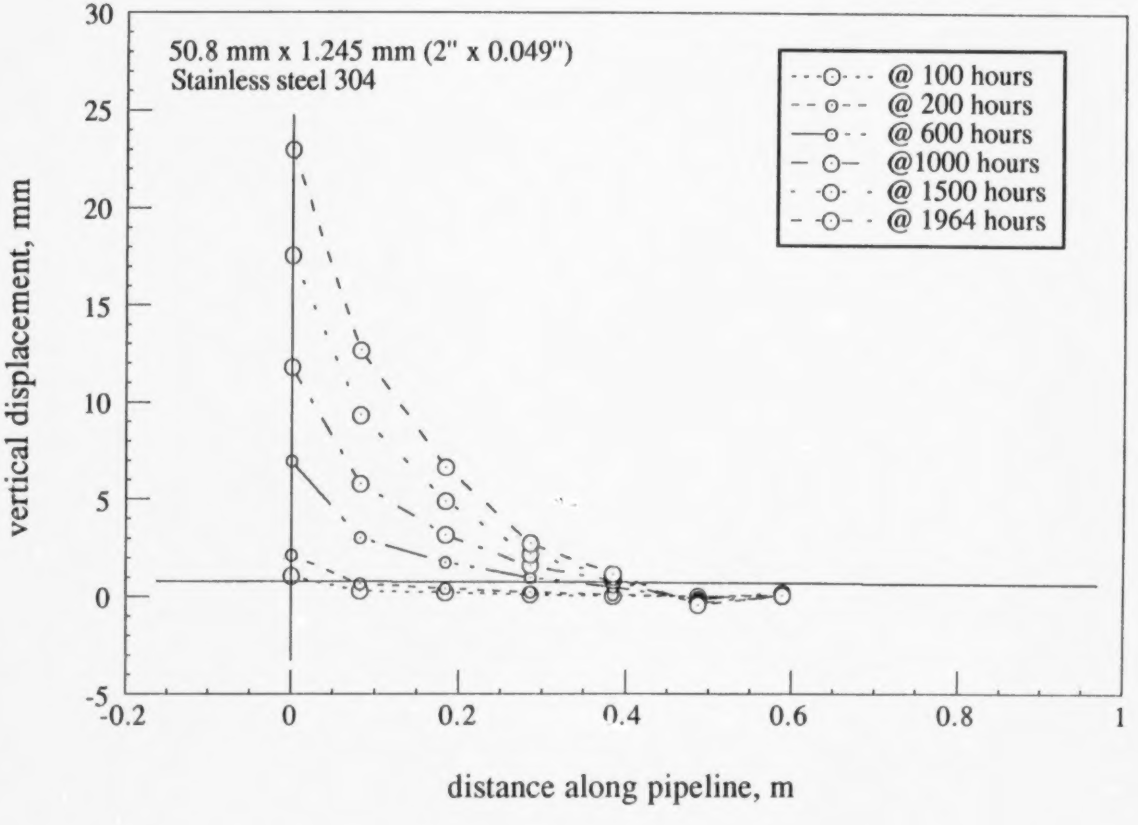

Figure 5.13b. Vertical displacement profile histories for pipeline model B.

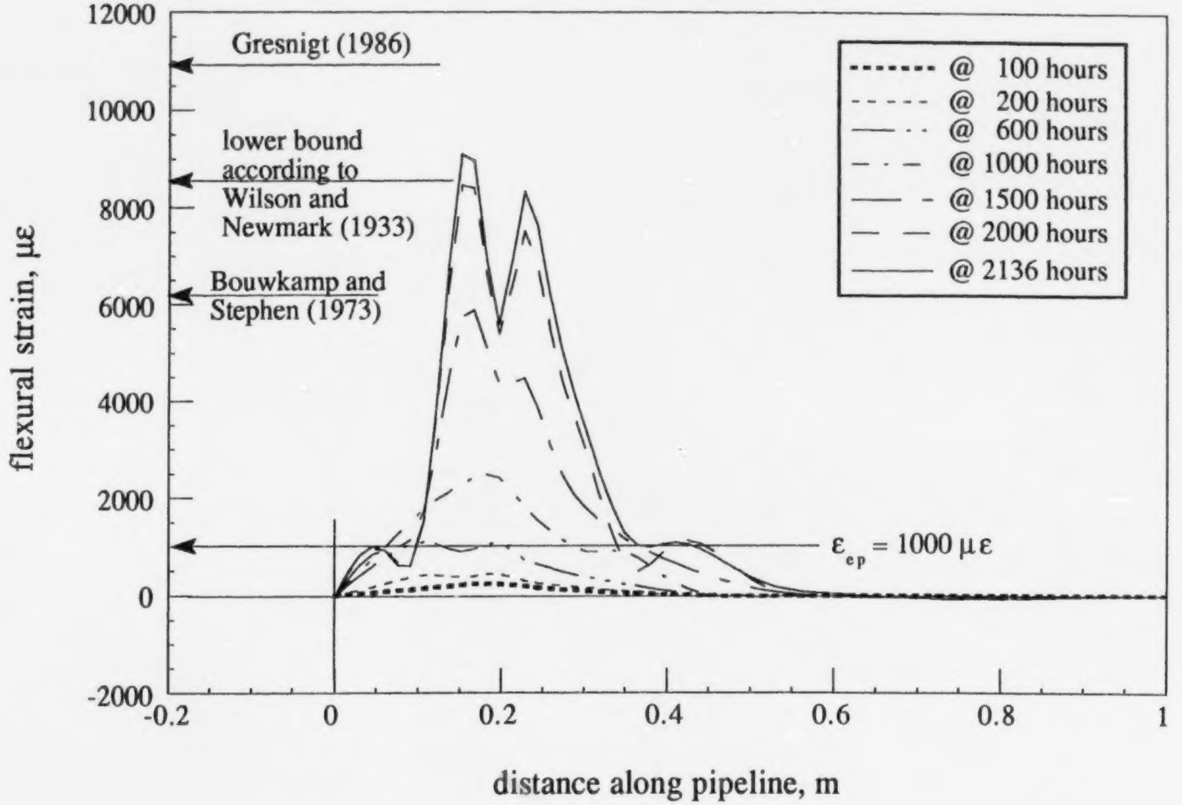

Figure 5.14a. Experimental flexural strain profile histories for pipeline model A.

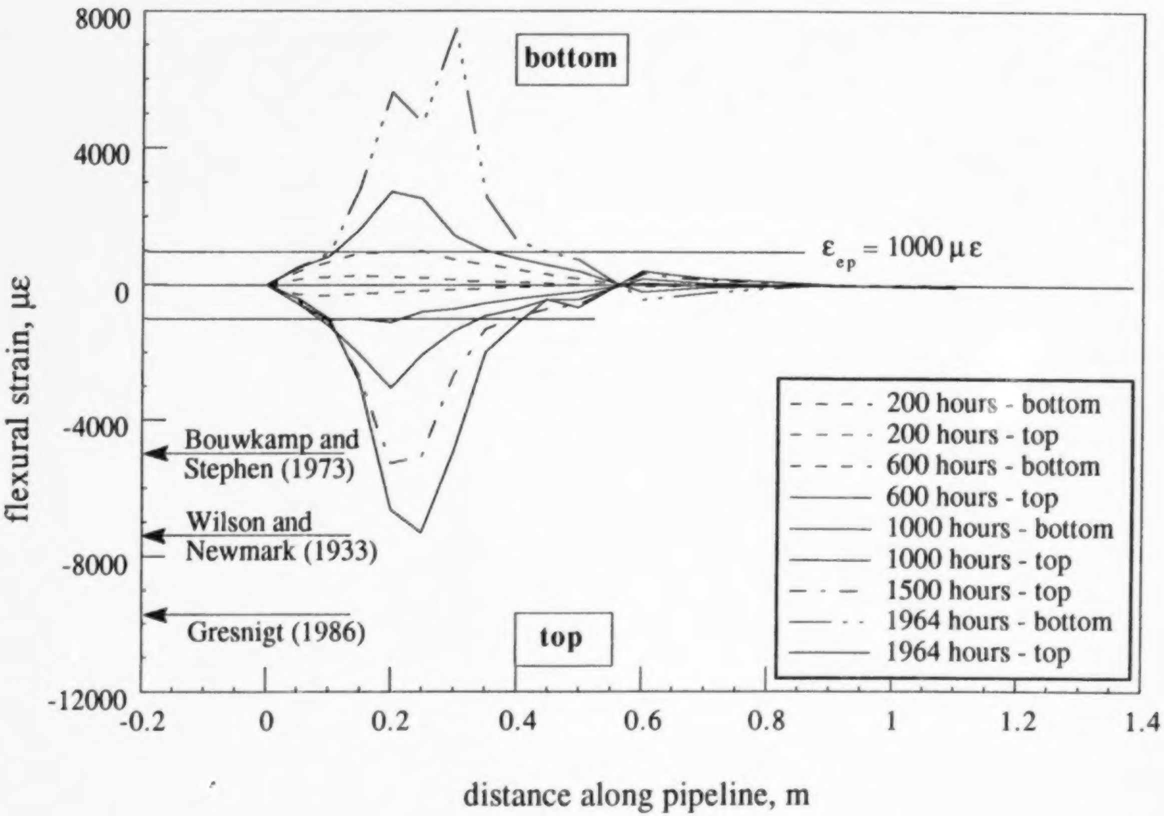

Figure 5.14b. Experimental flexural strain profile histories for pipeline model B.

pipeline model A is within the 100 - 300 kPa range. As noted before, the constant load creep data on polycrystalline ice indicates that primary creep is over after about 150 hours and consequently the application of Norton's secondary creep flow law for analysis is satisfactory for practical purposes. The strain profile is observed to be fairly smooth for the first 600 hours approximately for pipeline models A and B when the strains are below 0.1%. Thereafter the material of the pipeline model response is non-linear. After the tests were completed, the deformed profile of the bent pipeline models was obtained along the crest of the pipeline at 25 mm intervals. The final curvature was then estimated from the deformed shape using a three point finite difference formula. Since the determination of the curvature essentially involves numerical differentiation, the results can be very sensitive to small variations in the original data. However, the purpose of determining the flexural strains from the permanent deformed shape of pipeline models was only to confirm the final strains measured using electrical resistance strain gauges. A more elaborate procedure, such as fitting a cubic spline or a high order polynomial to the deformed shape, was not attempted for the same reasons stated earlier. The flexural strains were estimated from curvatures assuming that the neutral axis was still at the centre of the pipe. A comparison of the peak strains (Figures 5.15a and 5.15b) obtained from the two different methods indeed confirmed that the electrical resistance strain gauges had performed satisfactorily throughout the tests.

Circumferential measurements at different sections along the model pipelines were obtained to determine if significant ovality of the circular cross section had taken place. Figure 5.16 shows the deformed cross

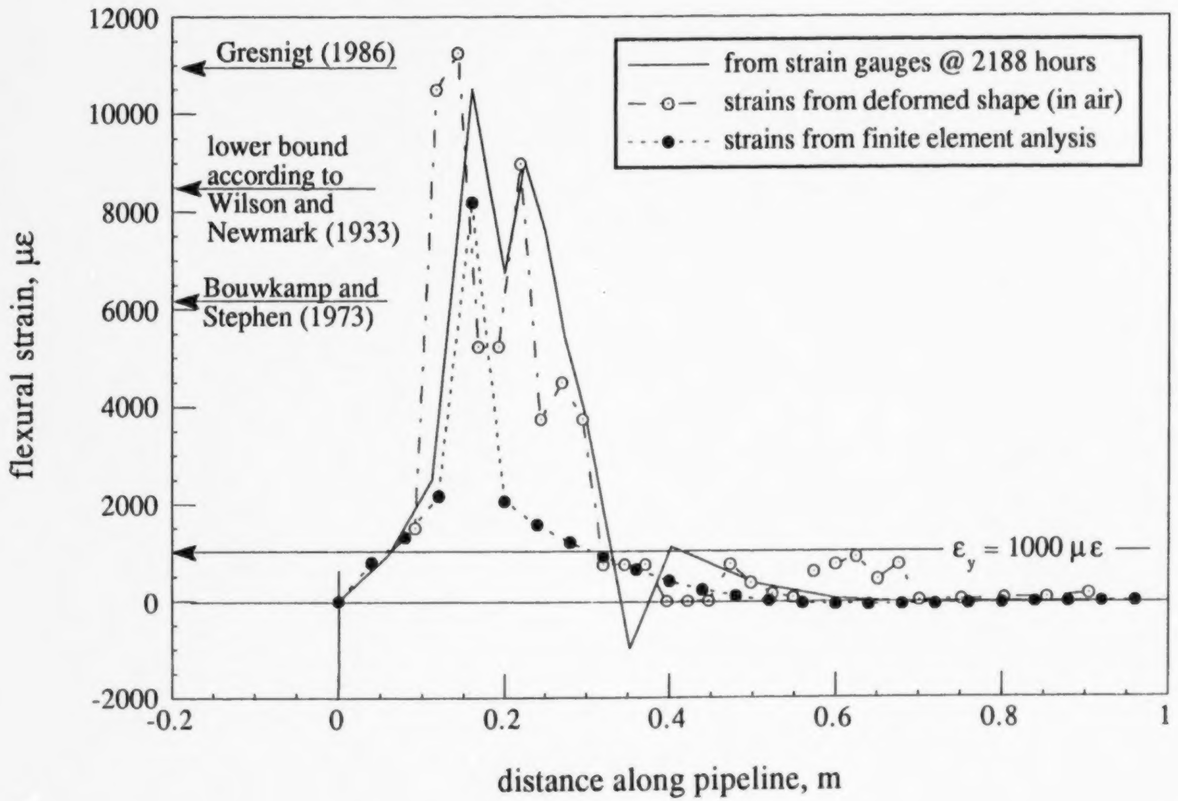

Figure 5.15a. Comparison of final flexural strain profiles before thaw, strains determined from deformed shape and predicted strains for pipeline model A.

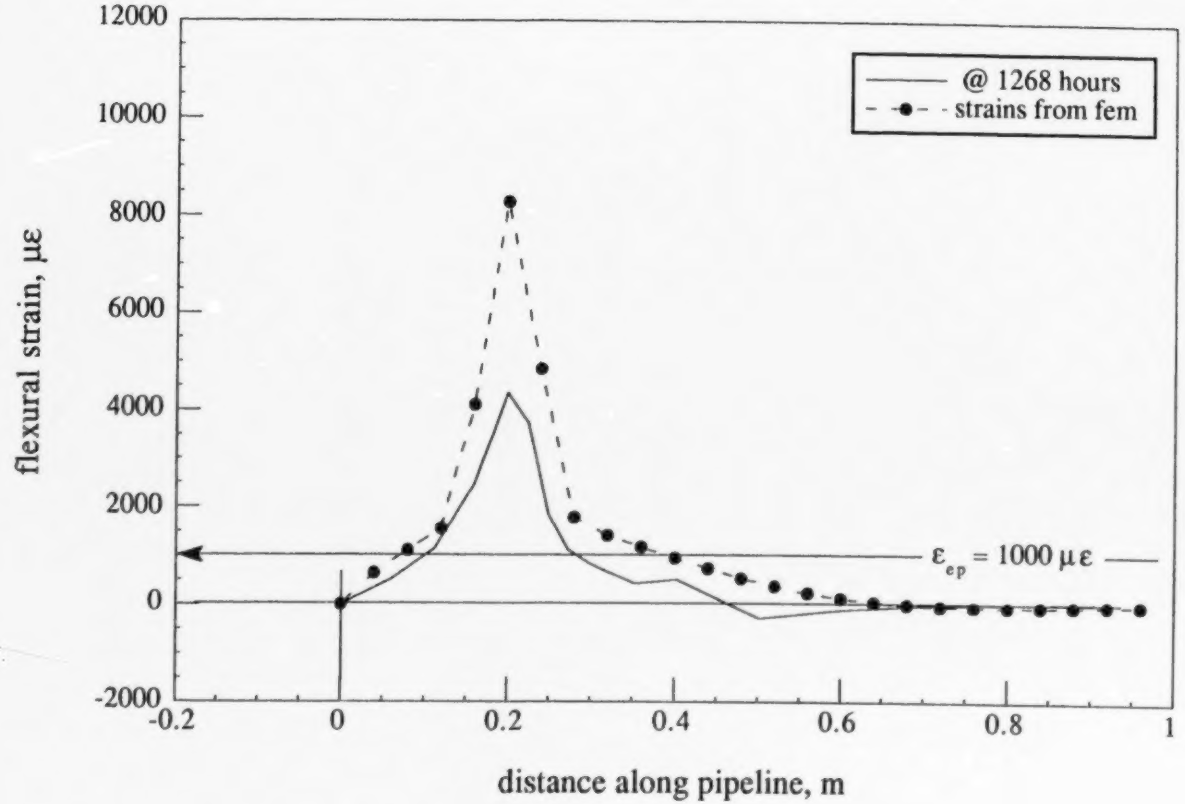

Figure 5.15b. Comparison of final flexural strain profiles before thaw, strains determined from deformed shape and predicted strains for pipeline model B.

sectional shape (exaggerated 20 times) of the pipeline at different sections of the pipeline. The circumferential readings were performed with a displacement dial gauge with an accuracy of 0.0254 mm (0.001"). These measurements were also confirmed independently using an electronic caliper. The maximum ovality, δ (inward) registered is in the order of 0.15 mm. In terms of the net diametrical change, $d_i(\%) = 2(\delta/b)100$, this amounts to a change of 0.78%. In fact the ovality is hardly discernable and no wrinkles or substantial local deformations were present.

If pipeline models A and B were to represent the prototype, then it is most probable that the pigging serviceability of these pipeline models would not be affected. Serviceability is not hindered in spite of the fact that all strain limits, as suggested by Wilson and Newmark (1933), Bouwkamp and Stephen (1973), Sherman (1976) and Gresnigt (1986), were exceeded (Figure 5.15a). It is most probable that the restraint offered by the surrounding stiff medium arrests the formation of wrinkles and substantially more flexural strain, as a result of frost heave, can be tolerated before serviceability would be severely hindered. Yun and Kyriakides (1990) found through analysis of shell buckling that imperfections have a dominant effect over the restraint offered by a stiff medium for the load carrying capacity for a pipeline subjected to axial loads. Even though the restraint offered by the surrounding stiff medium does not effect the load carrying capacity, it has a notable effect on the critical strain. It is important to make this distinction because design criteria are based on serviceability with respect to pigging as well as the need to avoid rupture when subjected to uplift due to frost heave. A similar

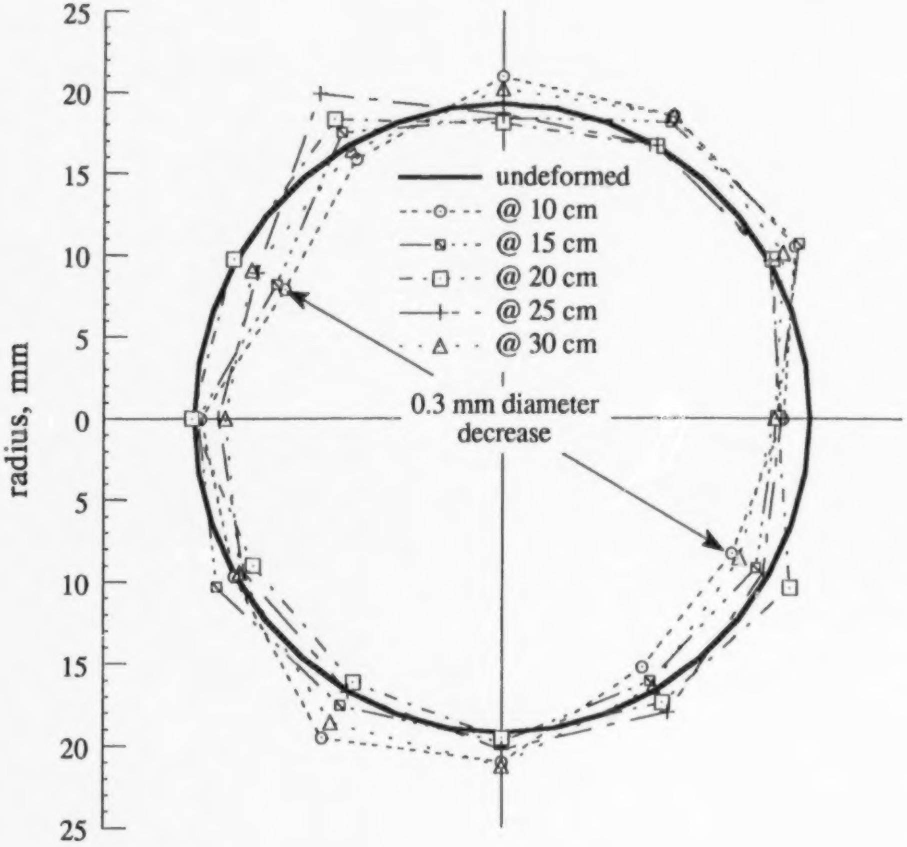

Figure 5.16. Out-of-roundness profiles exaggerated 20 times along the pipeline model A in the final deformed form.

situation (Yudovich and Morgan, 1989) arises for deep oil/gas casings where loading on the casings is imposed by the collapse of high porosity chalks in reservoirs at the Ekofisk site in the North Sea. Since these reservoirs are deep, the stiffness of the surrounding chalk would be high because its elastic modulus is dependent on the confining stress. Statistical analyses of casing serviceability and critical strain indicated that strains as high as 5-6% could be tolerated without posing a major hindrance for casing service.

Comparison of experimental behaviour with analysis

The numerical Winkler model developed for a beam embedded in a creeping medium in chapter 3 was used to evaluate the response of the model pipelines subjected to steady displacement for over 2000 hours. The finite element analyses were performed using Adina (1984) where the polycrystalline ice is represented by discrete creeping springs and the pipeline itself is represented by beam elements. Adina (1984) permits the specification of a tubular cross section whereby the material non-linearity can be taken into account in the simplest form. The material non-linearity of steel was limited to a bi-linear relationship along the lines suggested by the Committee on Gas and Liquid Fuel Lifelines (1984). All the pertinent data for individual components of the pipeline-polycrystalline ice that were discussed earlier helped to define all the relevant properties with minimal uncertainties.

The strain wave profile during the initial period, i.e. before 512 hours, helped to establish the elastic subgrade foundation modulus (i.e. elastic modulus of the surrounding ice). Since the solution for a beam embedded in a creeping medium is based on the correspondence principle, it is essential to match the elastic response with the form of the initial observed response. The procedure used was essentially the same as that discussed in chapter 4. Identification of the location of the peak strain permitted the determination of the most appropriate value of elastic or instantaneous modulus of ice which was estimated to be 61 MPa for both models A and B. The marked difference between the elastic modulus determined from sonic measurements and from pipeline-ice interaction is related to strain rate effects. Another source of discrepancy is perhaps in the limitation of Biot's (1937) or Vesic's (1961) formulae to translate the elastic continuum properties to foundation subgrade modulus. In the non-linear analysis an integration order of 5 x 3 x 5 (r, s, θ) was used for the pipe beam element. Tawfik (1986) argues that the tri-linear material model as proposed by the Committee on Gas and Liquid Fuel Lifelines (1984) for steel can lead to considerably higher estimated strains than would be obtained by a curvilinear material model like the Ramberg-Osgood model. This is primarily due to the fact that at large strains (> 4%) no stiffness is attributed to the material. This effect need not be of concern in the present analysis since the strains do not approach this strain limit. Nonetheless, Tawfik (1986) observes that when the material model is represented by the curvi-linear form, the strain wave is of an oscillatory nature near zones where plastic deformations takes place. A bi-linear stress strain relation for steel was selected for the finite element non-linear analysis and the prediction of peak strain was largely dependent on the elastic limit established from the uniaxial tests discussed earlier. If a bi-linear stress strain relation as suggested by the Committee on Gas and Liquid Fuel Lifelines (1984) is used, then the predicted peak strains are considerably reduced. This observation also confirms Tawfiks's (1986) findings that a discontinuous representation of the stress-strain relation for steel is not quite appropriate for realistic predictions.

Figures 5.17a and 5.17b shows the comparison of predicted and measured strain profiles at different time periods. The predicted and experimental flexural strain profiles match quite well for strains below the elastic strain proportionality limit (ε_{ep}) of 1000 $\mu\varepsilon$. However for strains beyond the elastic strain proportionality limit, the peak flexural strains (predicted vs measured) also compare well except that the extent of predicted plastic deformation is considerably less than that observed. The principal reason for this discrepancy is due to the fact that the pipeline is represented by a 2D beam elements in the finite element analyses and since the discretization is too coarse (typically one diameter of pipe) it is unable to account for stress redistribution that takes place in the pipeline as significant plastic strains develop. However, a 3D analysis, where the pipe is represented by shell elements and surrounding medium by 3D brick elements, would perhaps reproduce this redistribution of stresses more realistically, the analysis would be prohibitively costly.

Conclusions

A thorough description of the experimental procedure for carrying out model pipeline tests has been provided. Two different model size pipelines were tested in polycrystalline ice with continuous monitoring of flexural strains, displacements and temperature. The experimental data obtained

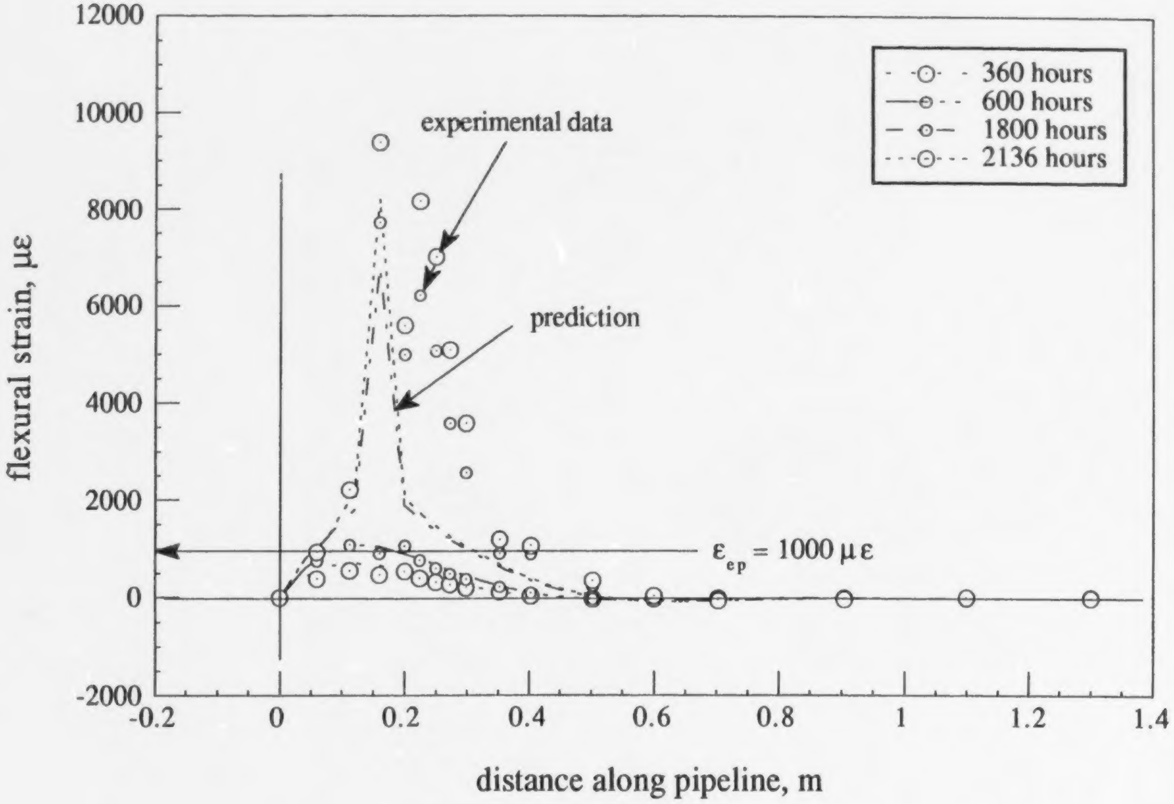

Figure 5.17a. Comparison of measured and predicted flexural strain profiles for pipeline model A.

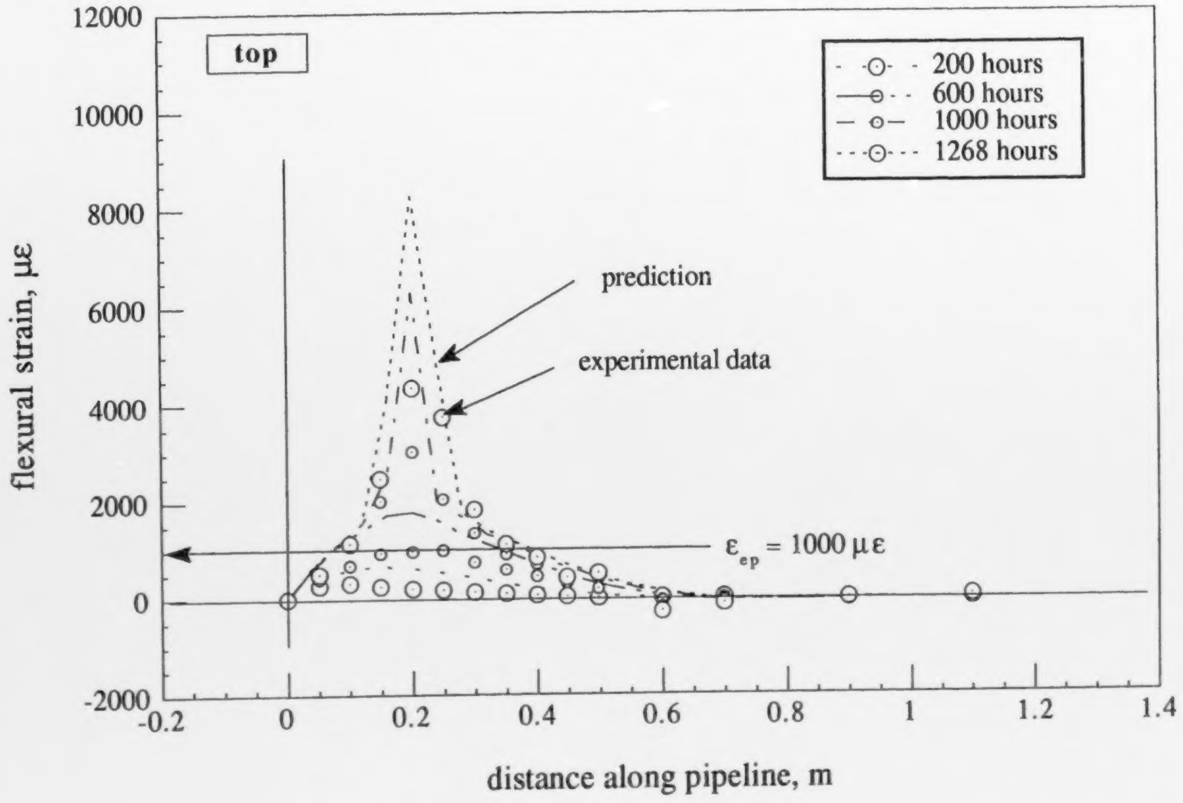

Figure 5.17b. Comparison of measured and predicted flexural strain profiles for pipeline model B.

generally confirms the findings of the simplified model of a beam embedded in a creeping medium. It seems that though the burial of the pipeline is shallow, for the purpose of this analysis it can be regarded as being deeply buried if the surrounding medium is very stiff. Though the strains exceeded currently accepted strain limits, the serviceability was not hindered. We therefore infer that the surrounding stiff medium retards the formation of wrinkles. This suggests that the critical strain limit can be increased considerably without jeopardizing the reliability of the pipeline. However, further tests need to be carried out with model pipelines of higher R/t ratios to further confirm these findings.

References

Adina - A finite element program for automatic dynamic incremental nonlinear analysis. 1984. Report AE 84-1, ADINA R&D, Inc., Boston, MA.

American Society of Civil Engineers. 1978. An overview of the Alaska highway gas pipeline: The world's largest project. National Convention of the American Society of Civil Engineers in Pittsburg, Penn. vi + 130p.

Biot, M.A. 1937. Bending of an infinite beam on an elastic foundation. Transactions, ASCE Journal of Applied Mechanics, **59** (A1-A7).

Bouwkamp, J.G. and Stephen, R.M. 1973. Large diameter pipes under combined loading. ASCE Journal of Transportation Engineering Division, **99**(TE3): 521-536.

Chen, J. and Kevorkian, V. 1971. Heat and mass transfer in making artificial snow. Industrial Engineering Chemical Process Design Development, **10**(1): 75-78.

Committee on Gas and Liquid Fuel Lifelines. 1984. Guidelines for the seismic design of oil and gas pipeline systems. ASCE. New York, NY.

Dallimore, S.R. and Crawford, H. 1985. Experimental observations of differential heaving and thaw settlement around a chilled pipeline. *In* Pipelines and Frost Heave. Proceedings of a seminar held at Centre de Geomorphologie, Caen, France. v + 75p.

Geotechnical Sciences Laboratories, Carleton University. 1986. Investigations of frost heave as a cause of pipeline deformation. Internal report - IR 50. Report prepared for Earth Physics Branch, Energy, Mines and Resources Canada, 71 pp.

Geotechnical Sciences Laboratories, Carleton University. 1988. The third freeze cycle of the Canada-France ground freezing experiment. Internal report - IR 54. Report prepared for Permafrost Research Section, Terrain Sciences Division of Geological Survey of Canada. 78 pp.

Geotechnical Sciences Laboratories, Carleton University. 1989. Canada-France pipeline-ground freezing experiment. Internal report - IR 58.

Report prepared for Permafrost Research Section, Terrain Sciences Division of Geological Survey of Canada. 81 pp.

Glen, J.W. 1955. The flow law of polycrystalline ice. Proceedings of the Royal Society, London, **228A**: 519-538.

Gresnigt, A.M. 1986. Plastic design of buried steel pipelines in settlement areas. Heron, **31**(4):1-113.

Hall, W.J. and Newmark, N.M. 1978. Seismic design criteria for pipelines and facilities. ASCE Journal of Technical Councils, **104**(TC1): 91-107.

Huff, C. M. 1990 Private communications, The Liquid Atomization Company, Ontario, Canada.

Instanes, A. 1992. Sonic and mechanical properties of spray ice. Ph. D. Thesis under preparation, University of Trondheim, Norway.

Jacka, T. H. and Lile, R.C. 1984 Sample preparation techniques and compression apparatus for ice flow studies. Cold Regions Science and Technology, **8**(3): 235-240.

Kennedy, R.P., Chow, A.W. and Williamson, R. A. 1977. Fault movement effects on buried pipelines. ASCE Journal of Transportation Engineering Division, **103**(TE5): 617-633.

Kim, H.O. and Velasco, P. 1988. Review of pipe buckling for arctic pipeline design. Proceedings of the Seventh International Conference on Offshore Mechanics and Arctic Engineering, ASME, New York, V:307-315.

Kyriakides, S., Yun, H.D. and Yew, C.H. 1983. Buckling of buried pipelines due to large ground movements. Earthquake Behaviour and Safety of Oil and Gas Storage Facilities, Buried Pipelines and Equipment, ASME. PVP, **77**:140-150.

Ladanyi, B. 1972. An engineering theory of creep of frozen soils. Canadian Geotechnical Journal, **9**: 63-80.

Langner, C.G. 1984. Design of deepwater pipelines. Proceedings, TNO-IWECO 30th Symposium on Underwater Technology, The Hague. Netherlands.

McRoberts, E.C., Law, T.C. and Murray, T.K. 1978. Creep tests on undisturbed ice-rich silt. Proceedings of the Third International Permafrost Conference, Vol. 1. Edmonton, Alberta, pp. 539-545.

Michel, B. 1978. Ice mechanics, Les Presses de L'Université de Laval, Québec. xxiii + 499p.

Morgenstern, N.R., Roggensack, W.D. and Weaver, J.S. 1980. The behaviour of friction piles in ice and ice-rich soils. Canadian Geotechnical Journal, **17**: 405-415.

Nixon, J.F. 1984. Laterally loaded piles in permafrost. Canadian Geotechnical Journal, **21**(3): 431-438.

Nixon, J.F., Morgenstern, N.R. and Ressor, S.N. 1983. Frost heave-pipeline interaction using continuum mechanics. Canadian Geotechnical Journal, **20**: 251-261.

Nyman, K. J. and Lara, P.F. 1986. Structural monitoring helps assess deformations in arctic pipelines. Oil and Gas Journal, **81**(11): 81-86.

O'Byrne, J.M. and Haynes, D. 1973. Use of a snow gun for production of a model snow material. East Snow Conference, Proceedings of the 30th Annual Meeting, Amherst, Mass., pp. 15-19.

Sayles, F.H. 1973. Triaxial and creep tests on Ottawa sand. Proceedings of the Second International Conference on Permafrost, Yakutsk, North American Contribution, pp. 384-391.

Sayles, F.H. and Haines, D. 1974. Creep of frozen silt and clay. U.S. Army Cold Regions Research and Engineering Laboratory, Hanover, NH. Technical Report 252, 50p.

Sego, D.C. 1980. Deformation of ice under low stresses. Unpublished Ph. D. Thesis, University of Alberta, Edmonton, Alberta. xxiii + 500p.

Sego, D.C. and Morgenstern, N., 1983. Deformation of ice under low stresses. Canadian Geotechnical Journal, **20**(4): 587-602.

Sego, D.C. and Morgenstern, N. 1985. Punch indentation of polycrystalline ice. Canadian Geotechnical Journal, **22**(2): 226-233.

Sherman, D.R. 1976. Tests of circular steel tubes in bending. ASCE Journal of Structural Division, **102**(ST11):2181-2195.

Sinha, N. K. 1989. Elasticity of natural types of polycrystalline ice. Cold Regions Science and Technology, **17**(2): 127-135.

Southwell, R.V. 1914. On the theory of elastic stability. Philosophical Transactions, Royal Society, London, **Series A. 213**: 187-244.

Tawfik, M.S. 1986. Analysis of pipelines under large soil deformations. Unpublished Ph. D. Thesis, Cornell University, xiii + 243p.

Vesic, A.S. 1961. Bending of beams resting on isotropic elastic solid. Proceedings of ASCE, **87**(EM2): 35-51.

Wilson, W. M. and Newmark, N.M. 1933. The strength of thin cylindrical shells as columns. Bulletin No. 255, University of Illinois. Experimental Station, Urbana, Illinois.

Yudovich, A. and Morgan, D.R. 1989. Casing deformations in Ekofisk. Journal of Petroleum Technology, **41**(7): 729-734.

Yun, H. and Kyriakides, S. 1990. On the beam and shell modes of buckling of buried pipelines. Soil Dynamics and Earthquake Engineering, **9**(4): 179-193.

Nomenclature

The following symbols are used in this chapter:

B = creep proportionality constant
c = critical strain criterion constant
D = pipeline diameter (=2R)
E = beam elastic modulus
E_T = steel strain hardening modulus
E_s = soil elastic modulus
h = embedment depth
I = beam moment of inertia
k_s' = foundation subgrade modulus
n = creep exponent in Norton relation
R = radius of model pipelines
t = pipeline wall thickness

$\dot{\varepsilon}_o$ = proof strain rate
ε_{ep} = elastic proportionality strain limit
γ = soil weight density
ν = steel Poisson's ratio
ν_s = soil Poisson's ratio

σ_{ep} = elastic proportionality stress limit

σ_y = steel yield stress

σ_o = proof stress

Appendix

Figures 5.A1, 5.A2 and 5.A3 show constant load multi-staged creep time histories for three more samples that were tested.

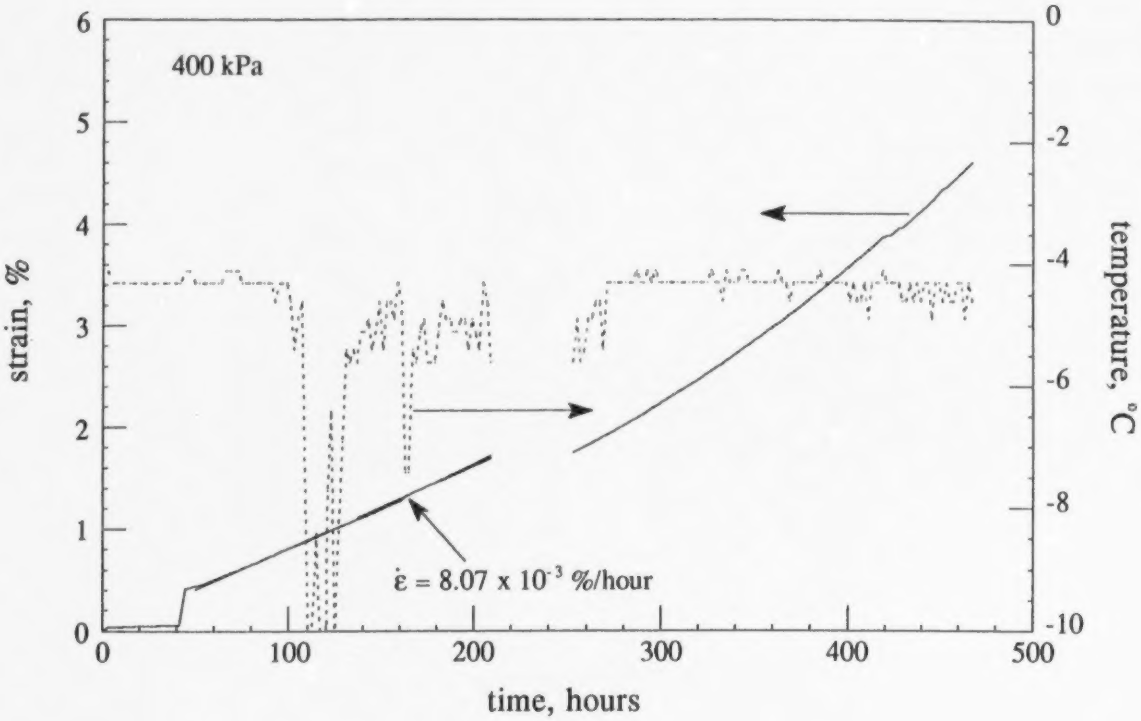

Figure 5.A1. Constant load creep test for polycrystalline ice sample T2-11/91.

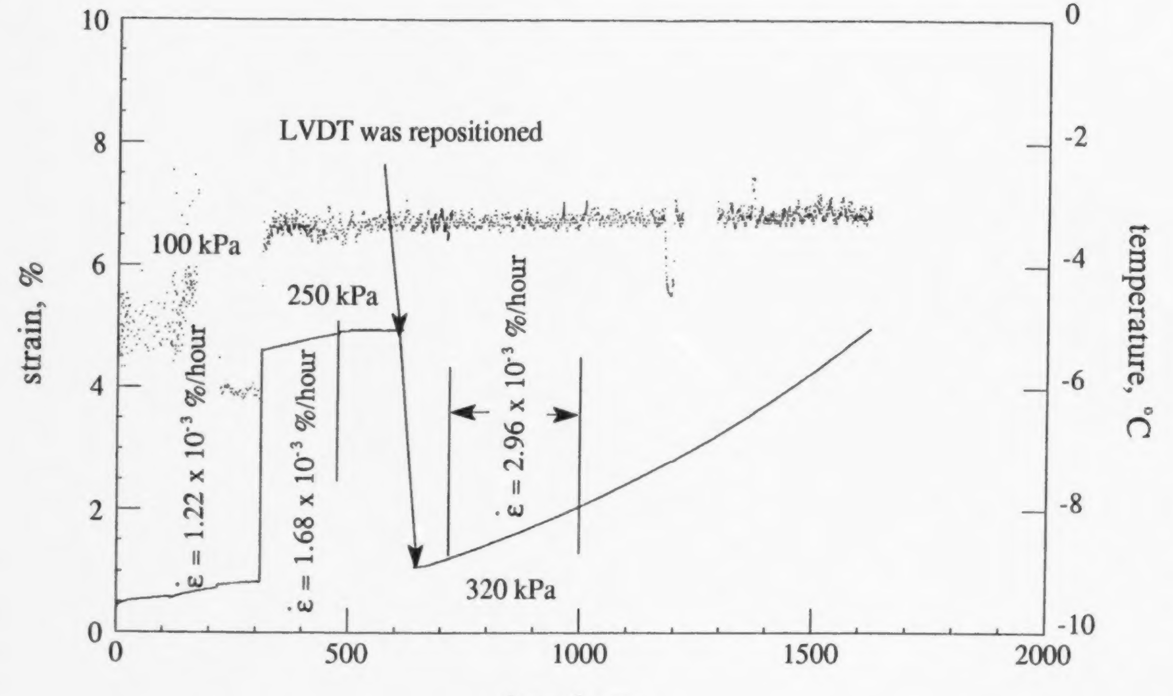

Figure 5.A2. Constant load creep test for polycrystalline ice sample A4-01/92.

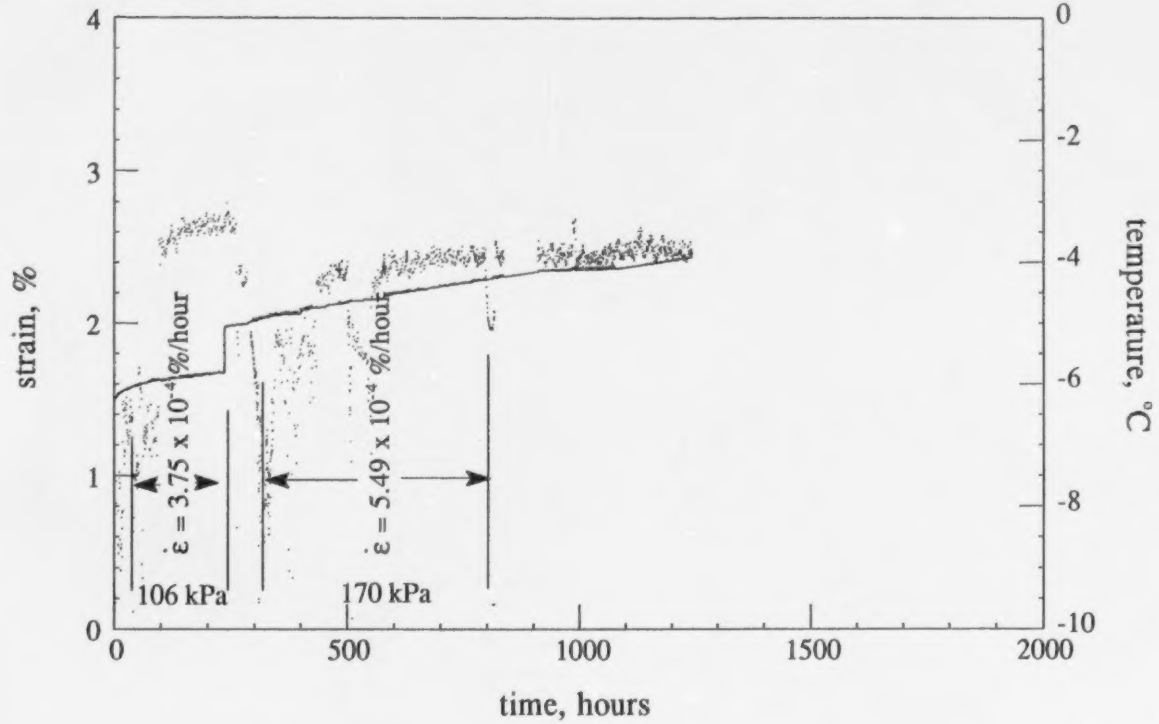

Figure 5.A3. Constant load creep test for polycrystalline ice sample B5-01/92.

Chapter 6

CONCLUSIONS

Frozen soil pipeline interaction

The principal problem associated with the design of a chilled buried gas pipeline subjected to frost heave is to identify the role of the specific characteristics of the frozen ground that significantly influence the behaviour of the pipeline. In order to improve the understanding of the problem, the pipeline frozen ground interaction study was undertaken in several stages with the development of simple analytical solutions that were later validated with the more complex finite element method.

In the first stage, particular attention was paid to the fact that the pipeline has a finite shallow burial and that the surrounding medium can be assumed to be an elastic perfectly-plastic material. It was found that the shallow burial can be accounted for by adjusting a bearing type capacity factor to evaluate the response of a pipeline embedded in an elastic perfectly-plastic medium. The developed model based on the beam on an elastic perfectly-plastic Winkler foundation was validated using a three-dimensional finite element discretization. Though the finite element model was coarse, it captures the principal characteristics of the response. The versatility of the Winkler model was demonstrated by solving the different problems of lateral loaded piles. The influence of the separation of the surrounding medium from the back of the pile was also demonstrated.

The next obvious step was to develop a similar model of a beam embedded in a creeping Winkler foundation to account for the specific fact that real frozen ground creeps according to Norton's flow law. The creep response obtained was based on the application of the correspondence principle. Upper and lower bound estimates were obtained using Raleigh-Ritz and Martin's inequality procedures since it is very difficult to obtain the exact solution for the resulting differential equation. These estimates were validated with the formulation of the discrete springs that can be readily used in the finite element method. The approximate solutions also established the non-dimensional parameters that clearly define the response of a beam embedded in a creeping medium subjected to an end load.

Several field and laboratory studies of timber, steel and aluminum piles subjected to lateral loads at the pile head have been performed in the last two decades and a few as late as 1991. These tests were carried out on piles installed in frozen silty clay, frozen sand and polycrystalline ice. The discrete Winkler finite element analyses of these pile tests were able to reproduce with good overall measure the observed behaviour using the available geotechnical data for frozen ground or polycrystalline ice. Subsequently, the application of the model to match the stress histories of the experimental pipeline at Caen, France, confirmed the robustness of the model in spite of its simplicity. These analyses demonstrated that the applicability of the correspondence principle is quite valid for the kind of problems under study in this thesis.

Two model pipelines embedded in polycrystalline ice and subjected to a steady upward displacement were tested. The models were thoroughly instrumented for flexural strains and upward displacements. Several constant load creep tests were performed on polycrystalline ice to determine its creep properties. The creep properties were found not to be too different from those obtained previously. The pipeline models were displaced so as to surpass currently stated strain limits on operational pipelines. Significant ovalization was not observed though the model pipelines were subjected to flexural strains exceeding 1%. These experimental results seem to suggest that large strains can be tolerated in the pipeline without significantly hindering its operation. The experimental results also confirm that, though the pipeline is buried at a shallow depth, as far as the analysis is concerned, it can be assumed that the overlying medium is semi-infinite because frozen ground is usually very stiff. The application of the solution for a beam embedded in a creeping medium demonstrated once again the robustness of the Winkler model as long as the model pipeline remains elastic.

Recommendations for future studies

The simple analytical solutions representing the pipeline as a beam embedded in a creeping medium have limitations because they do not account for material non-linearity of the pipeline material. Throughout the thesis it has been assumed that the elastic and creep properties are the same in tension as well as in compression. Since portions of the frozen medium are expected to be in tension, effort should be made to investigate whether there are significant changes in elastic and creep properties when the frozen material is in tension. Improvements should be attempted so as to take into account the effects of material non-linearity as well as ovalization. Nonetheless, every effort should be made to maintain the simplicity of the analytical solutions because a very complex finite element analysis is not always warranted for preliminary designs. Of course, these simple models should always be validated either with experiments or analyses of the finite element type.

There is a need for carrying out more experiments of the type described in this thesis but using model pipelines which have higher radius to wall thickness ratios, i.e. R/t in the range of 40 - 50. These model pipelines should explore the accentuated effects of wrinkling strain and whether the surrounding resistance by the stiff frozen medium significantly alters pipeline behaviour.